universität wien

MASTERARBEIT / MASTER'S THESIS

Titel der Masterarbeit / Title of the Master's Thesis

„Biological activity of platinum(IV)- and copper(II)-complexes and thiopyridone-based organometallics in three-dimensional cancer models“

verfasst von / submitted by

Dominik Wenisch, BSc

angestrebter akademischer Grad / in partial fulfilment of the requirements for the degree of

Master of Science (MSc)

Wien, 2021 / Vienna 2021

Studienkennzahl lt. Studienblatt / degree programme code as it appears on the student record sheet:	UA 066 863
Studienrichtung lt. Studienblatt / degree programme as it appears on the student record sheet:	Masterstudium Biologische Chemie
Betreut von / Supervisor:	o. Univ.-Prof. Dr. Dr. Bernhard Keppler
Mitbetreut von / Co-Supervisor:	

Abstract

Compared to the commonly employed two-dimensional (2D) cell culture approaches, three-dimensional (3D) models are much more similar to *in vivo* tumors or cancerous tissue in various aspects. Many cancer cell lines are capable of self-assembling to a spatial structure called multicellular tumor spheroid. This structure comprises multiple cell layers with gradually different access to nutrients, O_2 and growth factors. The same is true for cancerous tissues, which tend to show high interior heterogeneity regarding the access to nutrients by formation of blood vessels.

In this work, the effects of three classes of novel metal-based or metal-chelating anticancer compounds were for the first time studied in spheroid models, with a focus on cytotoxic activity, ROS production, and induction of apoptosis:

Octahedral Pt(IV) complexes are successors of the anticancer drug cisplatin (and its commonly used derivatives oxaliplatin and carboplatin), but are being developed to obtain better tolerable alternatives, as the Pt(II) drugs cause severe side effects. In the 3D approach, we demonstrated a broad range of cytotoxicities for the structurally diverse compounds (with sub- to low micromolar IC_{50} values for a few of them), but only modest induction of apoptosis. Some of the compounds induce high cellular ROS production, not necessarily correlating with cytotoxic potency.

Cu(II) chelators or complexes could also be promising alternatives to established classes of cancer chemotherapeutics. Thiosemicarbazones, which are continuously investigated for their anticancer effects, are known to preferentially chelate Cu(II). Resulting complexes may disrupt cellular processes due to the redox chemistry of the tightly regulated essential trace element. In multicellular tumor spheroid models, we could show combinations of thiosemicarbazones and copper(II) chloride yield IC_{50} values in a relatively narrow (one-digit to very low two-digit micromolar) range, despite structural variation with regard to methylation of the terminal nitrogen and presence of an estrone moiety. Cytotoxicity of the combinations was at least 4-5 times higher than that of the thiosemicarbazones alone. Terminal dimethylation seems to be favorable for induction of apoptosis, independent of the presence or absence of the hormone-like moiety.

Ru(II)- and Rh(III)-arene complexes are currently investigated due to their versatility in terms of ligand sphere. They may contain mono- or bidentate ligands that have an enormous impact on biological availability, and therapeutic side effects could be influenced by introducing minor changes to the ligands bound to those metals. A comparison of various thiopyridone-containing arene complexes indicated moderate to modest cytotoxic activity in the employed spheroid models, with the exception of a RAPTA-containing (Ru) complex that yielded IC_{50} values close to 1 µM in spheroids of two (out of four) cell lines. The same compound turned out to induce the generation of ROS most potently, which did not reflect in particularly strong induction of apoptosis (in the rather insensitive HCT-116 model, however). Since little is known about the mode of action for this class of compounds, we tested the interaction with the pUC-19 dsDNA plasmid in a cell-free approach. Five out of seven compounds showed an impact on DNA secondary structure, though to a quite low extent, making direct DNA interactions an unlikely cause for their cytotoxic effects on cancer cells.

For all three classes of compounds, results in multicellular tumor spheroids point to more or less pronounced differences between their representatives with regard to cytotoxicity, ROS production, and induction of apoptosis. Therefore, further preclinical evaluation is certainly warranted only for properly selected compounds.

Zusammenfassung

Verglichen mit den häufig untersuchten zweidimensionalen (2D) Zellkulturexperimenten, weisen dreidimensionale (3D) Modelle in vielerlei Hinsicht mehr Ähnlichkeiten zu *in vivo* Tumoren, beziehungsweise Krebsgewebe, auf. Viele Krebszelllinien haben die Fähigkeit, räumliche Strukturen durch Selbstassemblierung zu bilden, so genannte multizelluläre “Sphäroide”. Solche Strukturen bestehen aus vielen Zellschichten mit graduell unterschiedlichem Zugang zu Nährstoffen, Sauerstoff und Wachstumsfaktoren. Dasselbe Phänomen ist ebenfalls in Krebsgewebe zu finden, dessen heterogener Aufbau die Neubildung von Blutgefäßen benötigt, um besseren Zugang zu Nährstoffen zu gewährleisten.

In dieser Arbeit werden drei Klassen neuartiger, metallbasierender beziehungsweise metallchelatierender Krebstherapeutika und deren Auswirkungen vorgestellt, die erstmalig in dreidimensionalen Sphäroid-Modellen durchgeführt wurden. Der Schwerpunkt liegt dabei auf den Auswirkungen auf die Zytotoxizität, die Produktion von reaktiven Sauerstoffspezies und die Induktion von Apoptose:

Oktogonale Pt(IV) Komplexe sind Nachfolger des Krebstherapeutikums Cisplatin (und dessen häufig eingesetzter Derivate Oxaliplatin und Carboplatin), die entwickelt wurden, um besser verträgliche Alternativen zu haben, da Pt(II)-Chemotherapeutika erhebliche Nebenwirkungen aufweisen. In den 3D-Versuchen konnten wir eine weite Bandbreite an Zytotoxizitätswerten (mit IC_{50}-Werten einiger Komplexe im niedrigen mikromolaren Bereich) für strukturell sehr unterschiedliche Substanzen zeigen, wohingegen Apoptose in nur sehr geringem Ausmaß eingeleitet wurde. Einige dieser Komplexe produzieren hohe zelluläre ROS-Level, die nicht notwendigerweise mit der zytotoxischen Aktivität in Einklang zu bringen sind.

Cu(II)-Chelatoren beziehungsweise -Komplexe könnten ebenfalls eine vielversprechende Alternative zu den bereits etablierten Chemotherapeutika darstellen. Thiosemicarbazone, die fortlaufend auf ihre antitumoralen Effekte untersucht werden, sind bekannt dafür, bevorzugt mit Kupfer(II) Komplexe einzugehen. Diese Komplexe könnten, wegen der Redox-Aktivität des sehr stark regulierten essentiellen Spurenelements Kupfer, zelluläre Prozesse stören. In unseren multizellulären Sphäroiden konnten wir nachweisen, dass Kombinationen

von Thiosemicarbazonen und $CuCl_2$ eine relative enge Bandbreite an IC_{50}-Werten aufweisen (einstelliger bis niedriger zweistelliger mikromolarer Bereich), trotz einer strukturellen Diversität bezüglich der Methylierung des terminalen Stickstoff-Atoms und der Anwesenheit einer Estron-Komponente. Die Zytotoxizitätswerte dieser Kombinationen mit $CuCl_2$ waren zumindest um das Vier- bis Fünffache höher als die der einzelnen Thiosemicarbazone. Terminale Dimethylierung scheint für die Induktion der Apoptose von Vorteil zu sein, unabhängig davon, ob eine hormonähnliche Struktur vorhanden ist oder nicht.

Ru(II)- und Rh(III)-Aren Komplexe werden zurzeit wegen ihrer flexiblen Ligandensphäre untersucht. Mono- oder bidentate Liganden können enthalten sein, die einen starken Einfluss auf die biologische Verfügbarkeit haben, oder auch die geringfügige (strukturelle) Änderung von Liganden, die an diese Metalle gebunden sind, können zur Beeinflussung der therapeutischen Nebeneffekte führen. Ein Vergleich verschiedener Thiopyridon-enthaltender Aren-Komplexe wies auf geringe bis mäßige zytotoxische Aktivitäten in den getesteten Sphäroiden hin, mit der Ausnahme eines RAPTA-enthaltenen (Ru)-Komplexes, der IC_{50}-Werte nahe 1 µM in Sphäroiden von zwei (von insgesamt vier getesteten) Zelllinien aufwies. Derselbe Komplex zeigte zwar eine höchst wirksame ROS-Induktion in den Zellen der Sphäroide auf; dies lies sich jedoch nicht mit der relativ geringen Menge an apoptotischen Zellen (trotz der Insensitivität der HCT-116 Sphäroide) in Einklang bringen. Weiters testeten wir die Interaktion mit dem pUC-19 dsDNS-Plasmid in einem zellfreien Versuch, da über die genaue Wirkungsweise dieser Substanzklasse noch wenig bekannt ist. Fünf der sieben getesteten Komplexe hatten einen äußerst geringen Einfluss auf die Sekundärstruktur der DNS des Plasmids, sodass die direkte Interaktion der DNS mit den Substanzen als Grund für die zytotoxischen Effekte in Krebszellen unwahrscheinlich ist.

Für alle drei Substanzklassen zeigen die Ergebnisse der Zytotoxizitäts-, ROS- und Apoptose-Experimente in multizellulären Sphäroiden die mehr oder weniger ausgeprägten Unterschiede ihrer Vertreter an, weshalb weitere präklinische Beurteilungen für einzelne, ausgewählte Komplexe dieser Klassen auf jeden Fall gerechtfertigt sind.

Acknowledgements

This thesis, originating in the time of a pandemic in 2020/2021, was a hard, but also satisfying work. After finishing the practical part, it was not easy for me to sit down and start typing. While sitting in front of the present thesis, I talked or chatted with my supervisors, team members, family and friends, in order to motivate myself and being motivated by them.

For this reason, I want to thank all of you, who helped and supported me, especially my supervisor Prof. Dr. Dr. Bernhard Keppler and Dr. Michael Jakupec, who both gave me the opportunity to perform the practical parts of this work in their group. Of course, I am very grateful to my mentor Debora Wernitznig MSc, who introduced me into all practical aspects. Her support in all things happening before and during the pandemic was overwhelming.

Next, I also want to thank my team members Klaudia Cseh MSc, Michaela Hejl and Dr. Anton Legin, who always supported me with their knowledge and practical experience.

Then, “thank you” to all members, who attended and collaborated during this work. To name only few of them: Dr. Markus/Mathea Galanski, Dr. Éva Anna Enyedi and Dipl.-Ing. Dr. Wolfgang Kandioller, whose projects the studied compounds originated from.

Furthermore, I am grateful to my whole family, especially my three sisters, Kerstin, Bianca and Larissa, my father Helmut and my uncle Dr. Willibald Edinger, who always motivated me with constructive criticism, whenever necessary, and comforted me warmly.

Also, a big “thank you” to all my friends, who supported me at all times with jokes and talks, whenever possible. A special “thanks” I want to give is to Christina Schedl MSc, who always knows the perfect words to build me up.

A very special need to say “thank you” to, is my mother Monika Wenisch. You never let me down and always believed in what I and your daughters did to find our own path. You are one of the most prominent reasons why I am able to finish this thesis.

May you always be part of my/our future path, even if you are not able to go it with us physically. I only want to say: “THANK YOU”!

List of Contents

Abbreviations

BMI	Body mass index
BSA	Bovine serum albumin
DC	Dendritic cell
DCFH-DA	Dichlorodihydrofluorescein diacetate
DMSO	Dimethylsulfoxide
ER	Endoplasmic reticulum
FACS	Fluorescent-activated cell sorting
FCS	Fetal calf serum
FITC	Fluorescein isothiocyanate
ICD	Immunogenic cell death
MAP-K	Mitogen-activated protein-kinase
mAb	Monoclonal antibody
PBS	Phosphate buffered saline
PFA	Paraformaldehyde
PI	Propidium iodide
pta	1,3,5-Triaza-7-phosphaadamantane
RAPTA	Ruthenium-arene-1,3,5-triaza-7-phosphaadamantane
RB	Retinoblastoma protein
ROS	Reactive oxygen species
SAR	Structure-activity-relationship
STS	Steroid sulfatase
VEGF-R	Vascular endothelial growth factor receptor

Introduction

Global cancer statistics

Approximately 10 million people worldwide died from cancer in 2020, according to WHO statistics. One third of these deaths are estimated to have occurred due to (at least) one of the five most common behavioral risks:[1]

- Lack in physical exercise
- Unhealthy nutrition (low fruit and vegetable intake)
- High BMI
- Tobacco consumption
- Alcohol consumption

Although cancer ranks “only” second among death causes globally[2], its incidence, etiology and treatment are one of the most researched topics in biological/medicinal and issue-related institutions.

Worldwide, breast, lung and colorectal cancers are the most occuring types[3]; their respective incidences are for both sexes in all ages 11.7% for breast, 11.4% for lung, and 10% for colorectal types, as shown in *Fig. 1A (left)*. A total count of 19.292.789 cases in 2020 corresponds to 0.25% of today’s world population number of 7.8 billion.[4] According to *Fig. 1A (right),* almost half of these cases were lethal in 2020, whereby lung, colorectal and liver cancer caused the highest numbers of deaths.

With regard to the contintental distribution (*Fig. 1B*), Asia ranked first, with 49.3% of global cases and 58.3% of global cancer deaths in 2020. In the same year, Europe ranked second, with almost a fifth (19.6%) of all cancer deaths worldwide.

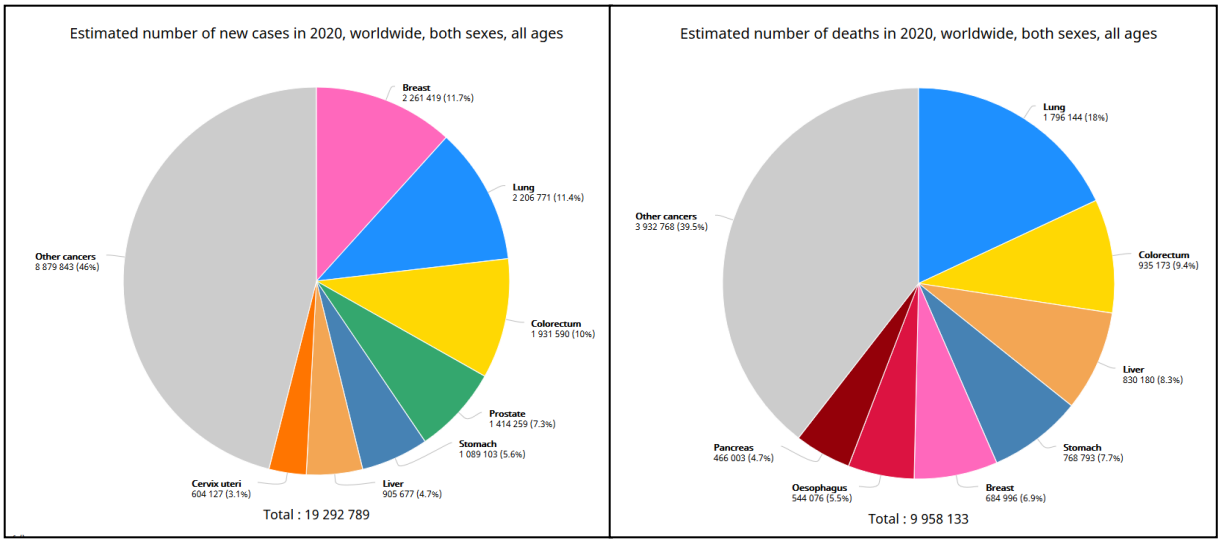

Fig. 1A: Incidence and mortality of various types of cancer worldwide in 2020. *Breast cancer types are most occuring, but are not the most lethal ones. Note that although cancers summarized as "Other cancers" comprise not frequently occuring types, their overall numbers account for more than two fifth of all incidence cases.*

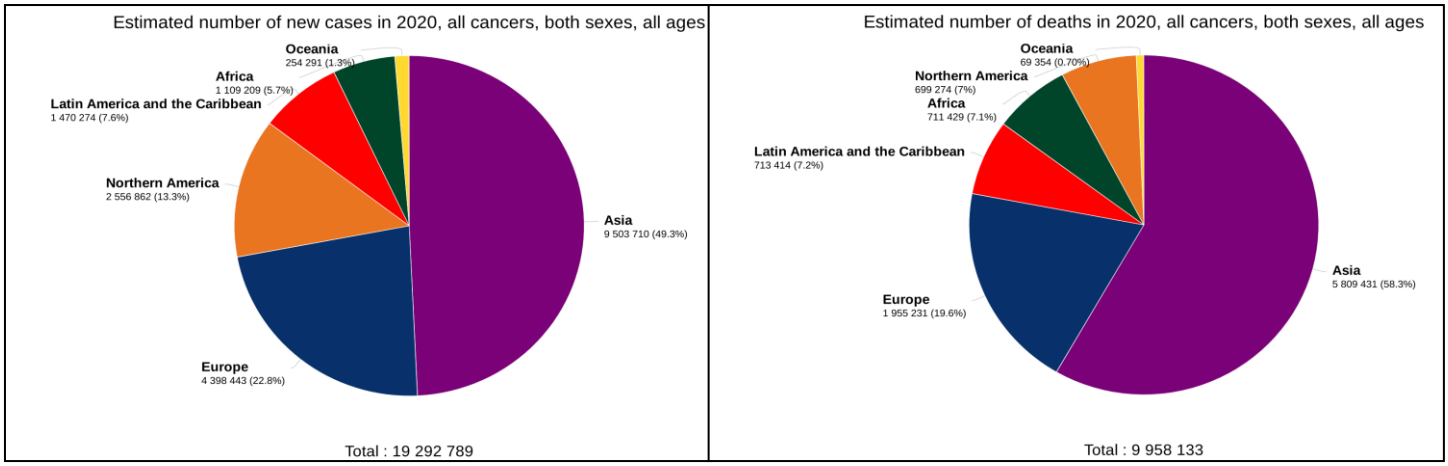

Fig. 1B: Continental distribution of cancer occurrence and its mortality in 2020. *Asia is the continent with highest numbers in both categories and Europe following with about half of Asia's incidence cases and approximately a third of its death rate.*

Cancer statistics in Austria

According to Statistics Austria, 20.969 people died of cancer in 2020.[5] Only cardiovascular diseases were more lethal (32.678 cases in total). In Austria, lung, prostate and breast tumors are the most lethal cancer types (*Fig. 2A*)[6] according to ASR values (ASR = "**a**ge-**s**tandardised **r**ate", a weighted mean of age-specific rates, adjusts the incidence rate as if the population had a standard age structure and thereby makes statistics of populations with different age structure comparable).[7] However, according to the unadjusted percentage distribution (*Fig. 2B*), lung-colorectal- and pancreatic-tumors are the most lethal ones.

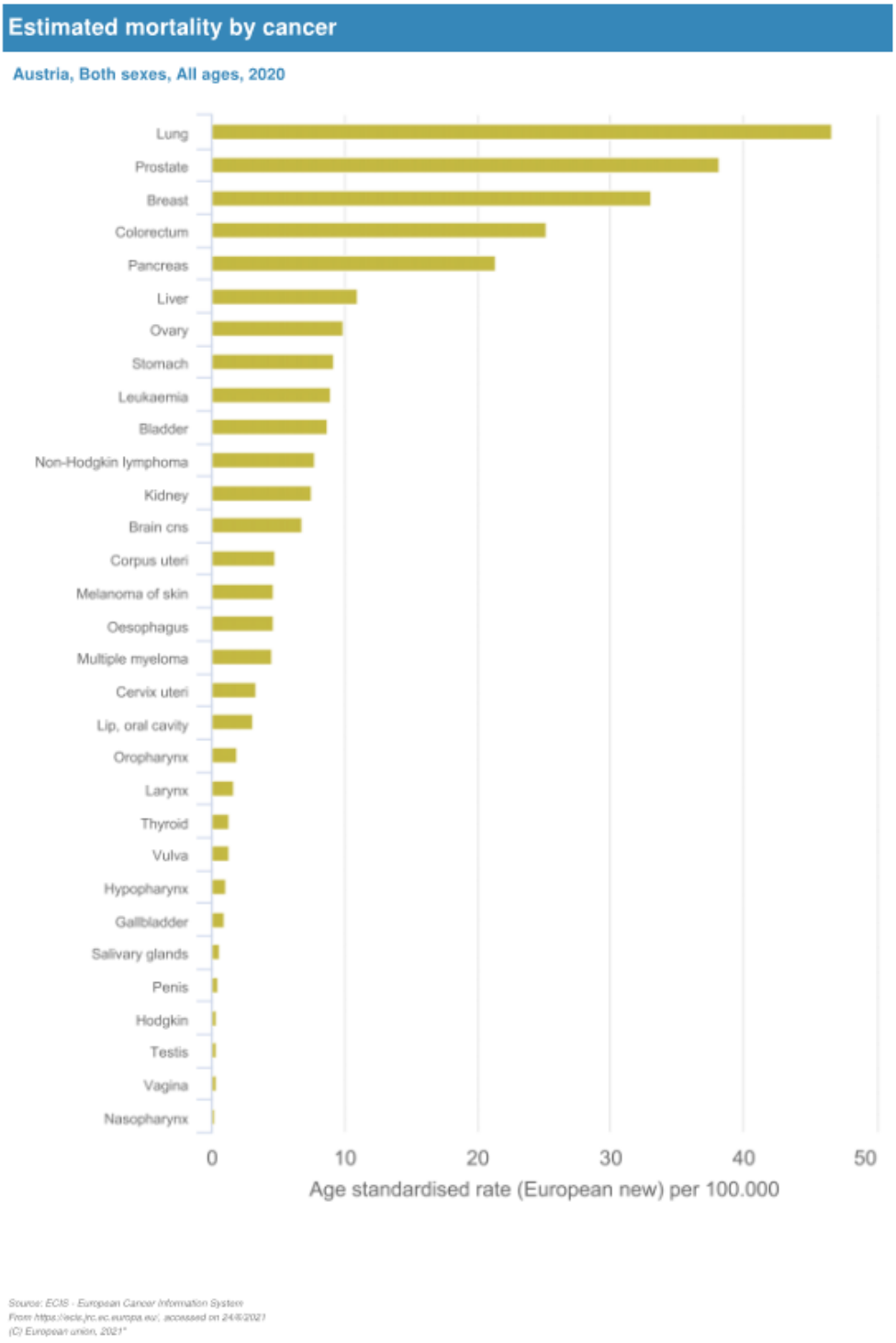

Fig. 2A: Cancer types and their respective ASR values per 100.000 people in Austria in 2020. *The three most deadly types in Austria are: lung with 46.6 people, prostate with 38,2 and breast with 33 deaths/100.000.*

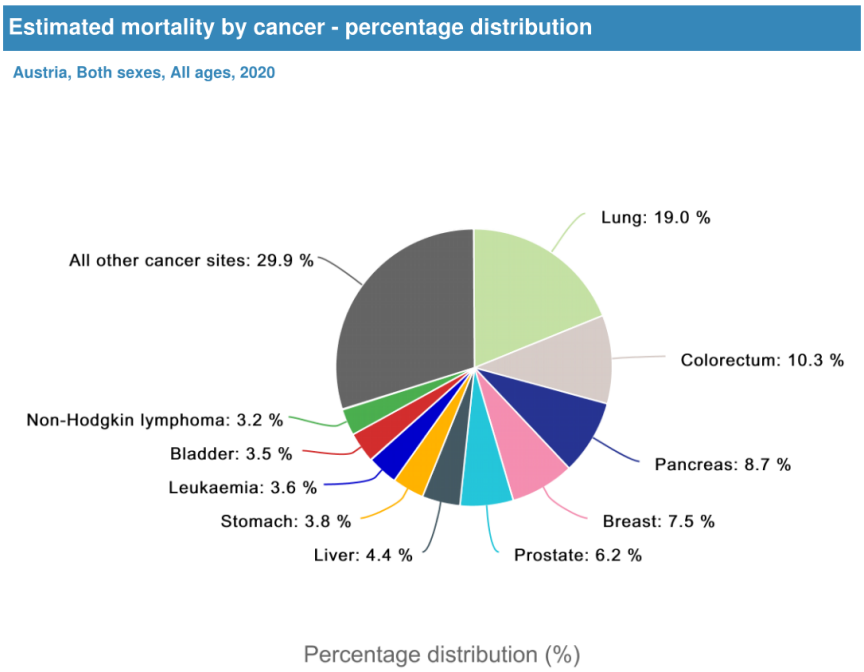

Fig. 2B: Austrian percentage distribution of cancer deaths by type in 2020. About *a fifth of Austrian cancer deaths is caused by lung tumors, followed by colorectal tumors (about 10%), while cancer types of rather low individual frequencies add up to almost 30% of cancer deaths.*

Cancer (general aspects)

"Cancer is the name given to a collection of related diseases. In all types of cancer, some of the body's cells begin to divide without stopping and spread into surrounding tissues."[8]

This general definition given by the U.S. National Cancer Institute reflects that each cancer arises from the abnormal proliferative behavior of a single cell, giving rise to clusters of cells that expand at their site of origin first, but eventually invade and disseminate into other tissues with severely detrimental effect.

In contrast to normal cells, cancer cells can divide uncontrollably due to changes in their transcriptional/translational behavior. Important growth factors[9] can be overexpressed or inhibitory proteins are mutated (and therefore inactivated), which both causes cells to grow and divide more often than usual.

Then, whole regulatory pathways of cells are blocked or altered. Even if only one protein is changed or inactivated in this pathway, the outcome is rigorously altered.

One of the most important and best investigated pathways is the mitogen-activated protein kinase (MAP-K) pathway.[10] Often inhibitory (tumor suppressor) proteins such as p53 or RB are silenced, which causes the cell to be constitutively overactive.[11]

Furthermore, cancer cells have a more invasive character than normal tissue cells. Especially EMT (epithelial-to-mesenchymal transition) transforms fully differentiated epithelial cells into a less differentiated stage with the potential of increased migratory ability and invasiveness.[12] This transition from normal-shaped- and integrated cells (benign cancer types)[13] to motile, intruding cells (malignant cancer types)[14] is the first step in the formation of metastases.

One more characteristic property of cancer cells is a fundamental conversion of metabolism: whereas normal cells use both glycolysis and the Krebs cycle in presence of oxygen to generate ATP as energy source, cancer cells transform glucose to lactate at a higher rate, even despite adequate oxygen levels. This quite inefficient form of generating energy is called Warburg effect or aerobic glycolysis.[15]

Considering all this, it is obvious, that cancer is a very complex disease with many aspects to be investigated and much work remains to be done to comprehend cancer in its entirety or even single characteristic cancer-associated features.

Classification of cancer[16]

Given its complexity, it is useful to classify cancer by different standards, like type of cell/tissue origin, stage of progression, extent of metastases, etc. Stages with low numbers are less harmful (benign or with better treatment prognosis), whereas stages with high numbers are more harmful (invasive tumors). The most common classifications are the UICC-stages and TNM-classification, which are outlined below:

UICC (Union internationale contre le cancer):

- Stage 0: benign neoplasias or tumor *in situ* without invasive properties
- Stage 1: small and middle-sized tumors, without lymph node involvement or metastases.
- Stage 2: middle-sized and huge tumors, without lymph node involvement or metastases.

- Stage 3: tumors of every size, with metastases in nearby lymph nodes without distant metastases (from primary tumor)
- Stage 4: tumors of every size, with metastases in lymph nodes and distant metastases (from primary tumor)

TNM (Tumor-nodes-metastases):

This classification method uses separate numbers for tumor size, extent of lymph node involvement and distant metastases:

- T (0-4): size of tumor
- N (0-3): number and position of lymph nodes involved
- M (0)/ M (1): absence or presence of distant metastases

Classification of cancer into these stages has consequences for the choice of adequate treatment of various cancer types.

Therapeutic ways to treat cancer

Depending on cancer type, progression of the disease, physical condition and many other factors, there are different ways of treating specific cancer types or tissues. Some are effective on their own, but therapy strategies often combine these basic treatment modalities in order to maximize efficacy or lessen side effects:[17]

Surgery

Removing the tumor tissue is often one of the first steps in treatment of solid tumors. Chances for curative effect are especially high if the tumor has not spread yet and its edges are still sharply distinguishable from normal tissue. Surgical intervention can contribute to prolong patients' lives, even by removing the bulk of tumor tissue only, since the cancer environments' production of growth and angiogenic factors is tremendously reduced, when the primary tumor is excised. [18] Despite the risk of tumor recurrence from only a few remaining tumor cells, there is still a good chance of improving and prolonging a patient's life. Under favorable conditions, even metastasized tumors may be excised, in order to inhibit "waves of metastases", which a primary tumor can emit, and by blocking these waves, lifespan can be prolonged.[19]

Radiation Therapy [20, 21]

This treatment modality uses high doses of photon or particle radiation, like γ-rays or electrons, in order to destroy cancer cells. Its effects are achieved either directly by causing damage to DNA strands, or indirectly by originating ROS or free radicals, which are then drivers of DNA damage. This leads to cell death, which can be accomplished in many ways: the most common are apoptosis (programmed cell death), necrosis or mitotic catastrophe, in which mitotic cells do not segregate their chromosomes correctly. Radiotherapy can take days to weeks to fully accomplish shrinking of tumors.

Chemotherapy

Treatment of cancer with cytostatic drugs is called chemotherapy. These drugs are pharmaceutical reagents which contribute to or directly induce cell death by their cytotoxic effects. Unfortunately, this approach is accompanied by many side effects for patients. Fatigue, loss of hair, or nausea are only the most conspicuous of them.[22] These adverse effects usually arise from unspecific drug activity affecting not only tumor cells, but also healthy tissue (typically proliferating tissues such as intestinal mucosa, hair follicles or bone marrow). The use of prodrugs, precursors of drugs which are activated only in immediate proximity to the tumor cells by conditions of the tumor environment may help to avoid them.[23]

Immunotherapy[24]

In principle, immunotherapy shall help a patient's immune system to fight cancer or other diseases by its own abilities. The immune system is, by this type of treatment, either stimulated or blocked, depending on the mode of action. If a type of cancer acts in an inhibitory manner on the immune system, application of naturally occurring proteins or designed substances, like monoclonal antibodies (mAbs), can help boosting the immune response against cancer cells. Other strategies employ cytokines or activation of T cells, which play a crucial role in the immune response.[25]

Targeted Therapy

Targeting specific biomarkers of cancer cells, like proteins which lead to faster proliferation or even angiogenesis, is the objective of this form of therapy. It aims to attack cancer cells preferentially over healthy ones, based on the overexpression of

certain proteins in cancer compared to normal tissue. Targeting is achieved either by small drugs, which are substances with low molecular weight capable of passing cell membranes easily, or by mAb's directed against receptors on the cell membrane.[26] Angiogenic factors, like the vascular endothelial growth factor (VEGF) and its receptor (VEGF-R), are targeted in a variety of cancers. Although targeted therapy has been established as a successful modality in cancer treatment, it can nevertheless cause severe side effects or be affected by resistance, because of the ability of cancer cells to use alternative pathways.[27]

Hormone Therapy

This strategy is used, when it comes to treat cancers with growth dependency on hormones, like breast, prostate or ovarian cancer.[28] Tamoxifen is frequently used in the therapy of hormone dependent breast cancers. By inhibiting estrogen receptors (ERs), tamoxifen prevents the growth signal cascade usually initiated by estrogens. Hence, cancer cells are not able to proliferate uncontrollably. Furthermore, a reduction of recurrence and mortality of ER-positive breast cancers treated with tamoxifen was showed.[29] Also, steroid sulfatase-inhibitors (STS-inhibitors) show promising results in fighting not only breast cancers, but also prostate cancer: STS is not only vital for the formation of the female hormone family of estrogens, but also the male hormone family of androgens. Therefore, its inhibition can be effective in both female and male hormone-dependent cancer types.[30]

Precision Medicine [31]

Precision medicine, also called personalized medicine is a treatment strategy aimed at finding the most appropriate therapy for each patient individually. Many cancer patients diagnosed with the same type of cancer and treated in the same way, regarding doses of radiation or choice of chemotherapy etc., show very different therapeutic results. These discrepancies can be caused by different mutations in cancer tissue. In order to determine the optimal cancer treatment for each patient, DNA-testing/sequencing should be performed after biopsies. Although, DNA sequencing is not readily being performed yet because of high costs, personalized medicine is a promising strategy to spare patients the side effects of ineffective therapies or better, to cure people from specific cancer types.

In the following chapters, metal-based drugs are explained in more detail, because they are the main part tested in this thesis. Hopefully, in the near future, they could be applied presumably in chemotherapy, targeted therapy or in combined therapies.

Metallodrugs in chemotherapy

Pharmaceutical agents containing metal ions are called metallodrugs.[32] Those metal-based drugs can be very diverse with regard to the elemental properties of the metal, like the ionic charge, coordination number, Lewis acid or redox properties, as well as regarding the ligands bound to them. Biological activities, like anti-viral, anti-bacterial or, central to this thesis, cytotoxic and anti-cancer activity, can either be due to the characteristic properties of metals and ligands themselves or, more frequently, a synergy between the metals and the ligands bound to them.[33,34] Change in ionic charge of the central metal (through redox reactions), e.g., leads to changes in overall drug structure, strength of ligand binding and hence biological activity. Ligands often consist of organic-chemical structures, which lead to changes in physico-(bio)chemical properties of the whole compound, like solubility, fluorescence, affinity to specific binding sites or uptake into the cell. Although those SAR-relevant characteristics[35] may be predicted to a certain extent, aiding in the rational design of novel anticancer drugs, the decisive question is how these compounds actually impact on biological systems. Addressing this question experimentally for a selection of compounds is the main part of this work.

The very first and most frequently used metallodrug in cancer chemotherapy, cisplatin (*cis*-diamminedichloridoplatinum(II)), is a Pt(II)-based substance with long history and outstanding characteristics: initially synthesized in 1844 by the Italian chemist Michele Peyrone (then the compound was known as Peyrone's chloride) and elucidation of its structure in the late 90's of the 19th century by Alfred Werner, its inhibiting effect on cell division was not known until Barnett Rosenberg investigated it 121 years after Peyrone's discovery. By serendipity, in his studies on electric fields and their effects on cell growth of the bacterium *Escherichia coli*, Rosenberg found cisplatin's most important effect: antiproliferative activity.[36-39] Today the *modus operandi* of cisplatin is relatively well known: After entering the cell, it loses a chloride ligand and a water molecule replaces it, due to the higher abundance of water than chloride. This loosely bound water molecule is replaced by nitrogen donors such as

those present in DNA, when aquated cisplatin enters the nucleus where it binds to the N7 of either of the two purine bases (adenine and guanine). By connecting two adjacent guanines in one strand (most frequently) or crosslinking two guanines on opposite strands, it inhibits DNA functionality, since even the repair systems of the cell are not able to fulfill their purpose properly. If DNA damage (like mismatch, breaks etc.) remains, death can be initiated and the cell dies eventually.[39,40] As a consequence of cisplatin-induced DNA damage, apoptosis is initiated, which might not be true for other metal complexes.

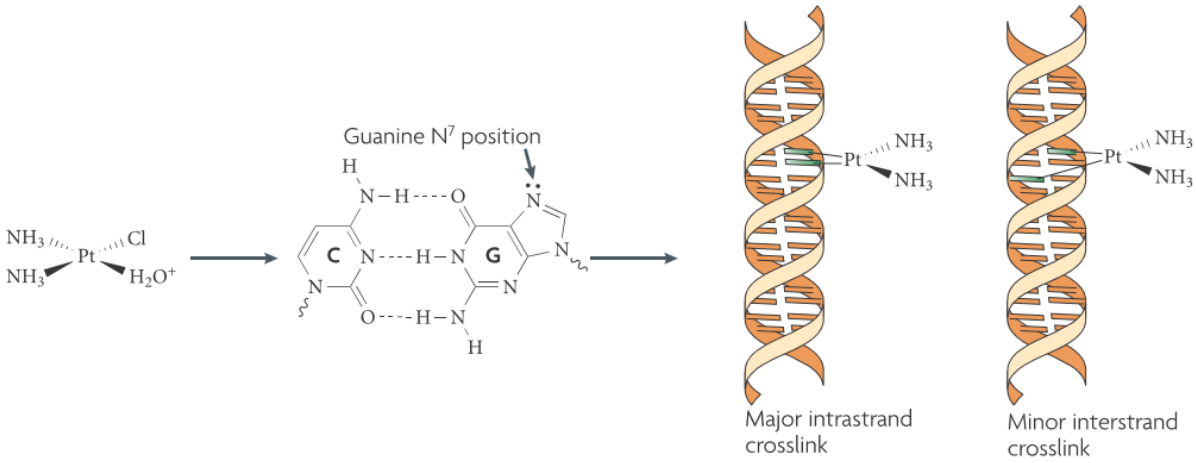

Fig. 3: Mechanism of aquated cisplatin. *Complexed water is removed when cisplatin enters the nucleus and, by its reaction with purine bases, the DNA structure is bent and, in most cases, it cannot be transcribed properly anymore, which results in cell death eventually (**adapted from ref. 41).***

For oxaliplatin and certain non-platinum metal-based drugs, like some ruthenium complexes, there is another way of cell death currently investigated: immunogenic cell death (ICD). ICD is particular in its *modus operandi*; whereas apoptosis is quite an intracellular process, ICD is crucially based on intercellular signaling. Induced, for example, by ER stress caused in cells by chemotherapeutic agents, the signaling cascade employs proteins, like calreticulin (CRT) or high-mobility group box (HMGB) proteins, to initiate an extracellular and enduring signal to the immune system. E.g., CRT is transported to the outer cell membrane, where it acts as signal for dendritic cells (DCs) to recognize cell damage and to stimulate the immune system by initiating maturation of T cells or by activation of NK cells, which can kill further tumor cells.[41,42] So, the immune system helps inducing a long-lasting signal to penetrate tumor tissue, beside the principal cytotoxic effect of metallodrugs.

Metals and novel complexes

For this thesis, four transition metals need to be considered in particular, as they are central atoms of novel anticancer reagents which are used and tested in the practical section of this work:

Platinum (Pt)

As mentioned above, most metal-based cytostatics in clinical use contain platinum(II) in their center, like cisplatin and its derivatives, carboplatin and oxaliplatin. Currently, Pt(IV) complexes are investigated intensively as prodrugs, due to their apparent suitability for cancer therapy.[43] Application of the "inactive" (+4)-form to patients could evade the problem of attacking tumor cells and healthy cells simultaneously. Pt(IV) drugs have the potential advantage of being reduced, and therefore activated, to their (+2)-form only at the site of tumor because of the reductive environment of the latter. Upon reduction, the mode of action is that of a Pt(II) drug (see above, *Fig. 3*).

Unfortunately, all reagents have both, advantages and drawbacks. Latest derivatives of cisplatin, like phenanthriplatin, show the desired result of distortion of DNA and the resulting death of tumor cells due to inhibition of transcription.[44] On the other hand, though, effectivity of classic or novel therapeutic compounds in cancer treatment can often be associated with severe side effects, like fatigue, loss of hair, (emesis (vomiting)), nephro- and/or ototoxicity etc.[44,45]

Regarding ototoxicity, studies in rodents reveal a major influence of copper-transporters, like *Ctr 1*, in the uptake and impact of the classic compounds cisplatin and carboplatin in cells of the cochlea.[45] This and other discoveries might have led to investigate the transition metal copper more intensively for anticancer effectiveness and evasion of side effects.

Copper (Cu)

One alternative to Pt-metallodrugs in cancer therapy might be complexes of redox-active copper, which is already abundant in cells. Given the intracellular usage for the proper activity of proteins, like *SOD* or *cytochrome C oxidase*, it is obvious that copper needs to be highly regulated. Disbalance of copper levels may lead to diseases and to formation of new blood vessels (angiogenesis), which is a main feature of malignant tumors.[48]

By exploiting the already available mechanisms of mammalian cells for copper transport or its reactivity, drugs with chelated Cu atoms could be very promising in cancer therapies. The core of Cu-containing drugs often consists of two or more metal ions coordinated by ligands which occupy different angles and distances, a feature determining bioavailability and cellular effects. Di-copper complexes may be more effective, due to being more cytotoxic and resistance-inhibiting than the widely used Pt drugs.[46] Among the variety of copper-chelating ligands, the family of thiosemicarbazones yielded promising results in anticancer studies.[47] Even enhanced cytostatic activities were demonstrated as the N-terminus of this chemical group was dimethylated.[51] Unlike platinum drugs, copper complexes frequently do not interact directly with DNA, but are prone to induce oxidative stress in cells. DNA-strand breaks and proteasome inhibition are initiated by ROS production, which leads to programmed cell death eventually.[48-50]

Ruthenium (Ru), Rhodium (Rh)

Ruthenium, rhodium (and osmium) are transition metals with higher variety in their oxidation states, therefore designing of novel antiproliferative drugs is much more challenging than with classic planary Pt(II) or octahedral Pt(IV) compounds. Changes in ligand position (equatorial, axial, out of plane etc.) or in their overall chemical structure, can induce an entirely different structural geometry, bioavailability or antineoplastic behavior. Alternatively, change in counter-ions of charged complexes, like KP1019 (Ru complex; indazolium salt) and KP1339 (same Ru complex, with sodium instead of indazolium), may result in better water solubility and improve its applicability to cancer patients.[52]

Ruthenium is the metal most extensively investigated for novel metallodrug candidates; in comparison, rhodium or osmium complexes are much less investigated, despite their similar features to Ru. Studies on designing Ru complexes and their outcomes in biological experiments revealed “piano-stool”-reagents as very promising, regarding high cytotoxicity and quite mild side effects. Such piano-stool complexes consist of an arene ligand in axial position and (usually complementing chloride ligands) varying organic ligands, either already bioactive or -inactive, in mono-, bi- or tridentate formation, which correspond to the three legs of a piano stool.

This piano-stool motif has also been investigated for Rh and Os complexes, which showed similar results.[53-55]

Considering specific bioactive ligands, naphthoquinones, for example, participate in redox-cycling of cells and contribute to the oxidation of DNA and other biomolecules. This property can be exploited for the design of new Ru and Os compounds with varying redox active compounds and their potential antiproliferative effect.[56]

The mode of action for those metal-containing substances is not fully understood yet, but many Ru/Rh/Os complexes do not interfere preferably with DNA, but they induce cellular stress, such as production of ROS and ER-stress or mitochondrial disintegration. They may also interact with cell-cycle proteins, which can lead to different forms of cell death or the inhibition of further tumor growth.[50,56]

2D vs. 3D methods

Experiments with mammalian cells are usually performed as a first step to get insights into the drug potency of test compounds.

Principally, there are two different approaches, which can be applied: 2D (two-dimensional) cell culture experiments, in which cells are seeded in plane-bottom plates to form a monolayer and, therefore, conditions for every single cell are uniform; or 3D (three-dimensional) cell culture approaches, in which cells are allowed to aggregate and form multilayer structures. The most commonly employed 3D models consist of aggregates in spherical shape ("multicellular spheroids"). However, different shapes can be formed, which *Kenny et al.*[61] investigated by using breast cancer cells. Those shapes can be round, mass-like, grape-like and stellate-like; each of them distinguishable by their overall spatial structure (*Fig. 4*).

Obtaining spheroids can be achieved by different techniques:

- A very simple, but effective approach is seeding of cells in specifically coated plates, which do not allow attachment of cells and thereby favor the formation of cell aggregates. By forming more cell-cell interactions and growing in spatial structures, the resulting aggregates show a certain similarity to actual tumors. Despite the absence of extracellular matrix components and angiogenesis,

this method is advantageous for drug screening, which is why this approach has been used here to obtain multicellular spheroids.[58]

- Furthermore, specific biological scaffolds or matrices can be used to support the formation of spheroids. Simple scaffolds, like collagen I, agar or hydrogels, help to mimic the microenvironment of solid tumors and favor spheroid formation.[57,58]

- Alternatively, though more sophisticatedly, cell sheets or microfluidic systems are used to mimic dynamic processes, like accumulation of waste products, formation of signal gradients or cellular differentiation.[57-58]

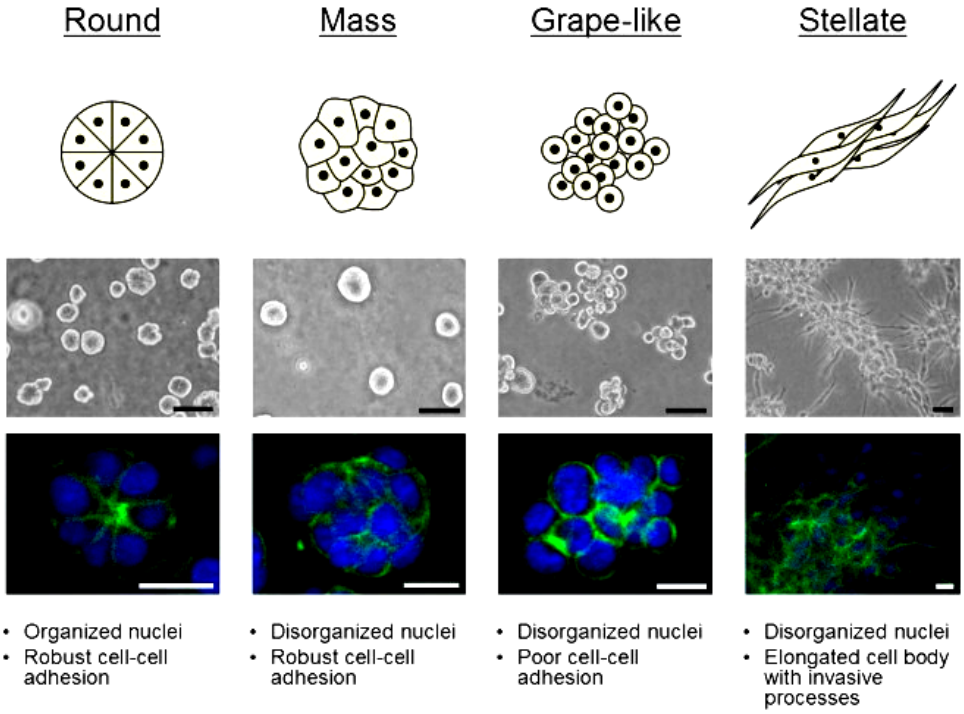

Fig. 4: Spatial structures of multicellular spheroids. *Breast cancer spheroid structures are predominantly spherical, whereby cell-cell junctions are crucial for their formation. If they are not robust enough, though, shapes can vary immensely. (**adapted from ref. 61**).*

Cells within a spheroid are in many respects more similar to those in actual tumors than cells in monolayers: cell shape, expression and organization of surface receptors, cancer gene expression levels, cell-stage heterogeneity and diffusion barriers within and between the zones formed in spheroids contribute to different

responses in 3D experiments compared to 2D approaches (*Fig 5*).[60] The fact that spheroids need longer time for their preparation before experiments can be started is outweighed by the chance that experiments in 3D cultures yield a more realistic prediction of drug efficacy than results obtained by experiments in 2D cultures alone.

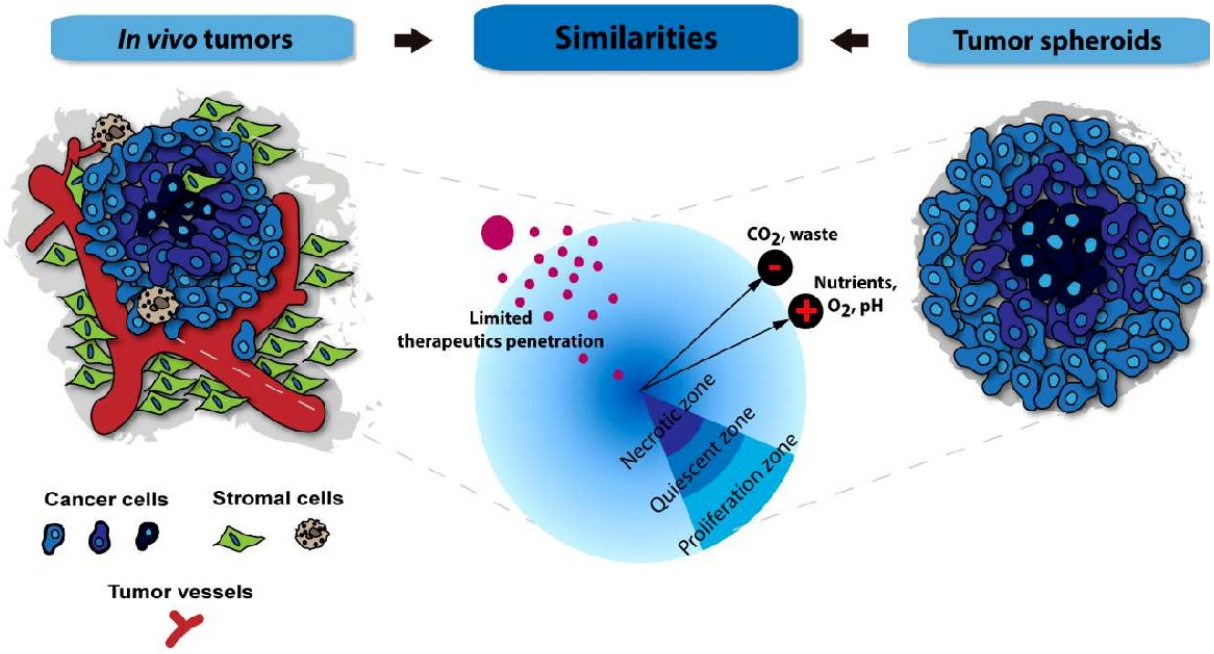

Fig. 5: Differences and similarities between *in vivo* tumors and tumor spheroids. Zone formation in spheroids resembles that in actual tumor tissue; the core does not obtain enough survival factors, like nutrients, O_2, hormones etc., whereas waste products accumulate. The bigger it grows, the more viable cells concentrate at the outer edge of the spheroid. Unlike *in vivo* tumors, spheroids do not contain vessels and other tissue structures, which are important for further growth and invasiveness of tumor species. Therefore, growth of simple spheroids is quite limited (**adapted from ref. 59).**

Materials and Methods

Cell culture conditions

The two colorectal carcinoma cell lines **HCT116**[62] and **HT29**[63] were kindly provided by the Institute of Cancer Research, Department of Medicine I, Medical University of Vienna, Austria. Both cell lines were cultivated in 75-cm^2 flasks (*Starlab*) at 37 °C under a humidified atmosphere containing 5% CO_2 in Mc-Coy's 5A medium (*Sigma Aldrich*) (supplemented with 10% (v/v) heat-inactivated fetal calf serum (FCS; *Biowest*) and 4 mM L-glutamine (*Sigma Aldrich*, 200 mM).

The cell lines **A549** (non-small cell lung cancer)[64] and **CH1/PA-1** (ovarian teratocarcinoma)[65] were kindly provided by the Institute of Cancer Research, Department of Medicine I, Medical University of Vienna, Austria, and the CRC Centre for Cancer Therapeutics, Institute of Cancer Research, Sutton, UK, respectively. Both cell lines were cultivated in 75-cm^2 flasks as described above, but in minimum essential medium (MEM, *Sigma Aldrich*) (supplemented with 10% (v/v) heat-inactivated FCS and 4 mM L-glutamine (*Sigma Aldrich*).

For passaging or harvesting of cells, flasks with subconfluent adherent cells were trypsinised with 2 ml trypsin-EDTA solution (*Sigma Aldrich*) and incubated at 37 °C for 5 minutes. Then, trypsinisation was stopped by addition of 8 ml of the respective medium and cells were subcultured as appropriate. For 3D experiments, the cell suspension was centrifuged at 2100 rpm (Megafuge 1.0R, *Thermo Scientific*) for 3 minutes, the supernatant aspirated and the cell pellet was resuspended in the respective medium. Cells were counted in a Neubauer improved counting chamber, 1:10 mixed with trypan blue (*Sigma Aldrich*) as a dead-cell marker. The appropriate volume of cell suspension was calculated for individual experiments. Each cell line was seeded in ultra-low attachment 96-well plates (*Corning*, round bottom). They were allowed to form spheroids in those plates within 96 hours with their respective medium in a humidified incubator at 37 °C.

AlamarBlue Assay

Theory[66]

The AlamarBlue assay is a simple and very effective way to determine cell viability and 50% inhibitory concentration (IC_{50}) values after drug treatment. In this assay, resazurin (known under the trademark “AlamarBlue”) in its oxidized form (blue color, non-fluorescent) is added to treated cells. The chromophore is incorporated and depending on metabolic activity of viable cells it is reduced (by NADPH, FADH etc.) to a pink, fluorescent derivative, resorufin. The extent to which this product is formed can be measured either colorimetrically or fluorometrically. This assay is advantageous due to its non-cytotoxic character and its handy application compared to other viability assays.

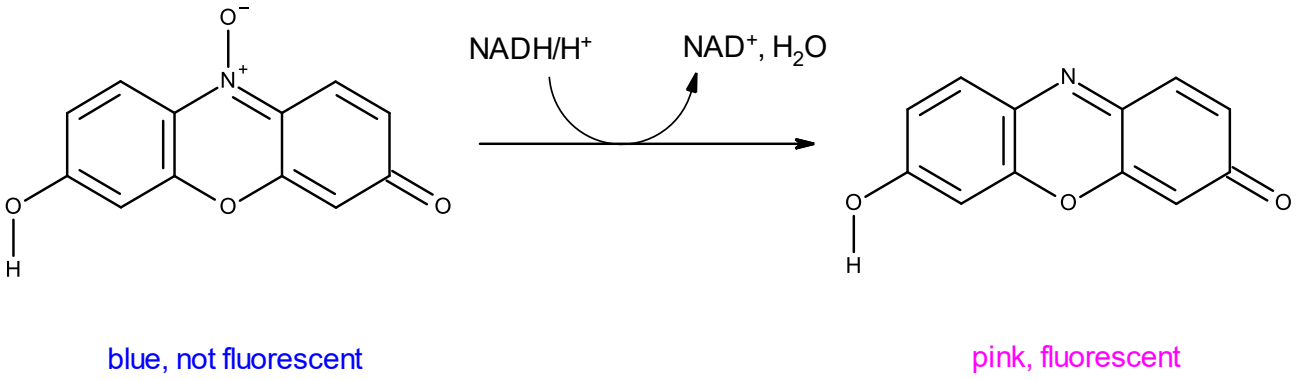

Fig. 6: Principle of AlamarBlue staining. Chemical reaction of the reduction of resazurin (blue, not fluorescent) to the highly fluorescent, pink resorufin. Only viable cells are able to induce the reaction due to production of the reducing agent $NADH/H^+$ (drawn with Biovia Draw 2016 software).

Application

For the 3D AlamarBlue assay, 500 cells/well were seeded in 100 µl/well into an ultra-low attachment 96 well-plate. Cells formed spheroids in appropriate size after 96 h of pre-incubation at 37 °C. After this period, drug candidates were dissolved in an appropriate volume of DMSO and vortexed or ultrasonicated. This stock solution was 1:100 diluted in the respective medium (see above). The resulting 1% DMSO-containing solution was serially diluted 1:1 with medium to obtain nine different concentrations for all tested compounds. When distributed over the 96-well-plate, the concentrations halved, as 100 µl of each dilution were added to 100 µl of medium

already present in the wells. Afterwards, the plate was incubated with the test compound for another 72 h, before 20 µl of a resazurin stock solution (~440 µM, in PBS) was added to each well. To obtain effective staining, cells were incubated with the dye overnight. Fluorescence was measured at 530/590nm (excitation/emission) with a multimode-microplate reader (*BIO-TEK*, Synergy HT), which measured three technical replicates per concentration simultaneously. IC_{50} values were automatically calculated from obtained concentration-effect-curves.

Growth of spheroids

Theory

Growth of cell aggregates or spheroids can be investigated by culturing them appropriately for a few days. The impact of test compounds on the growth behavior is monitored by taking pictures before and after treatment or on a daily basis, whereby diameters can be measured microscopically under the same settings. The feasibility of the latter, though, is highly cell-line dependent. For reliable results, cell lines that form strong cell-cell contacts should be chosen, due to the spherical appearance of the aggregates formed by them.[67] Other shapes (e.g. loosely grape-like or stellate) of spheroids cannot be measured adequately with this method.

Application

In this work, HCT116 cells were chosen for this approach, because their compact, spherical 3D aggregates were considered most suitable for this purpose.

First, 1000 cells/well were seeded into 96-well plates. After 96 hours pre-incubation, images of the spheroids were taken with a digital camera mounted onto an inverted microscope (*Olympus*, CKX 41) in 4x magnification. Diameters were measured with the CellF software. Afterwards, spheroids were treated with test compounds in the range of their IC_{50} values (+ standard deviation), which had been previously evaluated with the AlamarBlue assay. Compounds were dissolved in 100% DMSO and diluted in Mc-Coy's 5A medium to contain 1% DMSO. This solution was applied onto the cells, which were then incubated at 37 °C for 96 hours. Finally, images were taken once more (at 4x magnification) and diameters were evaluated with the CellF

software. Values of at least 6 spheroids (same conditions/concentrations) were taken into statistically account.

ROS Assay

Theory[68]

Hydroxyl radicals (·OH), superoxide anions (O_2^-) or hydrogen peroxide (H_2O_2) are reactive oxygen species (ROS), which are able to destabilize cell integrity if their levels are increased pathologically. Therefore, ROS is supposed to be an important factor in the disruption of cells, especially tumor cells. For measuring ROS in drug-treated tumor cells, different protocols are widely used, like the fluorimetric DCFH-DA assay.[69] An alternative easily applicable for multicellular spheroids, is the addition of CellRox, a fluorophore which exhibits bright fluorescence when oxidized in the presence of ROS. (This fluorophore is combined in this work with propidium iodide (PI) to exclude non-viable cells.) Thereupon fluorescence can be measured via flow cytometry. Basically, a flow cytometer consists of a capillary and a laser system, which detects cells in a fluid flow inside the capillary based on light scattering and fluorescence of one or more fluorophores.[70] The device converts the detected signals to be analyzed further with appropriate software.

Application

For this assay, the colorectal cancer cell line HCT116 was chosen, because of its ability to form tight spheroids.

1000 cells/well were seeded into 96-well plates and pre-incubated for 96 hours at 37 °C. Test compounds were dissolved in DMSO and diluted with medium to their respective IC_{50} (+ standard deviation). Spheroids were treated with the compounds for about 24 hours, before they were prepared for flow cytometric application:

Spheroids were harvested by pipetting and transferred into Eppendorf tubes. At least five spheroids per condition needed to be harvested in order to obtain enough viable cells for detection. Pooled spheroids were washed three times with PBS, trypsinized for 5 minutes at 37 °C with 400 µl TripLE Express (*Gibco*), and shaken vigorously by hand. Trypsinization was stopped by addition of 1 ml medium and the obtained single

cell suspension was centrifuged for 3 minutes at 2100 rpm (Minispin centrifuge, *Eppendorf*). Medium was aspirated and a 500 nM solution (obtained from a 250 µM stock solution in DMSO by dilution with medium) of CellRox (*Thermo Fisher*) was added. Cells were incubated with CellRox for 1 hour at 37 °C. Afterwards, 200 µl of cell/CellRox-suspension were transferred into a flow cytometer 96-well plate, to which 1.5 µl PI (*Invitrogen*, 1mg/ml) per well were added, and analyzed with a flow cytometer (Guava easyCyte 8HT, *Millipore*). Data were processed with FlowJo software.

Apoptosis Assay

Theory

The induction of apoptosis can be measured by flow cytometry of cells stained with a specific fluorophore-conjugated protein, annexin-V, as an apoptosis marker. It is known that cell membranes undergo a tremendous change when apoptosis is initiated. Mammalian cell membranes comprise lots of phospholipids which are usually distributed asymmetrically between outer and inner leaflet. One of those lipids is phosphatidylserine (PS), which can be found predominantly on the inner leaflet. If apoptosis occurs, though, the still intact membranes rearrange and PS is accumulated on the outer leaflet. Now, annexin V, a phospholipid-binding protein, can specifically recognize phosphatidylserine.[71,72] To differentiate from or exclude necrotic cells, PI can be used as a marker for the latter.

Application

Apoptosis was tested exclusively in HCT116 multicellular spheroids after treatment with the test compounds for the same reason as for the ROS assay.

1000 cells/well were seeded into 96-well plates and pre-incubated for 96 hours at 37 °C. Test compounds were dissolved in DMSO and diluted with medium to their respective IC_{50} (+ standard deviation). Spheroids were treated with the substances for 48 hours, before they were prepared for flow-cytometric application:

Spheroids were harvested by pipetting and transferred into Eppendorf tubes. At least five spheroids per condition needed to be harvested in order to obtain enough cells

for detection. Pooled spheroids were washed three times with PBS, trypsinized for 5 minutes at 37 °C with 400 µl TripLE Express, and shaken vigorously by hand. Trypsinisation was stopped by addition of 1 ml medium and the obtained single cell suspension was centrifuged for 3 minutes at 2100 rpm. Medium was aspirated and 250 µl binding buffer (10 mM Hepes/NaOH (pH 7.4); 140 mM NaCl; 2.5mM $CaCl_2$ in deionized water) and 1.5 µl annexin-V/FITC (FITC-labeled recombinant human annexin V, *Invitrogen*) were added. Cells were incubated for 15 minutes at 37 °C. Afterwards, 200 µl of cell/annexin-V-suspension were transferred into a flow cytometer 96-well plate, to which 1.5 µl PI per well were added, and analyzed with a flow cytometer. Data were processed with FlowJo software.

Immunocytochemistry

Theory

Immunocytochemistry makes use of antibodies conjugated to labels that allow to visualize the distribution of specific antigens in cellular microscopic samples. This approach was used here to identify viable cells within spheroidal aggregates and to visualize the apoptotic effects of test compounds in multicellular spheroids via confocal laser-scanning microscopy. For this purpose, spheroids need to be cut in sections to obtain high-resolution images at the confocal microscope.[74] Sections have to be fixed with paraformaldehyde (PFA)[73] and permeabilized for treatment with the respective antibodies. Different primary antibodies can be used simultaneously, e.g. to visualize either the viable or apoptotic state of treated spheroids. On the one hand, an antibody against KI-67 indicates the proliferative state of cells within spheroids.[75] On the other hand, antibodies against cleaved caspases 3 and 7, the mainly activated executioner caspases, indicate apoptosis. Caspase 3 is involved in apoptosis induced solely by mitochondrial dysfunction, whereas caspase 7 can be activated through a mitochondria-independent pathway as well.[76,77] A secondary antibody, conjugated to a fluorophore which generates the actual signal to be detected under the microscope, is added to form a complex with the primary antibody. This indirect approach employing two antibodies results in higher sensitivity and amplification of the signal.[78]

Application

HCT116 cells were chosen for this type of microscopic analysis, since their spheroids showed a proper stability during microsection and fixation.

After evaluating the sizes of treated spheroids (cf. “Growth of spheroids”), at least five spheroids per condition were transferred into a cryomold (*Sakura*) and embedded in Tissue-Tek (O.C.T compound, *Sakura*). Those samples were frozen at -81 °C (for at least a few hours) and stored for longer periods. For staining of samples, frozen blocks of spheroids were cut into 5 µm sections with a cryostat (CM3050 S, *Leica*) at -20 °C. Sections were gathered on glass slides and fixed with 4% PFA (in PBS) for 20 minutes. Slides were washed 3x with PBS (powder, *Gibco*; 9 g/L with deionized water) and cells were permeabilized with 0.1% Triton-X (in PBS) for 10 minutes. After washing 3x with PBS, samples were encircled with a hydrophobic-barrier pen and blocked with 10% goat serum/2% BSA (in PBS) for 30 minutes. Slides were washed 3x with PBS and respective primary antibody (Ab1) was added dropwise to the samples. The following Ab1’s were used: **KI67-Rabbit** (mAb, *Cell Signaling*); **cleaved caspase 3-Rabbit** (mAb, *Cell Signaling*); **cleaved caspase 7-Rabbit** (mAb, Asp198, *Cell Signaling*); each 1:1000 with 2% BSA in PBS. Sample slides were incubated at 4 °C overnight. The next day, slides were washed 3x with PBS and secondary antibody (Ab2) was added dropwise (Anti-Rabbit IgG Fab2 Alexa Flour 594, *Cell Signaling*). Samples were incubated in a dark box at room temperature for 1 hour. [For some samples a mouse Ab1 of the same quality and an anti-mouse Ab2 (Anti-Mouse IgG Fab2 Alexa Fluor 647, *Cell Signaling*) were used alternatively.]

After washing 3x with PBS, samples were mounted with DAPI (ProLong Gold antifade reagent with DAPI, *Invitrogen*), as a marker for nuclei, and covered with a glass slip. Fluorescence images were taken when slides were fully dried (at room temperature in the dark).

Plasmid Assay

Theory

For studies of novel anticancer compounds, it is reasonable to evaluate if changes in DNA conformation are involved in the drugs' mode of action. An established method to check for these effects employs the bacterial-derived plasmid "pUC19" in a cell-free assay. The 2686 base-pair-long plasmid is primarily found in its negatively supercoiled form.[79,80] Upon treatment with a drug candidate, its conformation can change, e.g., to its relaxed (open circular) or to its linear form, depending on initiation of single- or double-strand breaks (note: the linear form is not regarded in this thesis). Classic platinum drugs typically alter the mobility of the plasmid by gradual unwinding and bending imposed by bifunctional cross-links. Those changes in conformation can be visualized by separating distinct species via gel electrophoresis. Common gel electrophoresis separates species due to differences in mass; in this case, though, DNA is separated according to the apparent plasmid size associated with the different conformations. Supercoiled plasmid migrates fastest through the gel, followed by the spatially more relaxed open circular form, which moves slower.[81-83] Images of the gel can be taken when ethidium bromide as DNA intercalator is added.

Application[84]

400 ng of pUC19-plasmid were incubated with 50 µM of the test compound at 37 °C under continuous shaking for different periods of time (from 15 min to 6 h). After 6 h, interaction was stopped by cooling samples on ice. 20 µL of the probes were mixed with 4 µL 6x DNA loading dye (*Thermo Fisher Scientific*), and 20 µL of the obtained solutions were loaded onto a 1% agarose gel (in 1x TBE). Gel electrophoresis was accomplished in 1x TBE-buffer: Infiltration of the gel was achieved at 60 V for 5min and separation of the distinct DNA-conformations at 120 V for about 90min. Afterwards, the gel was stained for 20 min with ethidium bromide in 1x TBE (0.75µg/mL) under continuous shaking. Images of the stained gel were taken with a GelDoc-It Imaging System Fusion Fx7 (*Vilber Lourmat*), and quantitative evaluation was performed with ImageJ software.

Studied compounds

Platinum(IV) complexes (Project 1)

The following compounds were synthesized by the group of Mag. Dr. Markus/Mathea Galanski at the Institute of Inorganic Chemistry, Faculty of Chemistry, University of Vienna. All these compounds are octahedral platinum(IV) complexes with varying axial and equatorial ligands. All stable non-leaving groups comprise nitrogen donor species, like ethylenediamine (1a, 1c, 1d, 1e, 1g), ammonia and cyclohexylamine (1b), or tert-butyl-amine (1f).

Equatorial leaving groups are chlorido (1a, 1b, 1f) or acetato (1d, 1g) ligands, trifluoropropionic acid (1e) or small esters of succinic acid (1c).

Axial leaving groups are either acetato ligands (1b, 1c, 1e) or esters of succinic acid (methyl esters: 1a, 1d, 1f; pentanyl esters: 1g). With regard to the axial leaving groups all structures are symmetrical (*Fig. 6-1*).

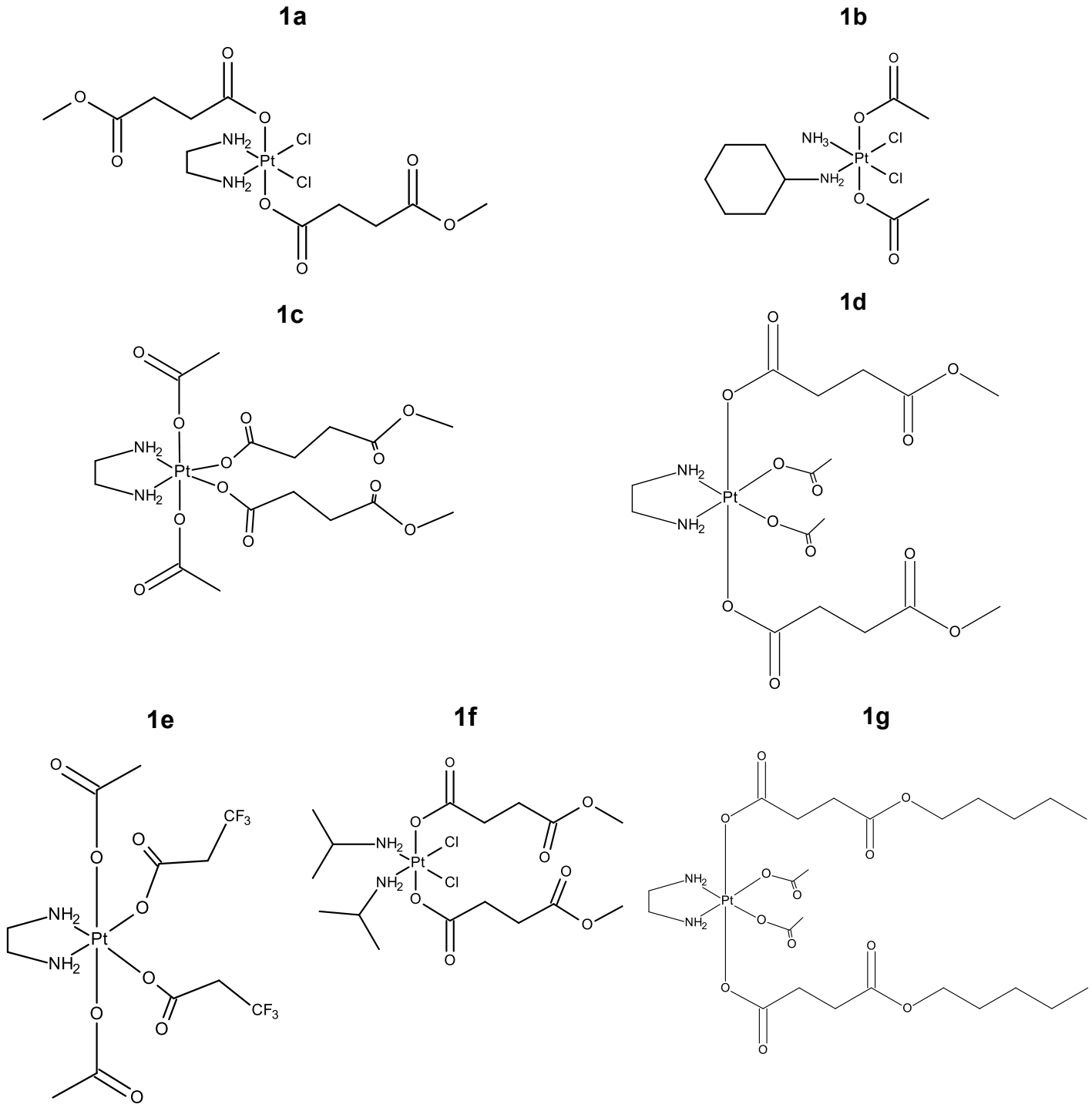

Fig. 6-1: Chemical structures of novel platinum(IV)complexes (drawn with Biovia Draw 2016 software).

Thiosemicarbazones (Project 2)

The following set of metal chelators was synthesized by the group of Éva Anna Enyedi, PhD, at the Department of Inorganic and Analytical Chemistry, University of Szeged, Hungary. These four derivatives are based on a mono or di-methylated thiosemicarbazonyl group. Two of them contain tetrahydronaphthalene derivatives (2a, 2b), the other two contain the estrogen derivative estrone (2c, 2d). Considering the high affinity for complex formation of copper with such a thiosemicarbazone moiety (cf. *ref. 48*), this project is aimed to show differences in biological activity between thiosemicarbazones with an estrone moiety, which could be of interest in therapy of hormone-dependent cancer types, and those with a tetrahydronaphthalene moiety instead.

For the experiments, copper was added to the thiosemicarbazones in order to build corresponding complex species *in situ*. Therefore, a copper(II) chloride-solution (c = 24.19 mM) was mixed equimolarly with the respective ligand.

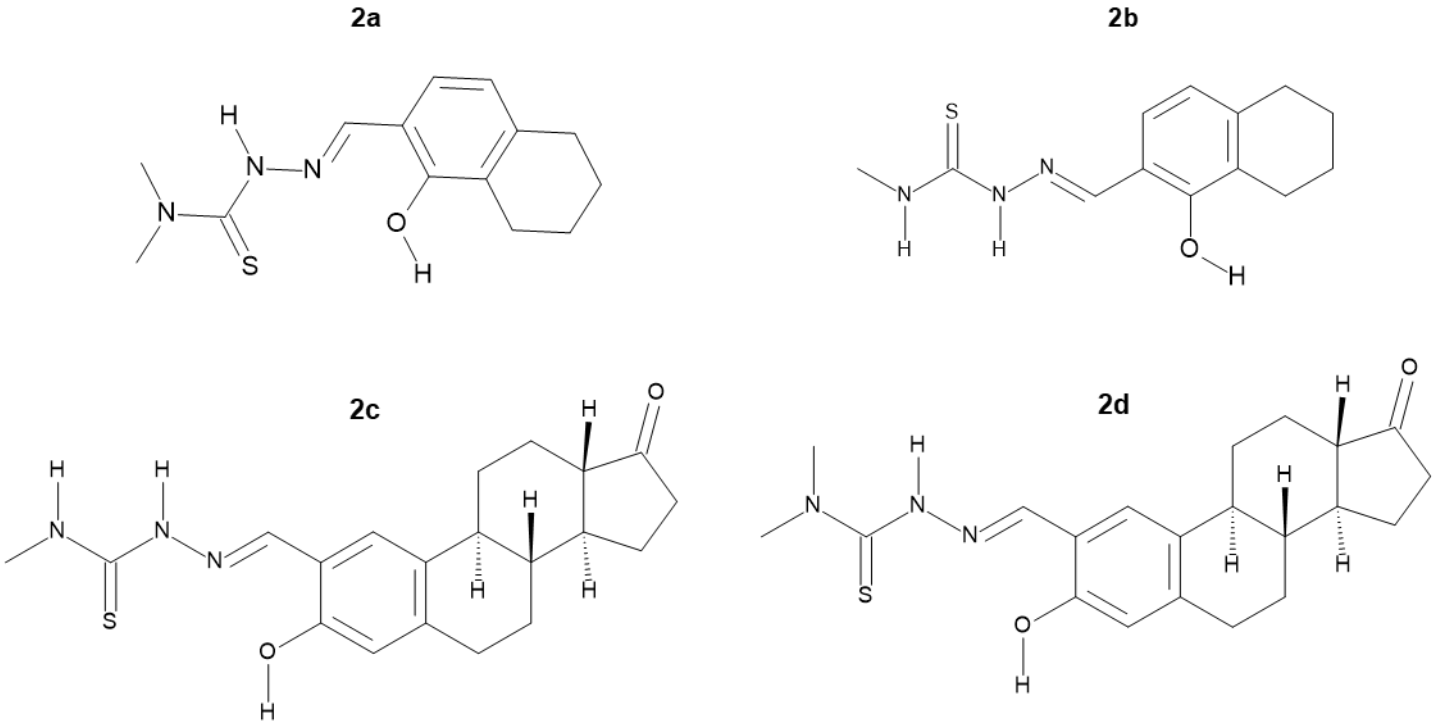

Fig. 6-2: Chemical structures of thiosemicarbazones containing either a tetrahydronaphthalene (2a, 2b) or an estrone moiety (2c, 2d) (drawn with Biovia Draw 2016 software).

Ru/Rh-arene complexes (Project 3)

Seven novel metal-arene compounds were synthesized by the group of Dipl.-Ing. Dr. Wolfgang Kandioller at the Institute of Inorganic Chemistry, Faculty of Chemistry, University of Vienna. Five of the seven investigated complexes contain Ru(II) as the central atom (3a, 3b, 3e, 3f, 3g), whereas the other two contain Rh(III) (3c, 3d). All complexes feature a bidentate thiopyridone moiety (either methylated or benzylated), but different leaving groups, such as methylimidazole (3a–3c), pta (3d–3f) and thiourea (3g). Axial ligands comprise either p-cymene or a cyclopentadienyl moiety (cf. *ref. 84*).

For Ru-, Rh- and even Os-containing metal complexes, the motif of the three-legged “piano stool” has indicated very promising antiproliferative properties (in 2D cell culture), which are not yet investigated well.

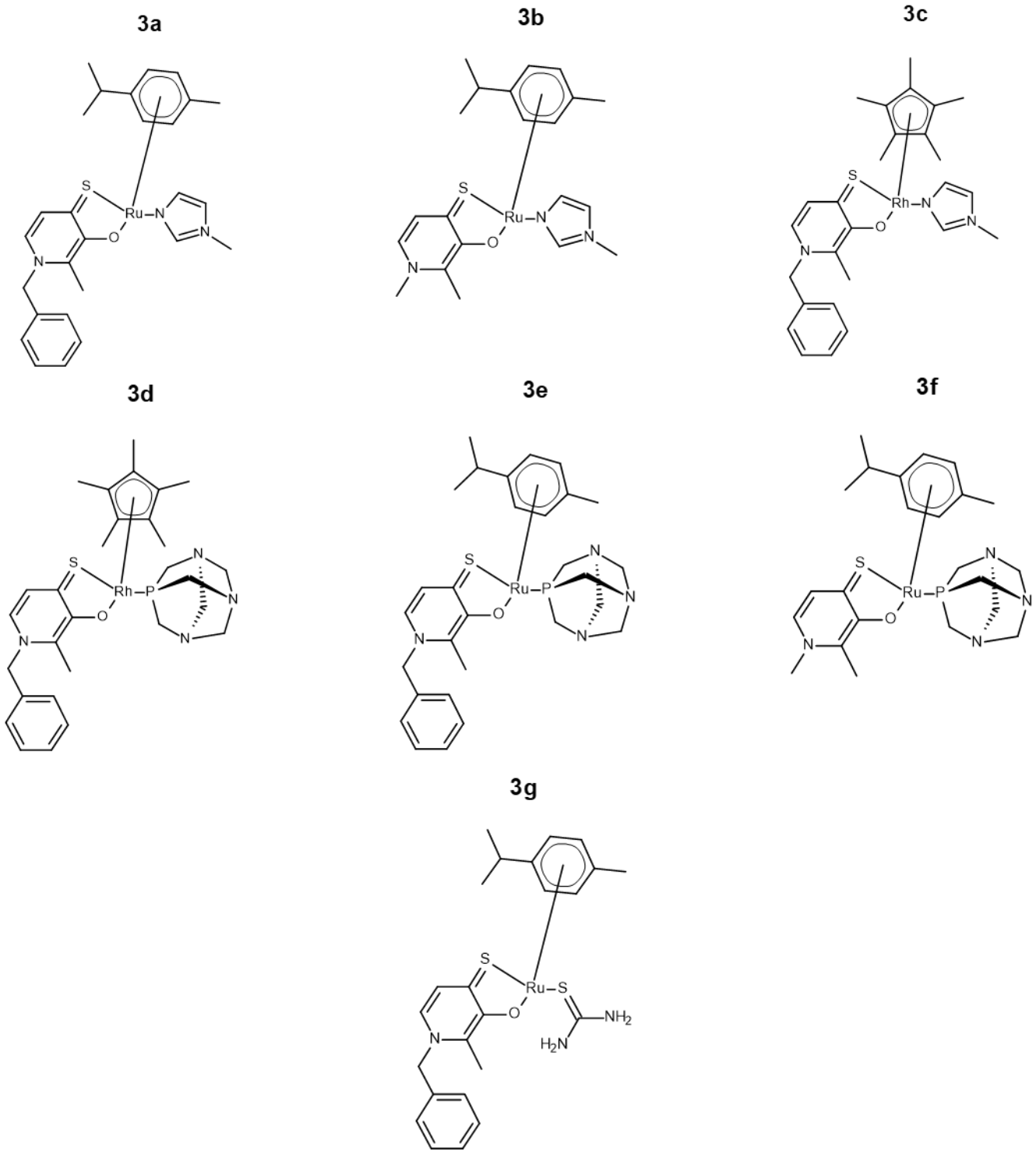

Fig. 6-3: Chemical structures of thiopyridone containing Ru(II) and Rh(III) "piano-stool" complexes: Stable bidentate thiopyridone and the different labile groups form the three legs of the piano stool, whereas the arene moiety resembles the seat (drawn with Biovia Draw 2016 software).

Results

Pt(IV) complexes (Project 1)

AlamarBlue Assay

The AlamarBlue assay in multicellular tumor spheroids revealed a wide diversity of cytotoxic potencies for the selected platinum(IV) complexes. Spheroids composed of CH1/PA-1-cells showed highest sensitivity throughout the whole spectrum of tested compounds. Monolayer cultures of this cell line are usually highly sensitive for treatment with platinum compounds, which is partially paralleled by the results in spheroid cultures here (cf. Table 1). Compounds **1b** and **1f** are remarkably active, with IC_{50} values <1 µM. In A549 and HCT-116 spheroids, values mostly indicate more moderate activity for these two compounds. Regarding their structure, both agents contain chlorido ligands in equatorial positions, which seems to be crucial for their high activity. From **1a**, another chlorido containing compound, **1f** only differs by its nitrogen donor ligands. This comparison reveals that the bidentate ethylenediamine ligand (present in **1a** instead of the two isopropylamine ligands in **1f**) lowers activity about 54-fold (CH1/PA-1), 31-fold (HCT-116) and 13-fold (A549). For **1b**, monodentate nitrogen donor ligands (ammonia and cyclohexylamine) apparently support cytotoxicity very effectively.

Compound **1e** shows intermediate potency, which is unequivocally associated with the presence of labile trifluoropropionato ligands in equatorial positions. Exchanging those ligands with monomethyl succinate (as in **1c**) lowers activity by 29-fold (CH1/PA-1), > 29-fold (HCT-116) and > 4-fold (A549).

Swapping axial and equatorial positions of acetate and monomethyl succinate leaving groups (as in **1c** compared to **1d**) only brought about a marginal 1.6-fold change of cytotoxic potency in CH1/PA-1 spheroids.

Elongating alkyl chains of axial ligands contributes to higher cytotoxicity (probably by increasing lipophilicity), as can be seen by comparing IC_{50} values of compounds **1d** and **1g**. Improving lipophilicity by exchanging methyl esters with pentanyl esters, seems to have tremendous effects on cytotoxicity in all three cell lines.

The overall rank order of compounds according to their cytotoxicity in multicellular tumor spheroids is equal for all three cell lines:

1f > 1b ≥ 1g > 1e > 1a > 1d ≥ 1c.

To conclude all above mentioned observations, the following apparent order of ligands' relevance for cytotoxic effects, regarding their size and position, was recognizable for this selection of platinum(IV) complexes: small leaving equatorial moieties > small, monodentate equatorial nitrogen-containing groups ≥ (large), lipophilic axial groups.

Table 1: IC_{50} values (in µM) obtained with the AlamarBlue assay after 96 h of treatment of multicellular tumor spheroids with platinum(IV) complexes. *Three different cancer cell lines (derived from diverse tissues) were used for assessing the cytotoxicity of novel compounds **1a–1g**. IC_{50} values (interpolated from concentration-effect curves in Fig. 7a and Fig. 7b) are represented by mean ± s.d. from at least three independent experiments. IC_{50} values larger than 400 µM are considered to indicate inactivity.*

compound	A549	CH1/PA-1	HCT-116
1a	115 ± 26	7.0 ± 1.6	44 ± 9
1b	27 ± 3	0.44 ± 0.06	4.4 ± 1.2
1c	> 400	115 ± 17	> 400
1d	> 400	74 ± 1	> 400
1e	95 ± 1	4.2 ± 1.1	14 ± 2
1f	9.4 ± 0.9	0.13 ± 0.05	1.4 ± 0.3
1g	33 ± 2	1.2 ± 0.8	4.0 ± 0.9

Concentration-effect curves, which resulted from measurements of single concentrations obtained with the AlamarBlue assay, were gathered and respective IC_{50} values were interpolated. HCT-116 and CH1/PA-1 multicellular spheroids formed stable aggregates, which resulted in quasi-sigmoidal concentration-effect curves, whereas A549 multicellular spheroids built elongated structures with likely loosely bound cells, which might be the reason for their irregular and jagged curves (cf. *Fig. 7a* and *Fig. 7b*).

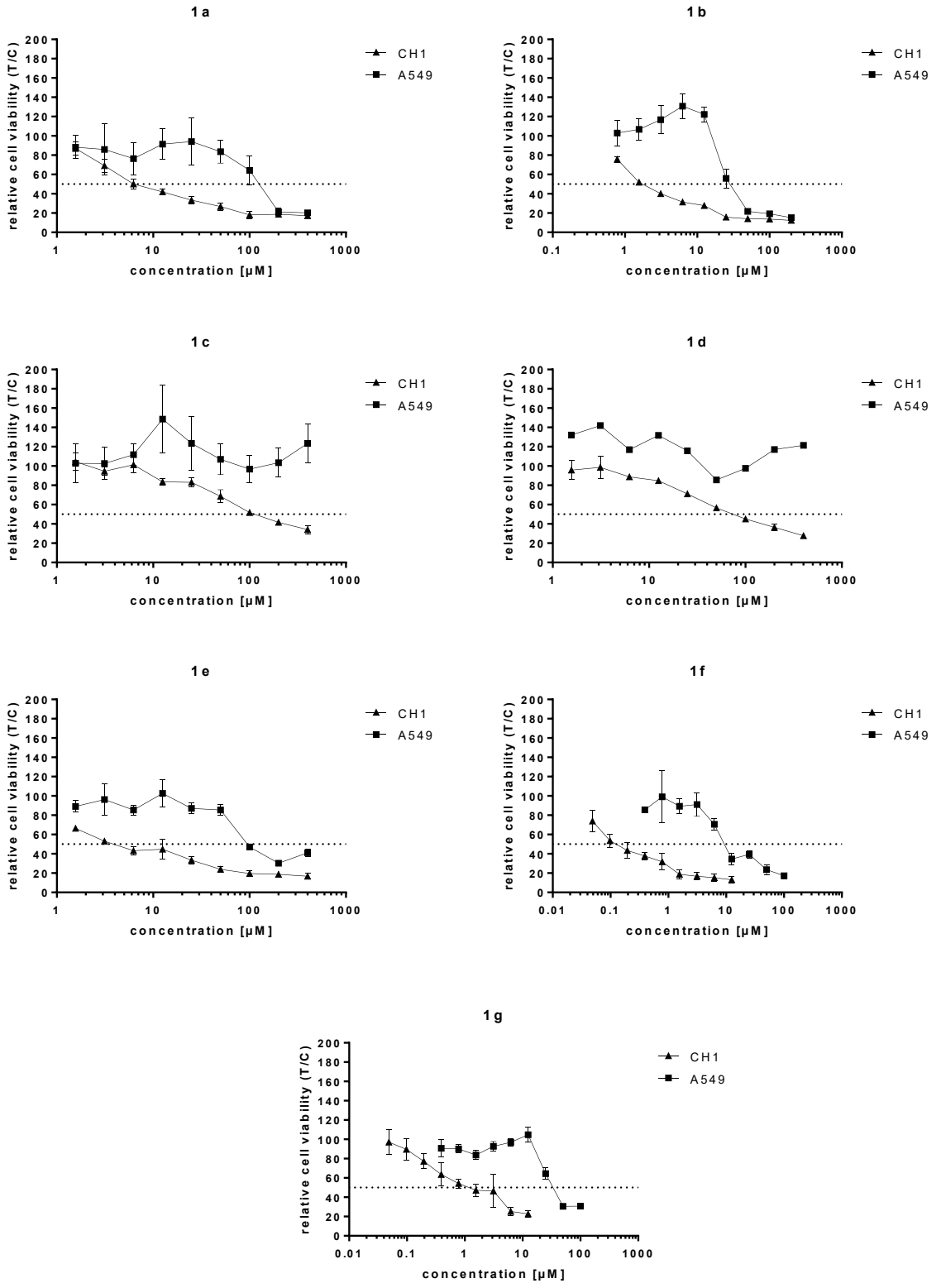

Fig. 7a: Concentration-effect curves of Pt(IV) complexes 1a–1g in A549 and CH1/PA-1 spheroids. *Depicted curves (relative cell viability vs concentration) were obtained for all seven tested compounds by means of the AlamaBlue assay. IC_{50} values were interpolated and are listed in Table 1.*

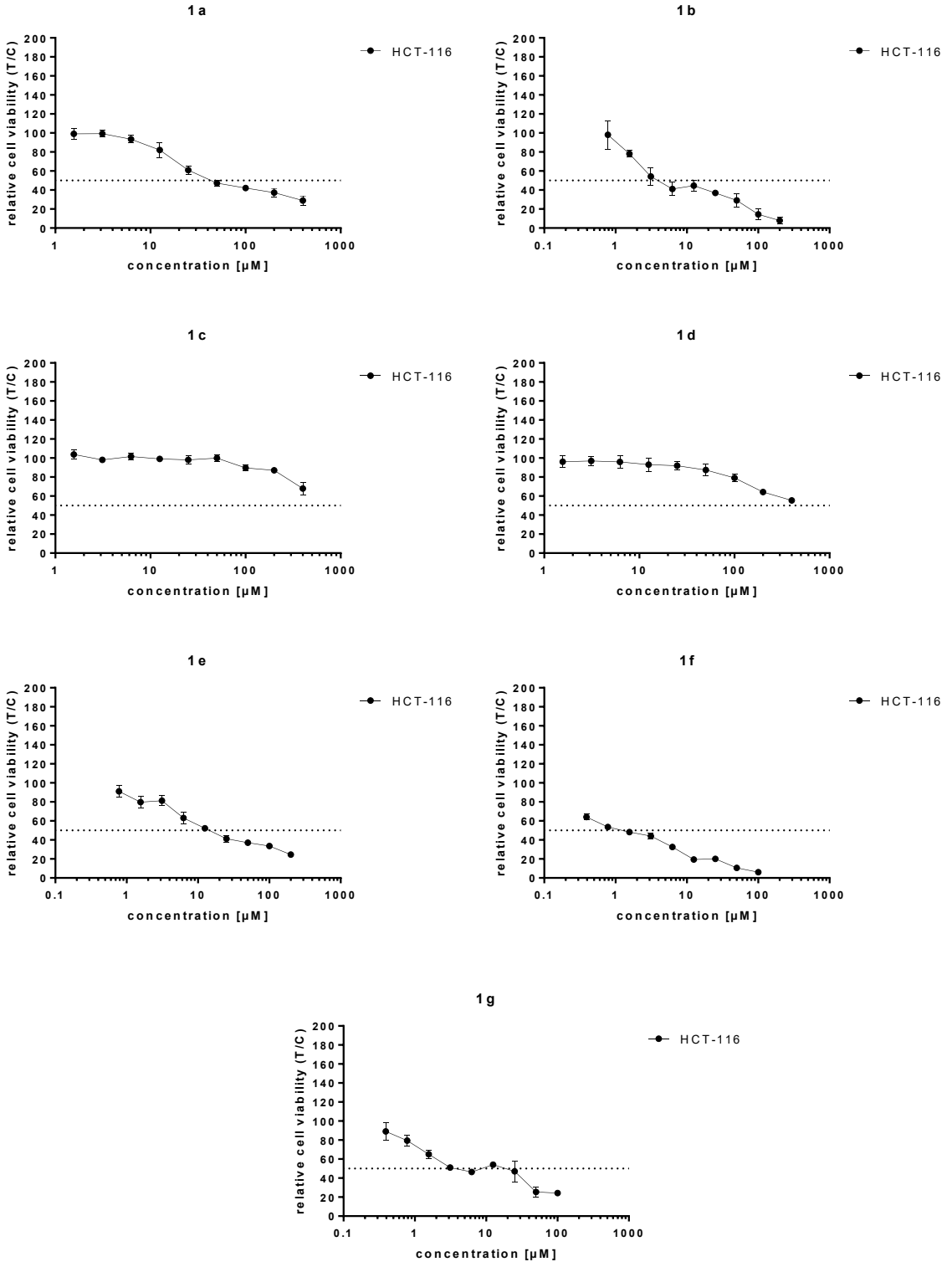

Fig. 7b: Concentration-effect curves of Pt(IV) complexes 1a–1g in HCT-116 spheroids. *The depicted curves (relative cell viability vs concentration) were obtained for all seven tested compounds by means of the AlamarBlue assay. IC_{50} values were interpolated and are listed in Table 1.*

Growth of spheroids

The impact of treatment on spheroids can also be assessed by measuring their sizes over time or at an endpoint. For this work, pictures of untreated spheroids 96 hours after seeding (= 0 h) and treated spheroids 192 hours later (= 96 hours after treatment) were taken and their diameters were calculated (with CellF software).

As shown in *Fig. 8 (top)*, untreated HCT-116 spheroids grew in diameter by about 200 µm in 96 hours. Compared to all treated spheroids, growth rate was reduced to half of the untreated spheroids at least. For spheroids treated with **1f**, even shrinking of spheroids was observable after 96 hours, which points to a more cytotoxic than cytostatic feature of that substance in this specific cell line.

Fig. 8 (bottom) shows representative pictures of all compound treatments plus the control spheroids (only medium) after 96 hours. It is apparent that diameters of treated spheroids are reduced compared to the untreated ones (CTL). The shape of untreated spheroids seems to be altered barely, whereas treatment seems to induce small irregularities, more or less distinct, at the edges of each spheroid, independent from compounds' chemical properties. Such local anomalies could be a hint on stressed or apoptotic cells. Furthermore, some cores look more densely packed than others, like spheroids treated with **1b**, **1c** and **1d**, with a ring of viable cells around them. The latter feature can also be noticed in untreated spheroids, but without irregularities at the spheroids' edges; but for these control samples, it must be assumed that, due to their large size after 8 days of growth under optimal conditions, core cells are not in a good condition anymore, because nutrients and O_2 do not penetrate that deeply (*cf. Introduction, 2D vs 3D methods* and *Fig. 5*).

Since the irregular edges mentioned above might be an indication for stressed spheroids, ROS levels and induction of apoptosis were assessed in the next steps.

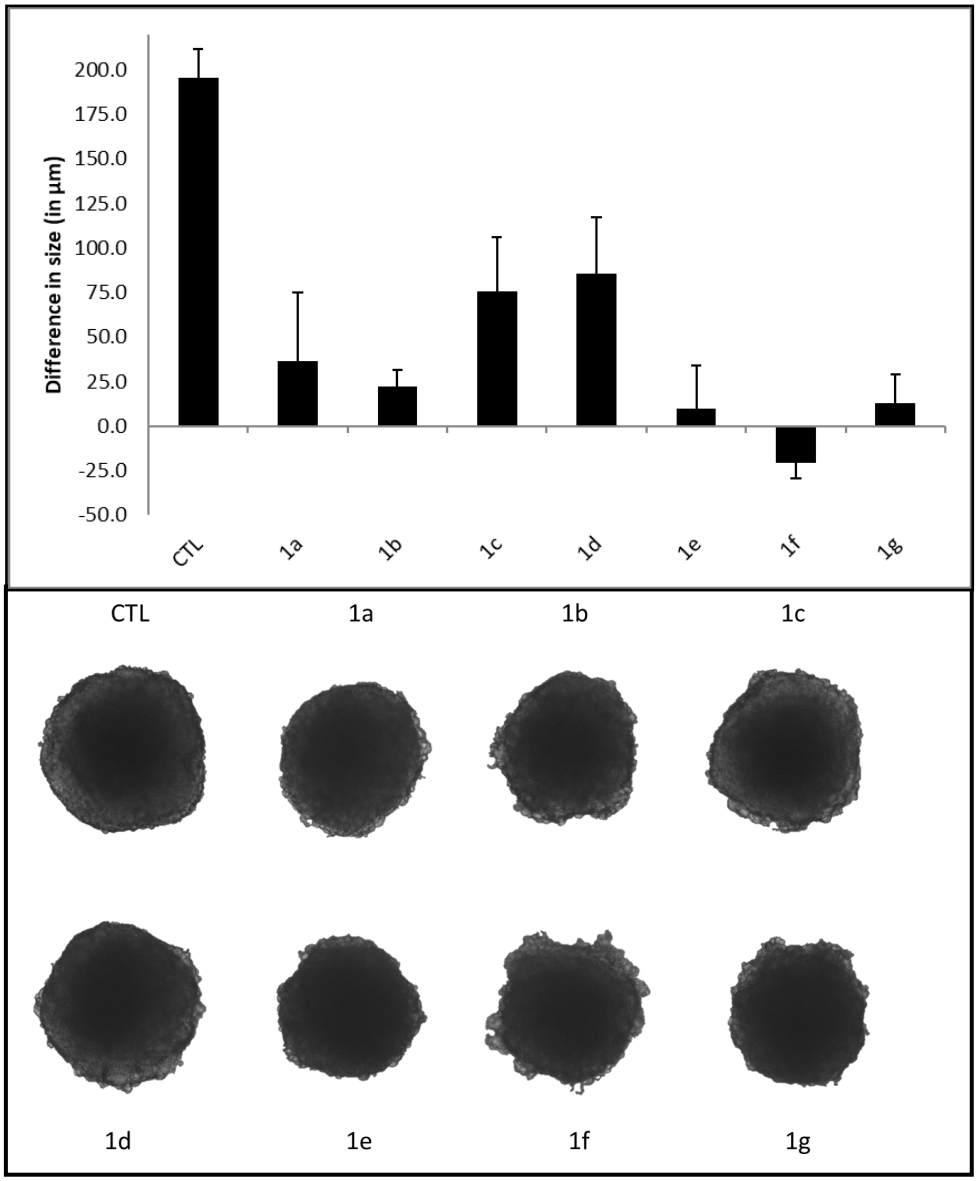

Fig. 8: Growth of HCT-116 spheroids within 96 hours of treatment with Pt(IV) complexes (1a–1g) compared to untreated control (CTL). *Size differences obtained by measuring spheroid sizes before (0 h) and after treatment (96 h) (top) compared to untreated controls (CTL). Representative pictures of spheroid shape and size after 96 hours of treatment with the respective compound (bottom). Values were averaged over at least 5–6 spheroids per condition. All spheroids were treated with the mean IC_{50} + s.d. of the respective compound, except for spheroids treated with* ***1d****, which was applied at a concentration of 200 µM.*

ROS Assay

In order to assess any oxidative stress that compounds might induce, the levels of cells with enhanced reactive oxygen species (ROS) were determined by flow cytometry. Spheroids were dyed with two fluorescent probes, which can be measured selectively. In this case, PI was used as red-fluorescent cell viability marker and CellRox as green-fluorescent marker for ROS levels in spheroids.

Fig. 9 depicts the levels of ROS induction in HCT-116 spheroids after 24 h of treatment with Pt(IV) complexes. Untreated spheroids show an increase in cells with enhanced ROS levels by less than 2% (of 5000 cells measured per condition). Compounds **1a**–**1c** do not show a significant increase in those levels compared to controls. On the other hand, compounds **1d**–**1g** raised the amounts of cells with enhanced reactive oxygen species by at least 6- to 11-fold.

The latter substances seem to stress cells more than the other tested substances, which should be investigated further.

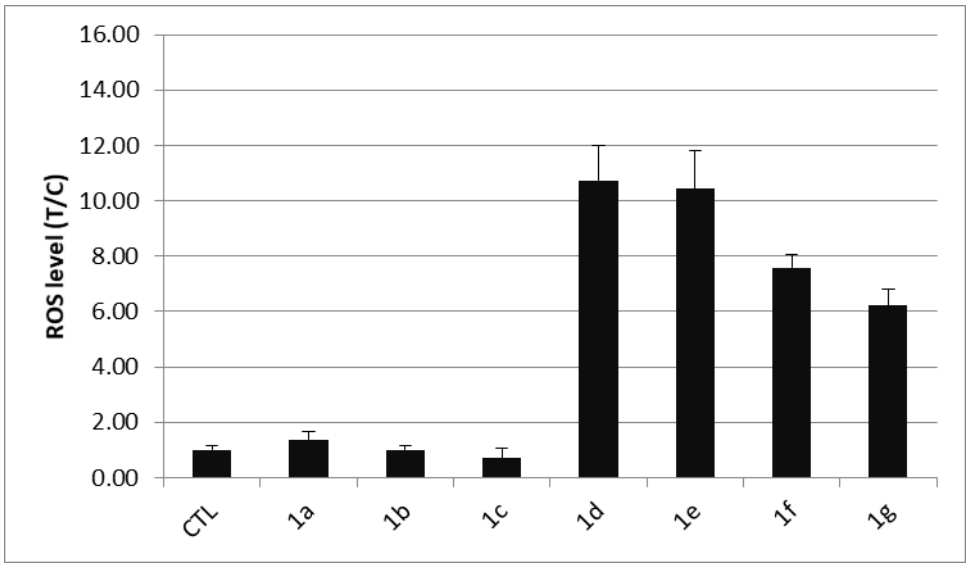

Fig. 9: ROS levels of HCT-116 spheroids after 24 hours of treatment with Pt(IV) complexes (1a–1g) compared to untreated control (CTL). *After exposure to test compounds at their respective IC_{50} + s.d. (except for **1d**, which was applied at a concentration of 200 µM), ROS levels in viable cells were measured via flow cytometry upon double-staining with PI (to exclude necrotic cells) and CellRox. Columns represent values (mean ± s.d.) obtained from at least 5-6 spheroids per condition in at least two independent experiments.*

Apoptosis Assay

After 48 hours of treatment with the respective compounds, the extent of apoptosis induction was measured independently from the above-mentioned ROS assay. ROS induction is usually a quite fast effect (therefore measured after one day of treating spheroids), whereas induction of apoptosis may require longer time. For this reason, a period of at least 48 hours was chosen for treatment with all studied compounds.

Fig. 10 demonstrates the percentages of apoptotic cells present in treated spheroids after 48 hours. Values were gained by flow cytometric measurements of 5000 stained cells, processed by FlowJo software. Treated and untreated samples were compared in order to assess substance effectivity in terms of apoptosis induction:

It can be concluded that substances **1c**, **1d**, **1e** and **1g** do not induce apoptosis in multicellular spheroids. Only compounds **1a**, **1b** and **1f** yielded slight increases in apoptotic cells by 1.2-, 1.7- and 1.5-fold, respectively, at the applied concentrations.

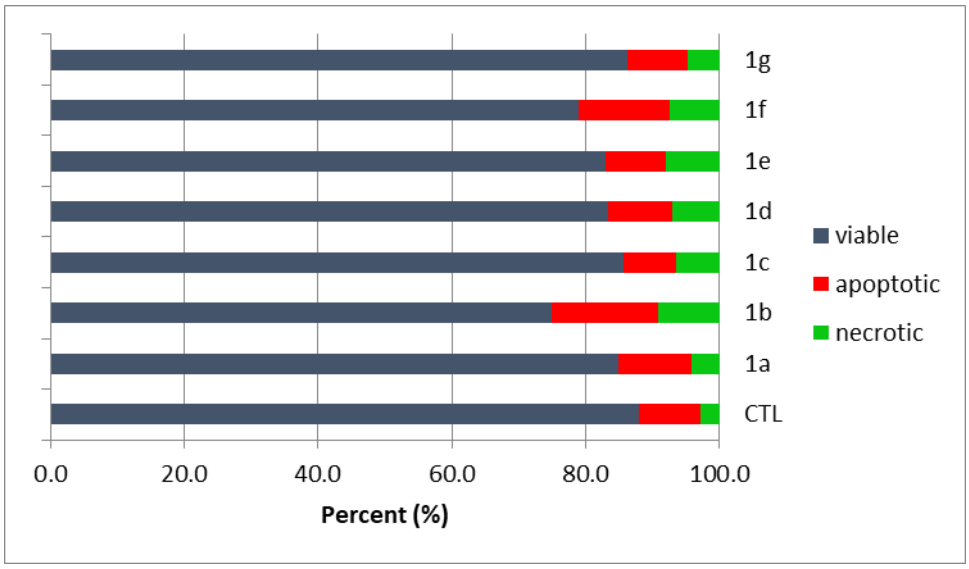

Fig. 10: Apoptotic/necrotic cells in HCT-116 spheroids after 48 hours of treatment with Pt(IV) complexes (1a–1g) compared to untreated control (CTL). *The percentages of apoptotic and necrotic cells in spheroids were assessed by flow cytometry upon exposure to the compounds at their respective IC_{50} + s.d. (except for **1d**, which was applied at a concentration of 200 µM) and application of an apoptosis-specific fluorescent protein (annexin V-FITC) as well as PI. Bars represent mean values from analysis of at least 5–6 spheroids per condition in at least two independent experiments.*

Immunocytochemistry

This method was applied qualitatively to assess induction of apoptosis after 96 hours of treatment.

For this purpose, cryo-samples had been cut in 5 µm thin sections before staining was accomplished. Three different primary antibodies were used to indicate viable and apoptotic cells within treated spheroids. Viable cells could be marked with a KI67-tagging primary antibody (*Fig. 11a*). All samples showed significant amounts of viable cells, in the core region as well as in the periphery of the spheroids. Apparently, all treated spheroids even demonstrate an increase in KI67-staining, compared to a negative control. On the contrary, the markers of apoptosis, cleaved-caspases 3 and 7 (*Fig. 11b* and *Fig. 11c*), yielded only sparse dots throughout the spheroids, indicating no significant induction of apoptosis after 96 hours of treatment with Pt(IV) compounds at the chosen concentrations, except for compound **1f**. For this compound, staining of cleaved caspase 7 resulted in a much higher number of dot signals (dispersed throughout the entire spheroid section) than for any other compound, which suggests a more cytotoxic character.

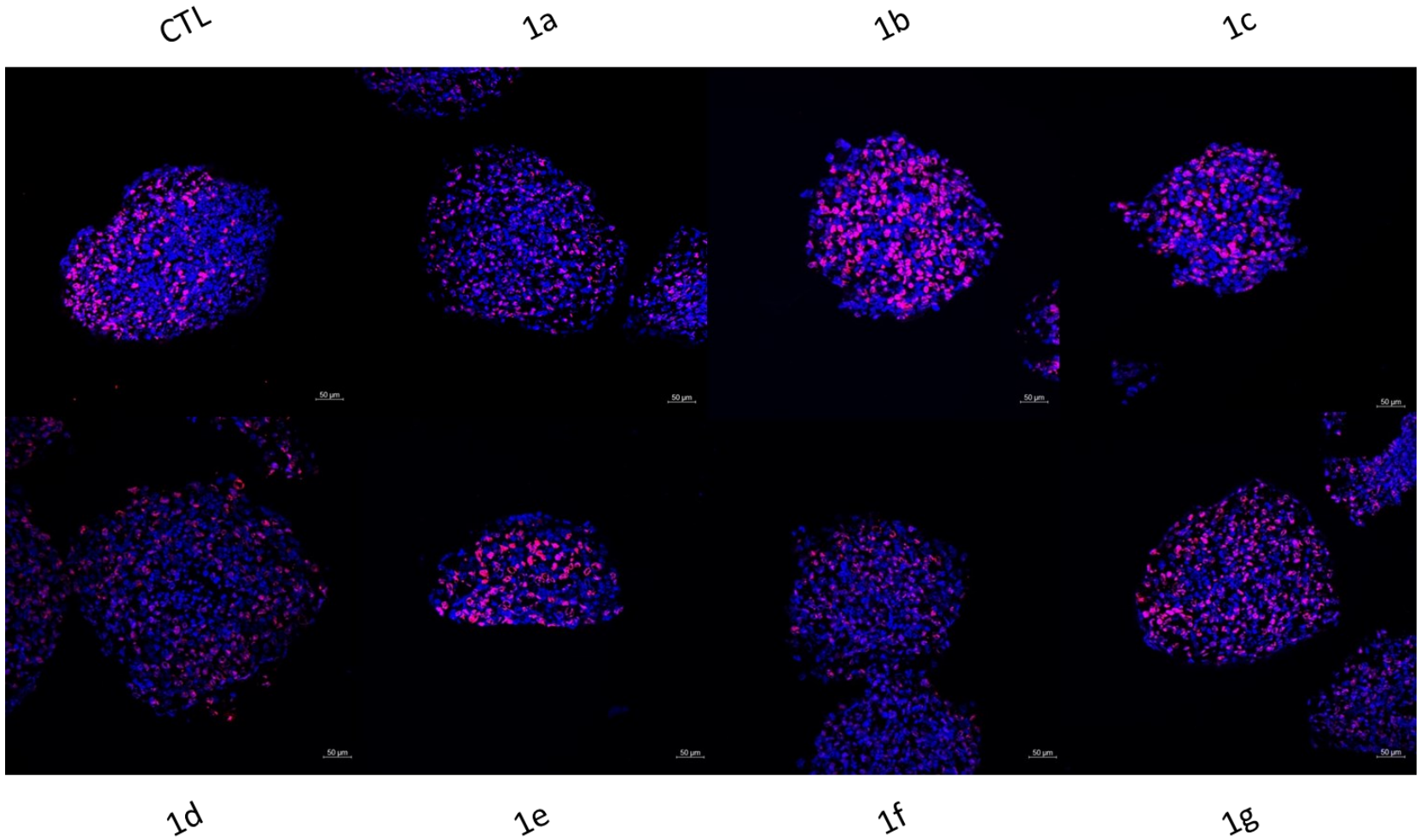

Fig. 11a: Representative immunocytochemical images of HCT-116 spheroids stained against KI67 after 96 hours of treatment with Pt(IV) complexes (1a–1g) compared to untreated control (CTL). *Spheroids were initially tagged with a primary antibody against the proliferation marker KI67 and then with a fluorescently labeled secondary antibody (= red dots). Additionally, DNA was stained with DAPI to visualize the nuclei (= blue dots). Spheroids were treated in the range of IC_{50} + s.d. of the respective compound. Pictures were taken with a confocal laser-scanning microscope (Zeiss LSM 800) with a 20x magnification lens.*

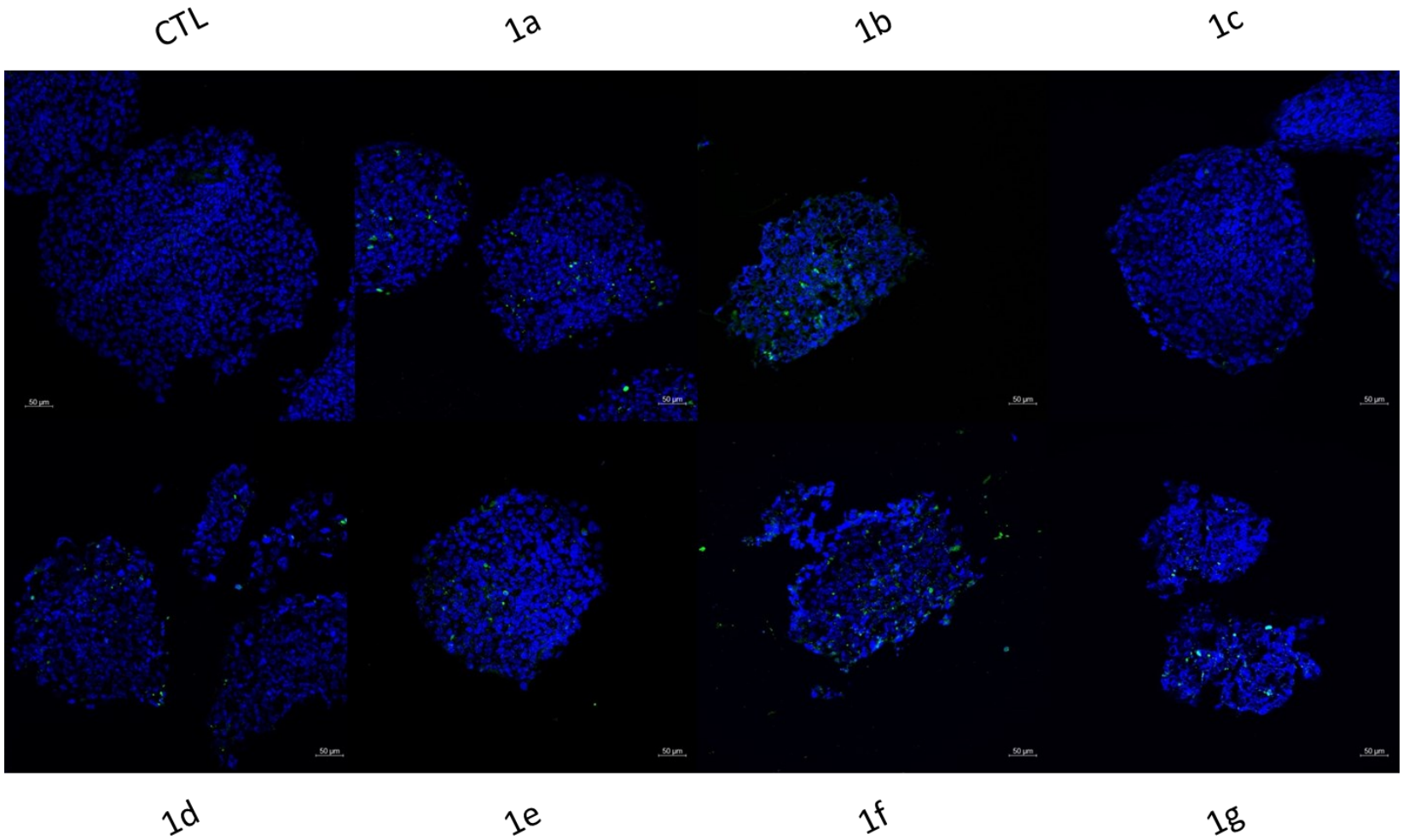

Fig. 11b: Representative immunocytochemical images of HCT-116 spheroids stained against cleaved caspase 3 after 96 hours of treatment with Pt(IV) complexes (1a–1g), compared to untreated control (CTL). *Spheroids were initially tagged with a primary antibody against an apoptosis-specific marker, cleaved caspase 3 (active form of caspase 3), and then with a fluorescently labeled secondary antibody (= green dots). Additionally, DNA was stained with DAPI to visualize the nuclei (= blue dots). Spheroids were treated in the range of IC_{50} + s.d. of the respective compound. Pictures were taken with a confocal laser-scanning microscope (Zeiss LSM 800) with a 20x magnification lens.*

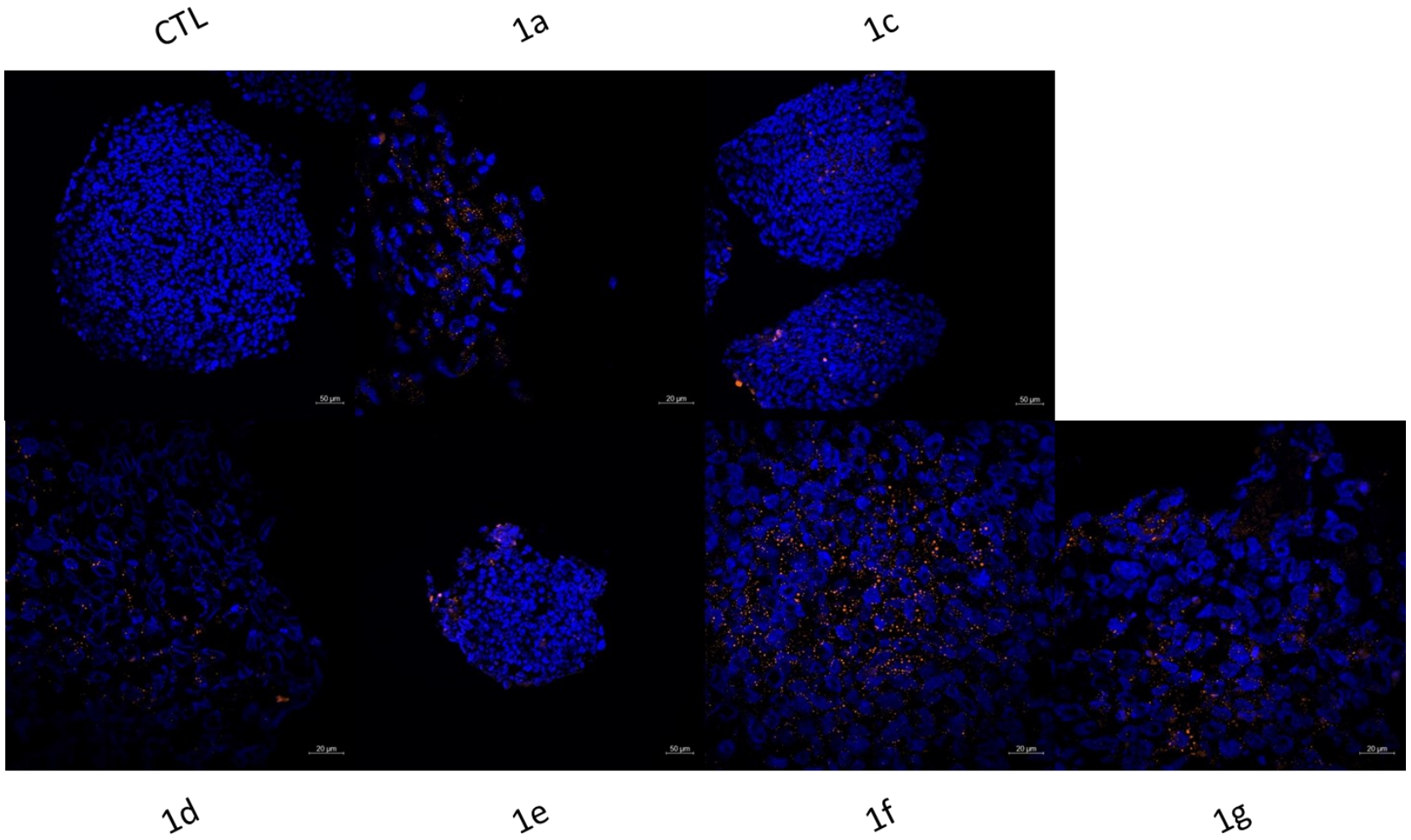

Fig. 11c: Representative immunocytochemical images of HCT-116 spheroids stained against cleaved caspase 7 after 96 hours of treatment with Pt(IV) complexes (1a–1g) compared to untreated control (CTL). *Spheroids were initially tagged with a primary antibody against another apoptosis-specific marker, cleaved caspase 7 (active form of caspase 7), and then with a fluorescently labeled secondary antibody (= orange dots). Additionally, DNA was stained with DAPI to visualize the nuclei (= blue dots). Pictures of* ***1b****-treated spheroids were not possible to take, probably due to inadequate sample preparation or staining procedure. Spheroids were treated in the range of* IC_{50} *+ s.d. of the respective compound. Pictures were taken with a confocal laser-scanning microscope (Zeiss LSM 800) with 20x and 63x magnification lenses.*

Synopsis of Project 1

Octahedral Pt(IV) complexes tested in this work demonstrated the following main results:

A consistent order of activities of the different substances in all tested cell lines was observed, whereby **1f** was the most promising compound in the cytotoxicity tests. Small leaving equatorial moieties, as well as small, monodentate equatorial nitrogen-containing groups and (large), lipophilic axial groups seem to have high impacts on cytotoxicity of Pt(IV) complexes.

All platinum complexes caused a deceleration in spheroid growth after 96 hours of treatment. The outstanding properties of **1f** were confirmed, as this compound not only decelerated growth, but decreased spheroid size.

ROS assay in 3D-models indicated that four of seven tested compounds increased the levels of cells with enhanced reactive oxygen species, whereas three of them did not show any effects.

A quantitative apoptosis assay after 48 hours did not show high induction of apoptosis, and qualitative immunofluorescence after 96 hours even revealed an increase in viable, proliferating cells (compared to a negative control). Only **1f** indicated quite a high amount of the apoptotic marker cleaved caspase 7. The other tested compounds lacked comparable properties at the tested concentrations.

In summary, for all compounds a more or less distinct cytostatic behavior was observable, but only **1f** showed pronounced cytotoxic properties in terms of apoptosis induction.

Thiosemicarbazones (Project 2)

AlamarBlue Assay

The second project introduced in this work also revealed new insights into the biological activity of copper(II)-complexing thiosemicarbazones. These compounds had to be mixed with copper chloride, since the corresponding complexes had not been isolated by the time this work was performed.

Cytotoxicity tests showed relatively high activity in all three cancer cell lines used (*Table 2* and *Fig. 12*). Despite of the hormone-like character of **2c** and **2d**, no clear difference was observed in A549 and HCT-116 models, which are supposed to be quite hormone-independent cell lines by their origin from lung and colorectal cancer tissue, respectively, and the usually highly sensitive cell line CH1/PA-1. Results even demonstrated highest activities in the colon carcinoma spheroids (HCT-116), which was chosen as the main cell line for subsequent experiments within this project.

Table 2: IC_{50} values (in µM) obtained with the AlamarBlue assay after 96 h of treatment of multicellular tumor spheroids with combinations of thiosemicarbazones and copper chloride, as well as each compound alone (only in HCT-116). *Three different cancer cell lines (derived from diverse tissues) were used for assessing the cytotoxicity of the test compounds (copper chelators **2a–2d** in the presence of equimolar Cu^{2+}) (left). The single copper chelators, as well as the copper(II) solution were tested independently in HCT-116 spheroids (right). IC_{50} values (interpolated from concentration-effect curves in Fig. 12) are represented by mean ± s.d. from at least three independent experiments.*

compound	**A549**	**CH1/PA-1**	**HCT-116**	**compound**	**HCT-116**
***2a* + Cu^{2+}**	16 ± 2	17 ± 5	4.8 ± 0.6	***2a***	21 ± 1
***2b* + Cu^{2+}**	10 ± 5	5.4 ± 1.2	3.9 ± 1.0	***2b***	>25
***2c* + Cu^{2+}**	10 ± 2	10 ± 1	3.9 ± 0.4	***2c***	>25
***2d* + Cu^{2+}**	13 ± 2	7.3 ± 2.4	3.9 ± 1.2	***2d***	20 ± 2
				Cu^{2+}	>25

AlamarBlue tests of either the four ligands or copper(II) chloride solution alone, did not show activity comparable to the mixtures that are expected to give rise to complex species. In fact, IC_{50} values were at least 5 times higher for ligands and

copper(II) chloride in HCT-116 spheroids (concentration-effect curves not shown in this thesis) than those of the equimolar mixtures. Those results demonstrated the dependency of the biological activity of tested ligands on their copper complexation, but a relative independency of the chemical nature (with or without estrogen moiety) of the ligands themselves.

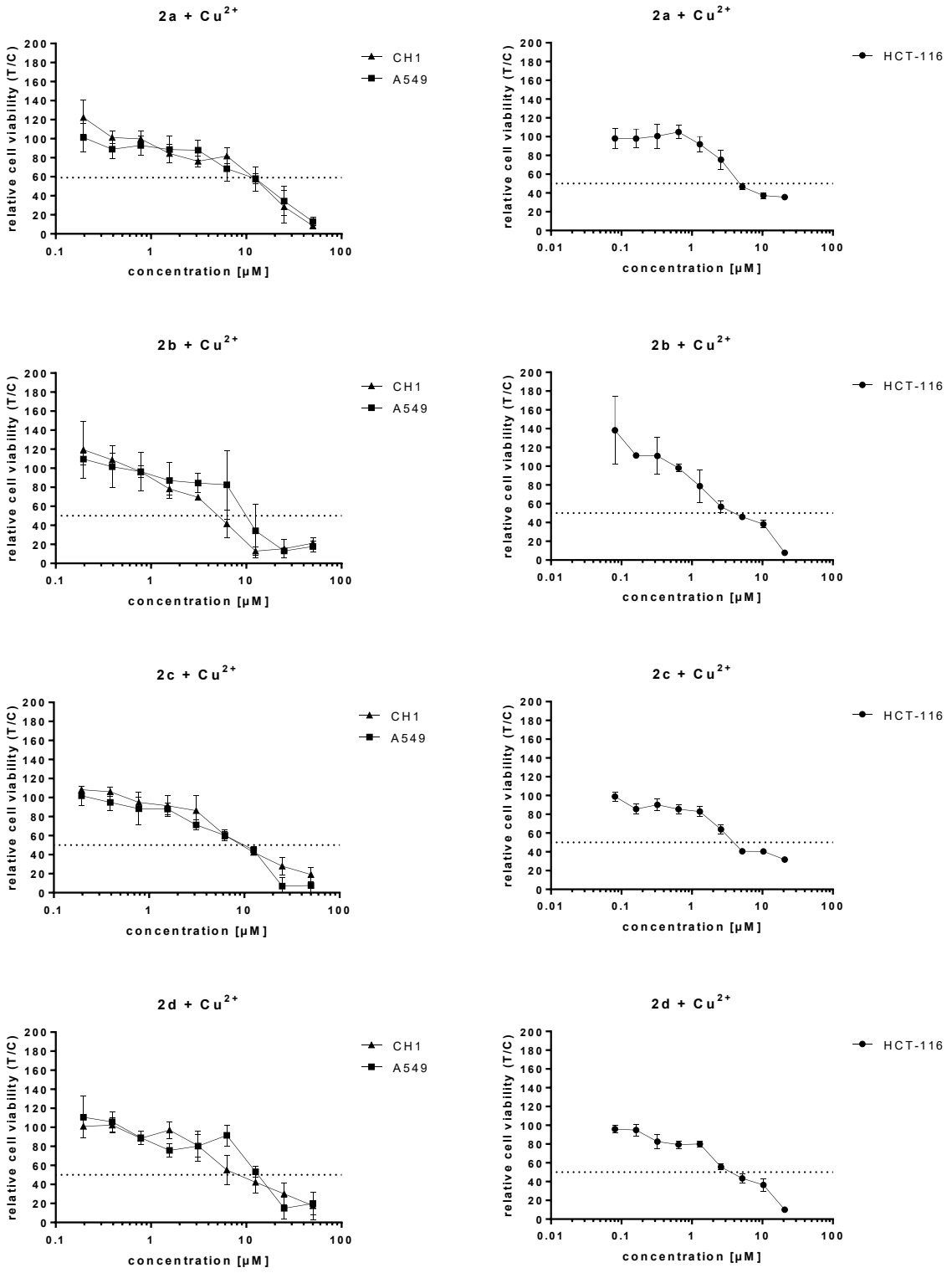

Fig. 12: Concentration-effect curves equimolar mixtures of thiosemicarbazones (2a–2d) and copper(II) chloride in A549, CH1/PA-1 (left) and HCT-116 (right) spheroids. *IC_{50} values are listed in Table 2.*

Growth of spheroids

HCT-116 spheroids were tested on their size and shape changes after treatment with thiosemicarbazones combined with copper(II) chloride. For all treated spheroids, smaller sizes compared to control spheroids can be observed after 96 hours of treatment (*Fig. 13, bottom*). Three out of four tested compounds revealed cytostatic properties by diminishing growth dramatically, whereas **2b** even caused an overall reduction in spheroid size by approximately 11% compared to that at the beginning of the experiment (*Fig. 13, top*).

Spheroids treated with **2a** and **2b** demonstrated a dense core of probably stressed cells, whereas their edges show less densely packed cells, which start to form outgrowths. For **2c**- and **2d**-treated spheroids, the dense core was not surrounded by loosely packed viable cells, but small outgrowths were detectable. Hence, the following structure-activity relationship could be inferred from these observations: only non-hormone-like substances **2a** and **2b** seem to induce a contrast between a dense spheroid core and a ring of more loosely aggregated cells, whereas hormone-like compounds **2c** and **2d** seem to reduce the spheroid to a structure that is compact and dense throughout.

To assess whether spheroids were affected by oxidative stress or undergo apoptosis upon treatment with these compounds, appropriate experiments were performed next.

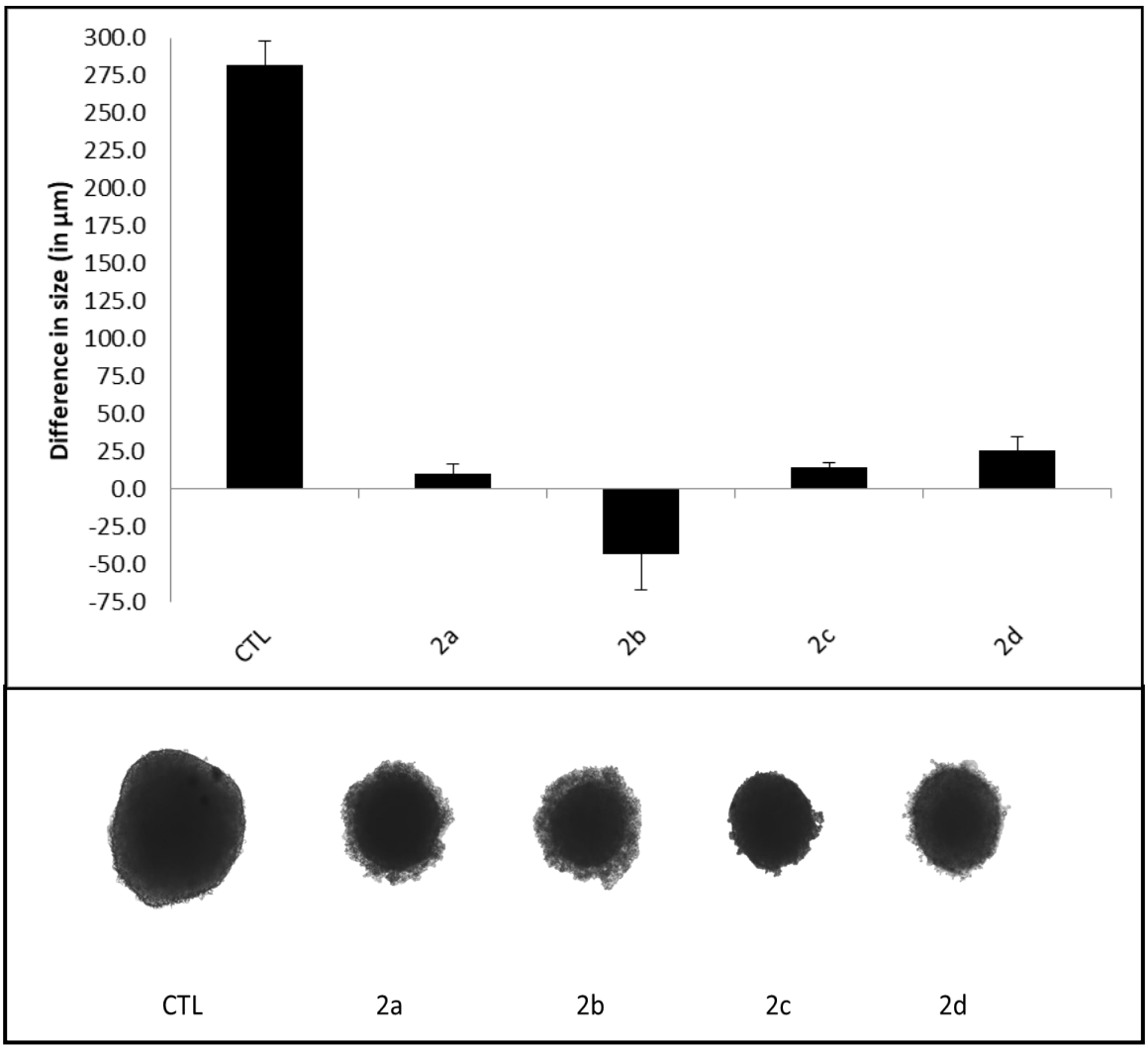

Fig. 13: Growth of HCT-116 spheroids within 96 hours of treatment with equimolar combinations of thiosemicarbazones 2a–2d and copper(II) chloride compared to untreated control (CTL). *Size differences obtained by measuring spheroid sizes before (0 h) and after treatment (96 h) (top) compared to untreated controls (CTL). Representative pictures of spheroid shape and size after 96 hours of treatment with the respective compound (bottom). Values were averaged over at least 5–6 spheroids per condition. All spheroids were treated with the mean IC_{50} + s.d. of the respective compound.*

ROS Assay

Flow-cytometric assessment of ROS levels in spheroids upon treatment with the investigated thiosemicarbazones (all in combination with copper chloride) demonstrated increases in cells with enhanced ROS levels by 1.6-fold and 1.4-fold upon treatment with **2b** and **2d**, respectively. For **2c** the highest induction (with a 2.8-fold increase) could be observed. Only **2a** seemed to decrease the number of cells with enhanced ROS, though insignificantly by 7%, of the control level.

Although **2b** did not induce ROS as strongly as **2c** (approximately half as much), it became obvious that those two monomethylated thiosemicarbazones had more influence on ROS levels than the demethylated analogs **2a** and **2d**. Those results indicated the importance of the thiosemicarbazone moiety, whereas the hormone-like part has less influence in this assay.

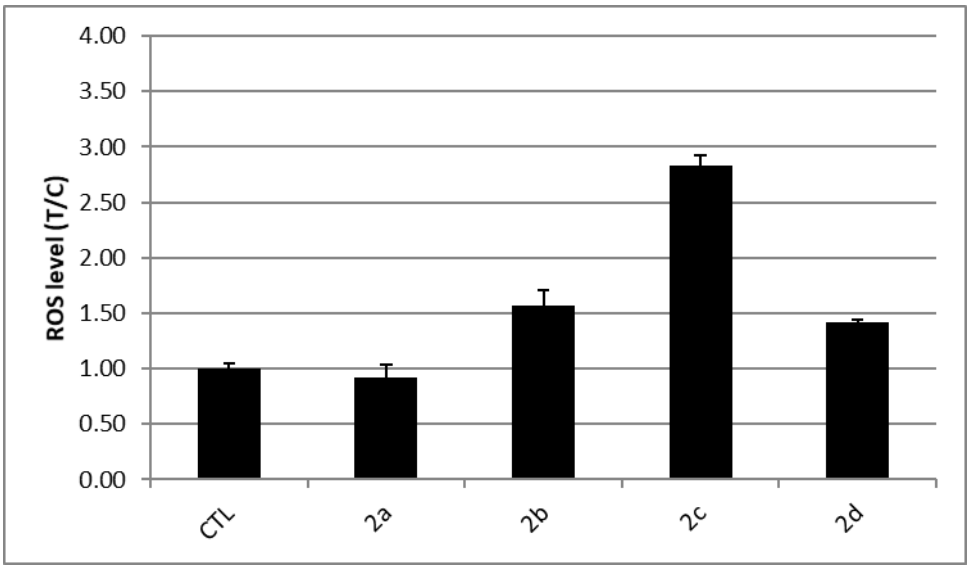

Fig. 14: ROS levels of HCT-116 spheroids after 24 hours of treatment with equimolar combinations of thiosemicarbazones 2a–2d and copper(II) chloride. *After exposure to test compounds at their respective IC_{50} + s.d., ROS levels were measured via flow cytometry upon double-staining with PI (to exclude necrotic cells) and CellRox. Columns represent values (mean ± s.d.) obtained from at least 5–6 spheroids per condition in at least two independent experiments.*

Apoptosis Assay

Quantification of apoptotic cells within HCT-116 spheroids by using a fluorophore-tagged annexin V showed that all four tested substances combined with copper(II) chloride induce apoptosis after 48 hours. In spheroids treated with **2c** the smallest amount of 17% apoptotic cells in could be observed, followed by 21% in **2b**-treated spheroids. The highest percentages of apoptotic cells (24% and 26%) were found in **2d**- and **2a**-treated spheroids.

Apparently, the methylation status of the terminal nitrogen of the thiosemicarbazone moiety is important with respect to apoptosis: bi-methylation seems to favor apoptosis induction more strongly than mono-methylation. Dependency on the presence or absence of the hormone-like moiety does not seem to occur.

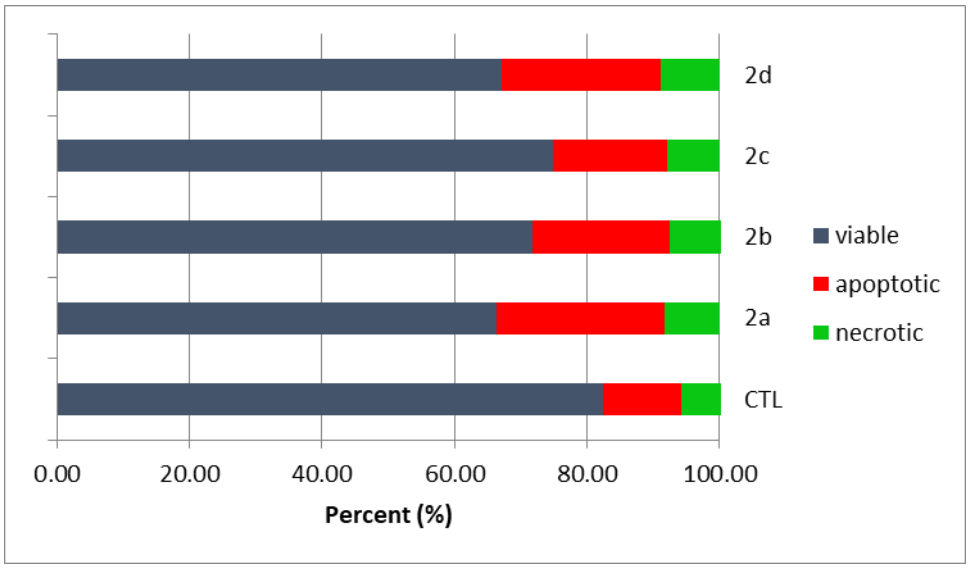

Fig. 15: Apoptotic/necrotic cells in HCT-116 spheroids after 48 hours of treatment with equimolar combinations of thiosemicarbazones 2a–2d and copper(II) chloride compared to untreated control (CTL). *The percentages of apoptotic and necrotic cells in spheroids were assessed by flow cytometry upon exposure to the compounds at their respective IC_{50} + s.d. and application of an apoptosis-specific fluorescent marker (annexin V-FITC) as well as PI. Bars represent mean values from analysis of at least 5–6 spheroids per condition in at least two independent experiments.*

Immunocytochemistry

Qualitative assessment of apoptosis was achieved by immunocytochemistry after 96 hours of treatment with the respective compound (at IC_{50} + s.d.).

Compared to controls, KI-67 staining for HCT-116 spheroids treated with combinations of compounds **2a**–**2d** and copper(II) chloride demonstrated roughly comparable amounts of proliferating cells, but stained cells seemed to accumulate primarily at the outer edge, except for **2d**-treated spheroids where proliferation appears reduced (*Fig. 16a*).

Pictures taken from the edges of spheroids, which were stained against cleaved caspases 3 and 7, revealed a complementary pattern: apoptosis staining occurred mainly in the core region of spheroids under three out of the four tested conditions. **2a**, **2c** and **2d** seemed to induce apoptosis almost exclusively in spheroid cores (more or less distinct), whereas **2b**-treated spheroids did not seem to accumulate apoptotic cells in any region (*Fig. 16b* and *16c*).

Additionally, qualitative pictures of cleaved caspase 3 and 7 stainings (*Fig. 16b* and *Fig. 16c*) confirmed that compounds **2a** and **2d** induce higher amounts of apoptotic cells (compare section above).

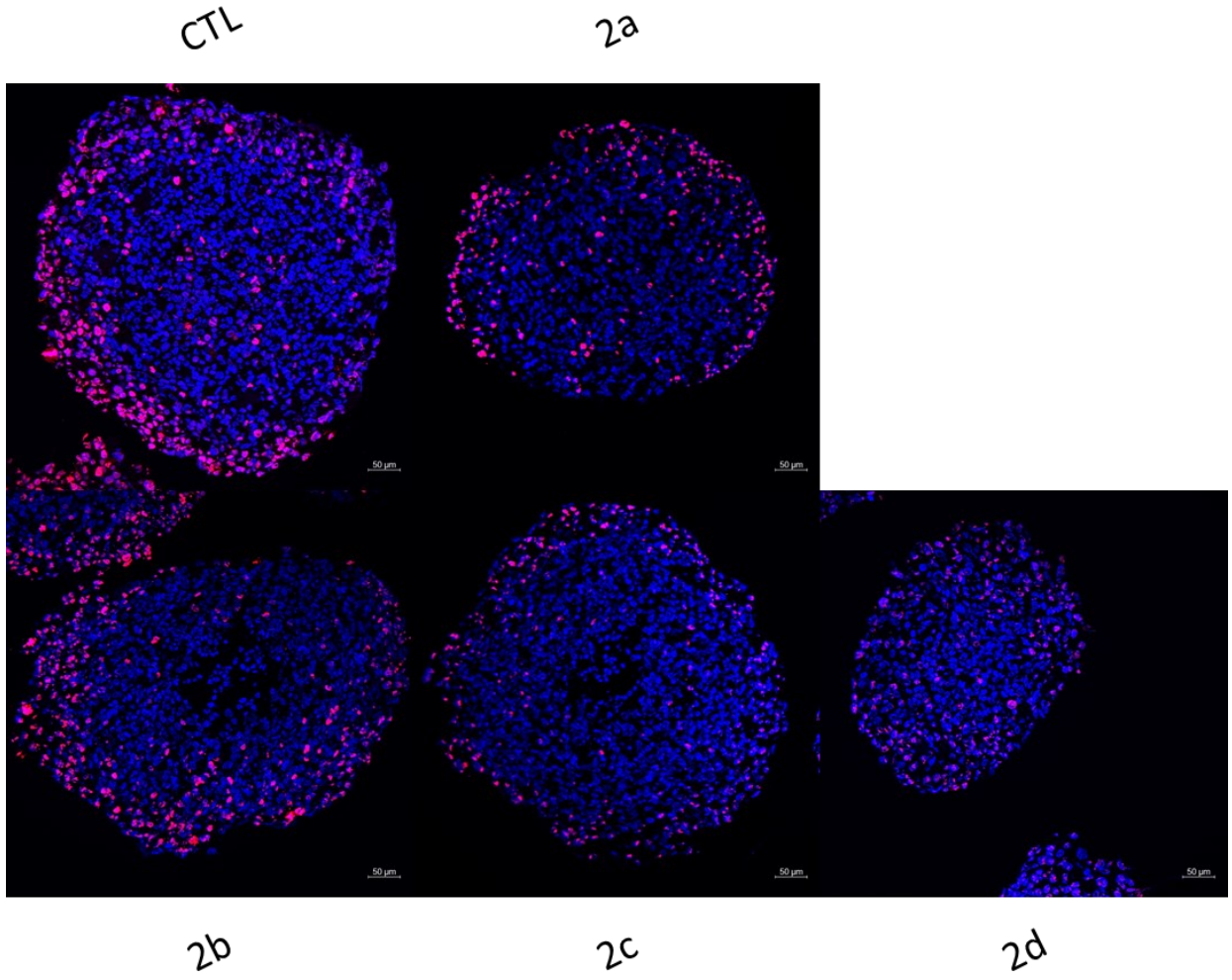

Fig. 16a: Representative immunocytochemical images of HCT-116 spheroids stained against KI67 after 96 hours of treatment with 2a–2d [+ Cu^{2+}] compared to untreated control (CTL). *Spheroids were initially tagged with a primary antibody against the cell proliferation marker KI67 and then with a fluorescently labeled secondary antibody (= red dots). Additionally, DNA was stained with DAPI to visualize the nuclei (= blue dots). Pictures were taken with a confocal laser-scanning microscope (Zeiss LSM 800) with a 20x magnification lens.*

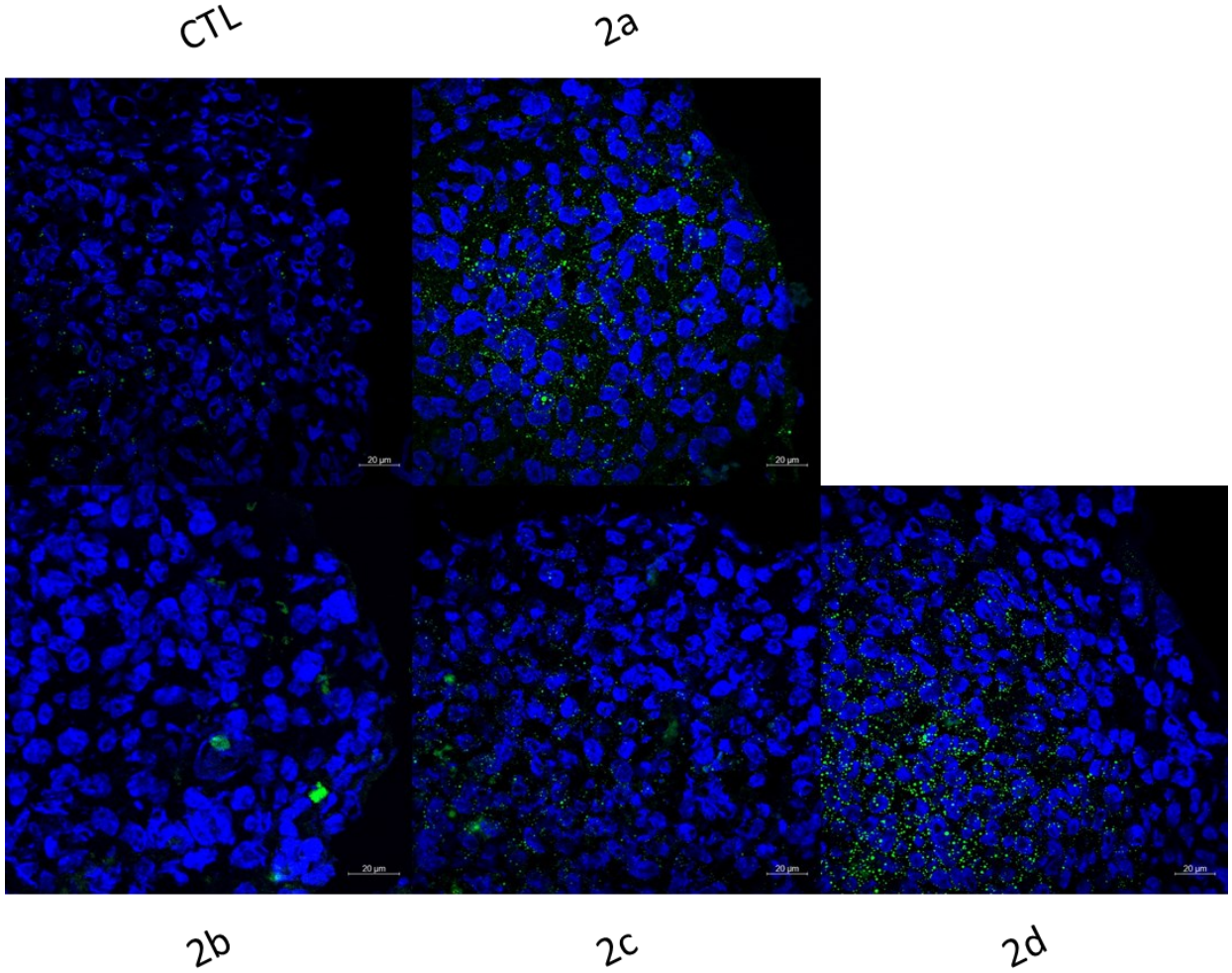

Fig. 16b: Representative immunocytochemical images of HCT-116 spheroids stained against cleaved caspase 3 after 96 hours of treatment with 2a–2d [+ Cu^{2+}] compared to untreated control (CTL). *Spheroids were initially tagged with a primary antibody against the apoptosis-specific marker cleaved caspase 3 (active form of caspase 3), and then with a fluorescently labeled secondary antibody (= green dots). Additionally, DNA was stained with DAPI to visualize the nuclei (= blue dots). CTL (neg. control) showed no to low signals, as expected. Pictures were taken with a confocal laser-scanning microscope (Zeiss LSM 800) with a 63x magnification lens.*

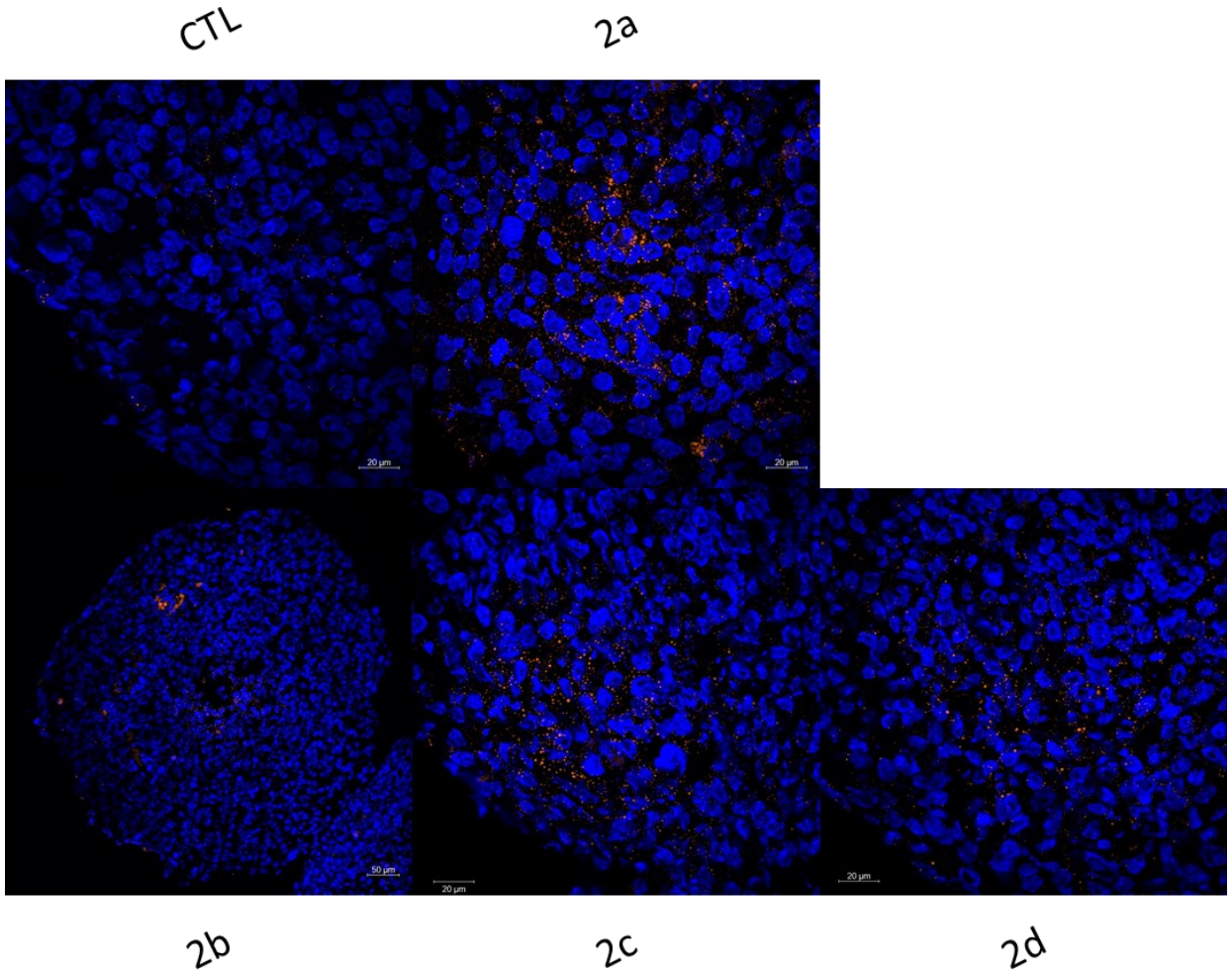

Fig. 16c: Representative immunocytochemical images of HCT-116 spheroids stained against cleaved caspase 7 after 96 hours of treatment with 2a–2d [+ Cu^{2+}] compared to untreated control (CTL). *Spheroids were initially tagged with a primary antibody against the apoptosis-specific marker cleaved caspase 7 (active form of caspase 7), and then with a fluorescently labeled secondary antibody (= orange dots). Additionally, DNA was stained with DAPI to visualize the nuclei (= blue dots). CTL (neg. control) showed no signals, as expected. Pictures were taken with a confocal laser-scanning microscope (Zeiss LSM 800) with a 63x magnification lens.*

Synopsis of Project 2

For the combination of thiosemicarbazones and copper(II) chloride the following results were obtained:

Cytotoxicity tests yielded IC_{50} values in a rather narrow one-digit to low two-digit micromolar concentration range in all tested spheroid types, with no dependency on the chemical structure. Three out of four complexes caused deceleration of spheroid growth and one even decreased their sizes.

Tests for ROS induction in multicellular tumor spheroids indicated that three of the four compounds increased the levels of reactive oxygen species, but to different extent with no clear-cut structure dependency.

A quantitative apoptosis assay (48 hours exposure) showed induction of apoptosis, which was confirmed by a qualitative immunofluorescence method (after exposure for 96 hours). Additionally, the importance of a bi-methylated thiosemicarbazone moiety was observable in the quantitative assay and supported by immunocytochemical images.

Ru/Rh-arene complexes (Project 3)

AlamarBlue Assay

The compounds of the last project comprised of Rh(III) and Ru(II) in the center of piano-stool structures featuring a bidentate thiopyridone moiety and methylimidazole (**3a**–**3c**), pta (**3d**–**3f**) or thiourea (**3g**) as a leaving group. IC_{50} values in multicellular tumor spheroids grown from four different cancer cell lines were obtained by the AlamarBlue assay and are listed in Table 3.

Most of the complexes showed rather low activities in all four investigated cell lines, only the Ru complex **3f** demonstrated very high activity in the lung carcinoma cell line A549 and in the ovarian teratocarcinoma cell line (CH1/PA-1). For the two colon carcinoma cell lines (HCT-116 and HT29) low to no activity was observable for this compound. For the Rh complexes **3c** and **3d**, moderate IC_{50} values in all cancer cell lines or at least in A549 and CH1/PA-1 spheroids were obtained, respectively. It is hence tempting to speculate that a Rh-pentamethylcyclopentadienyl analog of compound **3f** might combine the most favorable features.

Table 3: IC_{50} values (in µM) obtained with the AlamarBlue assay after 96 h of treatment of multicellular tumor spheroids with Ru/Rh-arene complexes. *Four different cancer cell lines (derived from diverse tissues) were used for assessing the cytotoxicity of compounds **3a**–**3g**. IC_{50} values (interpolated from concentration-effect curves in Fig. 17a and Fig. 17b) are represented by mean ± s.d. from at least three independent experiments. IC_{50} values >400 µM were not determined and compound considered inactive in the respective spheroid model.*

compound	A549	CH1/PA-1	HCT-116	HT29
3a	130 ± 6	146 ± 5	108 ± 10	236 ± 14
3b	> 400	253 ± 16	283 ± 7	235 ± 59
3c	127 ± 5	65 ± 4	56 ± 10	74 ± 2
3d	245 ± 29	71 ± 1	17 ± 10	176 ± 7
3e	154 ± 23	39 ± 1	263 ± 43	> 400
3f	0.44 ± 0.10	1.4 ± 0.6	318 ± 8	> 400
3g	139 ± 2	117 ± 4	242 ± 29	293 ± 28

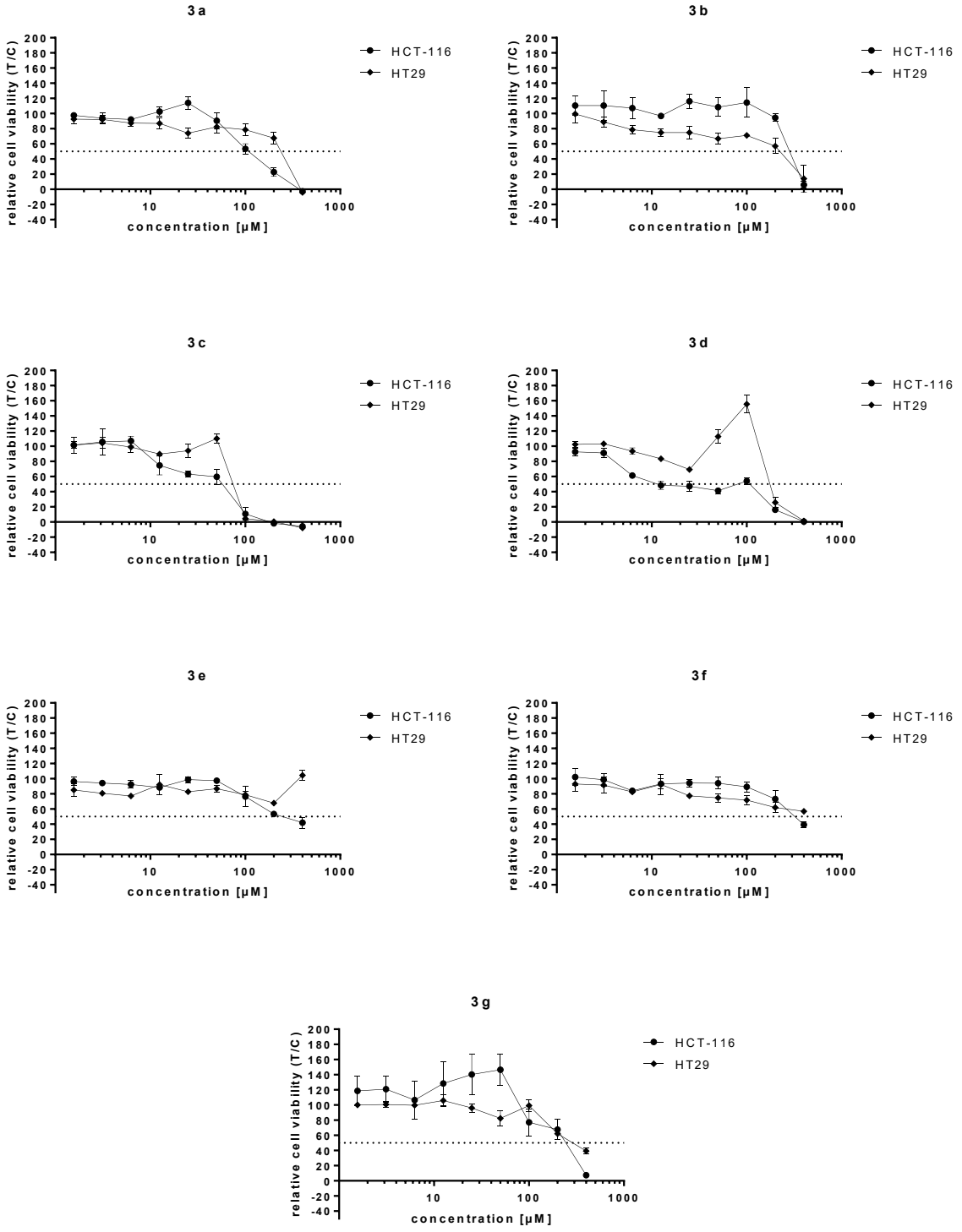

Fig. 17a: Concentration-effect curves of Ru(II)- and Rh(III)-thiopyridone complexes 3a–3g in HCT-116 and HT29 spheroids. *The depicted curves (relative cell viability vs concentration) were obtained for all seven tested compounds by means of the AlamarBlue assay. IC_{50} values were interpolated and are listed in Table 3.*

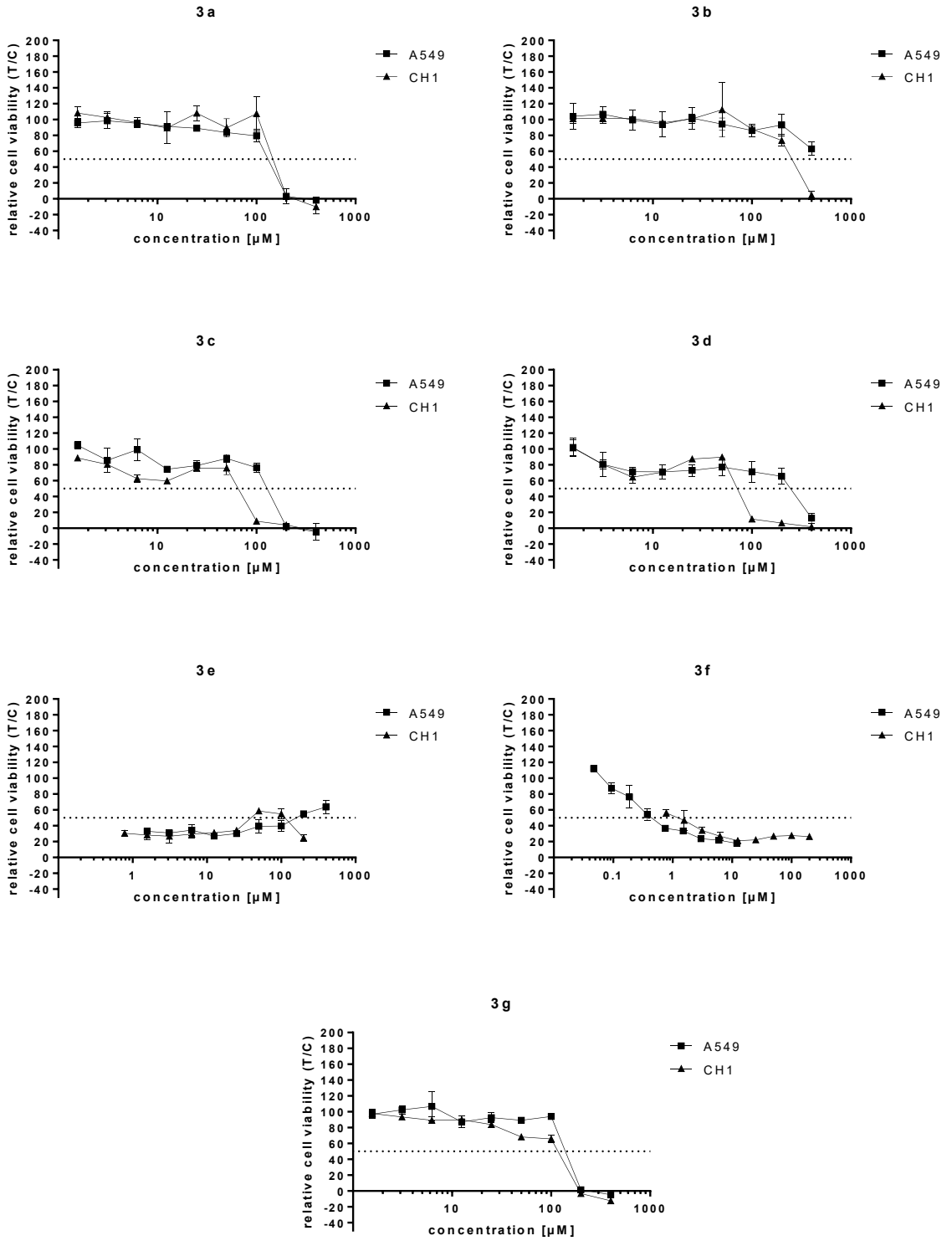

Fig. 17b: Concentration-effect-curves of Ru(II)- and Rh(III)-thiopyridone complexes 3a–3g in A549 and CH1/PA-1 spheroids. *The depicted curves (relative cell viability vs concentration) were obtained for all seven tested compounds by means of the AlamarBlue assay. IC_{50} values were interpolated and are listed in Table 3.*

Growth of spheroids

The impact of compounds **3a**–**3g** on spheroid growth was assessed with HCT-116 cells.

This experiment demonstrated the effectivity in slowing down growth over 96 hours. One of the compounds (**3g**) even reduced spheroid size compared to the initial diameter by approximately 13% (*Fig. 18*, *top*).

Regarding the effects on shapes of spheroids (*Fig. 18*, *bottom*), **3b** caused the most conspicuous changes: treated spheroids presented with a dense core surrounded by an enormous ring of quite loosely bound cells and irregular outgrowths. None of the other complexes induced such drastic changes, but all of them caused to some extent an appearance consisting of a compressed core (taken for measurements of spheroid diameters) and small outgrowths. (Note: Spheroids before and after treatment with **3e** showed more ovoid forms than all the others; this might be explained by the fact of precipitated compounds of FCS within the medium. During the experiment it was observable that a few spheroids grow along such precipitated factors, which determined another overall structure for the spheroids.)

With this experiment, the cytostatic features of Ru(II) and Rh(III) complexes could be demonstrated, whereby one Ru compound (**3g**) revealed a pronounced cytotoxic behavior.

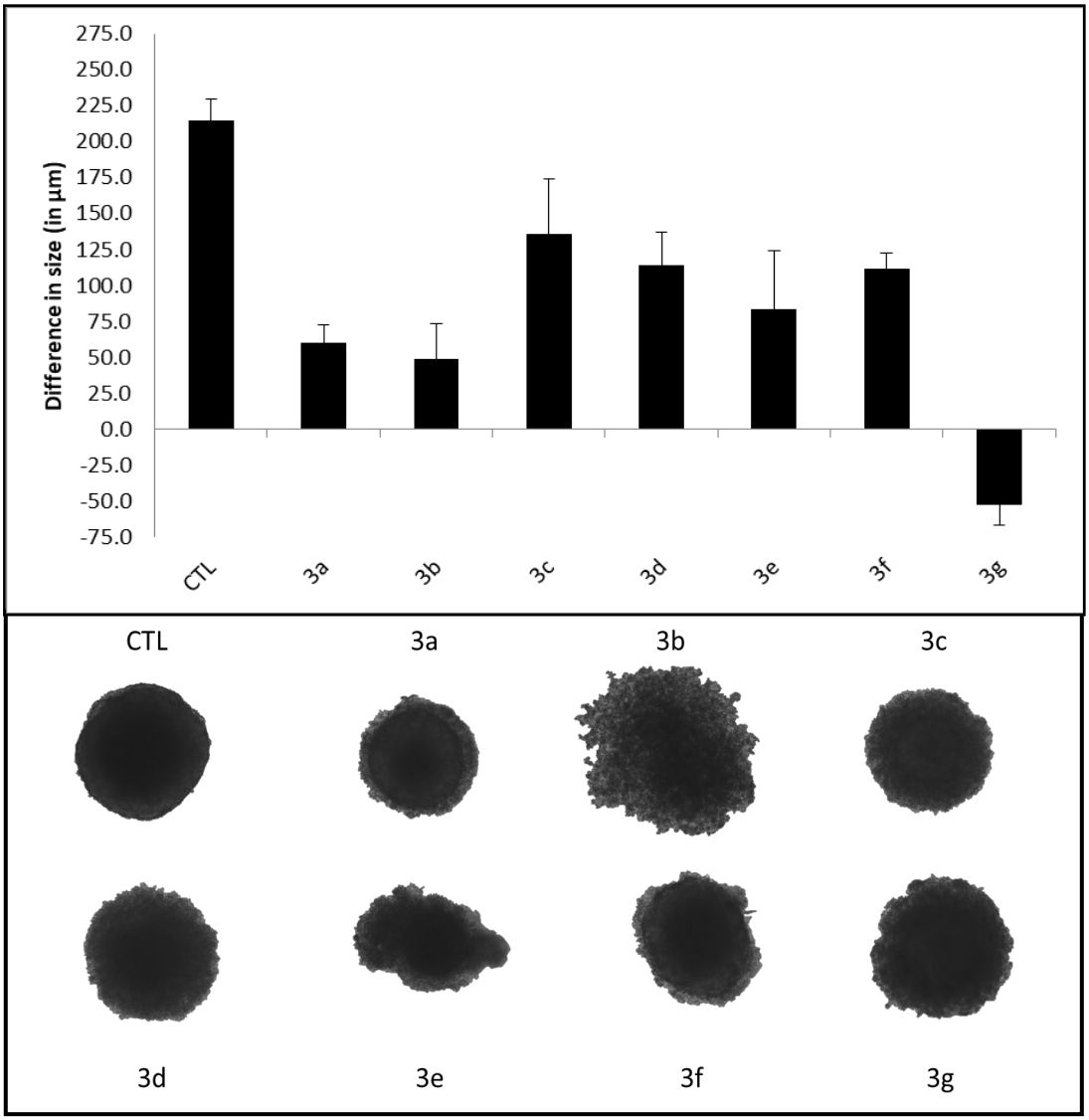

Fig. 18: Growth of HCT-116 spheroids within 96 hours of treatment with Ru(II)/Rh(III)-thiopyridone complexes 3a–3g. *Size differences obtained by measuring spheroid sizes before (0 h) and after treatment (96 h) (top) compared to untreated controls (CTL). Representative pictures of spheroid shape and size after 96 hours of treatment with the respective compound (bottom). Values were averaged over at least 5–6 spheroids per condition. All spheroids were treated with the mean IC_{50} + s.d. of the respective compound.*

ROS Assay

ROS induction in spheroids was measured by flow cytometry after 24 hours of treatment with the test compounds and results are depicted in *Fig. 19*. Compared to untreated controls, three substances (**3a**, **3c** and **3d**) did not alter the levels of cells with enhanced ROS significantly, whereas **3e**, **3f** and **3g** increased these levels by 2.3-fold, 4.2-fold and 2.3-fold, respectively, and **3b** decreased them by 77%. Hence, this approach revealed tremendous activity for two substances (**3b** and **3f**) which, interestingly, showed opposing effect. For further insights, apoptosis was assessed quantitatively and qualitatively, as described in the next section.

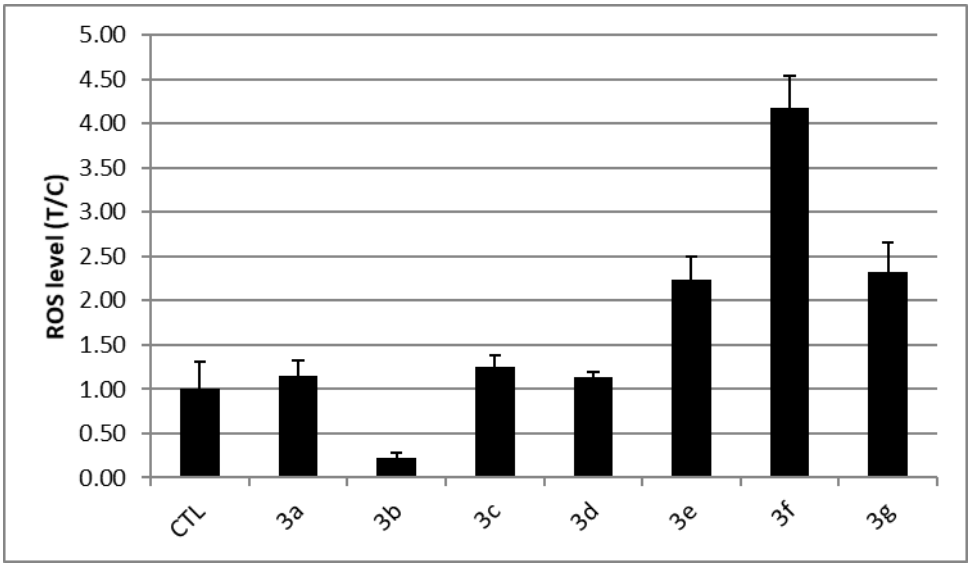

Fig. 19: ROS levels of HCT-116 spheroids after 24 hours of treatment with Ru(II)/Rh(III)-thiopyridone complexes 3a–3g. *After exposure to test compounds at their respective IC_{50} + s.d, ROS levels were measured via flow cytometry upon double-staining with PI (to exclude necrotic cells) and CellRox. Columns represent values (mean ± s.d.), which were obtained from at least 5–6 spheroids per condition (IC_{50} + s.d.) in at least two independent experiments.*

Apoptosis Assay

The quantitative approach of measuring apoptotic and necrotic cells within HCT-116 spheroids after treatment with Ru/Rh-thiopyridone complexes revealed that all ot these substances induced a considerable extent of apoptosis after 48 hours of treatment (*Fig. 20*). Values varied between 2-fold (**3c**) and 7-fold (**3b**) increases, compared to control samples. Intriguingly, although ROS levels decreased after 24 hours of treatment, **3b** seemed to enormously induce apoptosis after 48 hours. Those results point to different triggers (other than reactive oxygen species) in the induction of apoptosis by this specific compound.

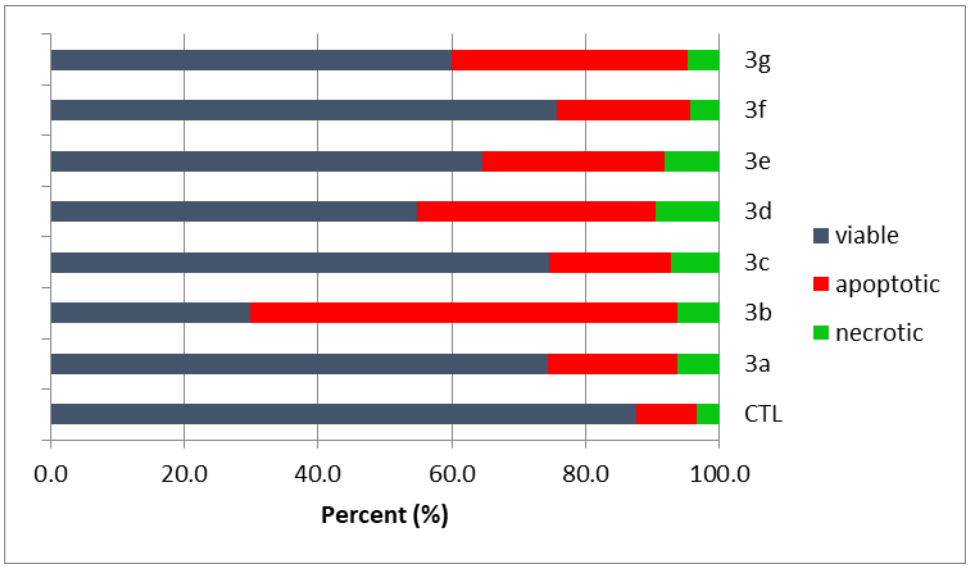

Fig. 20: Apoptotic/necrotic cells in HCT-116 spheroids after 48 hours of treatment with Ru(II)/Rh(III)-thiopyridone complexes 3a–3g compared to untreated control (CTL). *The percentages of apoptotic and necrotic cells in spheroids were assessed by flow cytometry upon exposure to the compounds at their respective IC_{50} + s.d. and application of an apoptosis-specific fluorescent marker (annexin V-FITC) as well as PI. Bars represent mean values from analysis of at least 5–6 spheroids per condition in at least two independent measurements.*

Immunocytochemistry

Qualitative assessment of apoptotic cells within HCT-116 spheroids did not correspond well with results of the quantitative assay, however: Images taken upon KI-67 staining (*Fig. 21a*) show that spheroids contained viable, proliferative cells in tremendous amounts, but their distribution appeared quite dependent on the test compound. **3c**-, **3d**-, **3e**- and **3g**-treated spheroids showed a distribution of proliferating cells throughout the entire cross-sections, whereby **3c**- and **3d**-spheroids seemed to comprise less of them than the other ones. In control samples and **3f**-treated samples, concentration of proliferating cells at the edge of spheroids was observed. On the contrary, **3a**-treated samples showed a concentration of proliferating cells in the spheroid cores.

Apoptosis staining (*Fig. 21b* and *Fig. 21c*) did not yield the anticipated results: against expectation, only a few stained cells per spheroid cross-section were actually observable. But although the number of apoptotic cells was not as high as expected, a small increase was found in treated samples compared to untreated ones. Unfortunately, no pictures could be taken of **3b**-treated spheroids. Most likely, the fixation step before staining was not appropriate for those spheroids. The peculiar appearance mentioned above and discernible in *Fig. 18 (bottom)*, suggests that cell-cell contacts might have been lost or substantially weakened, which is why spheroid sections were washed off the slides.

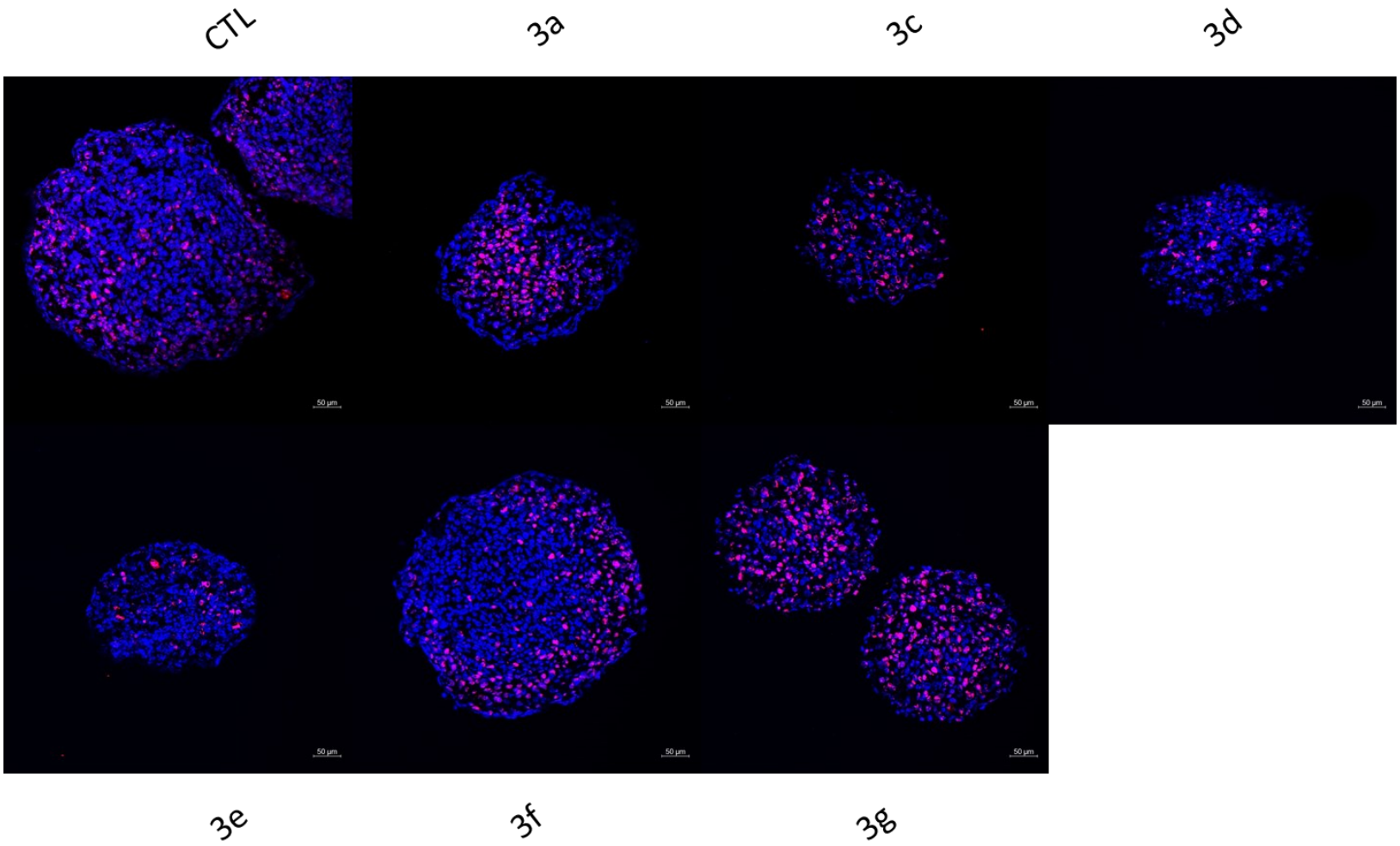

Fig. 21a: Representative immunocytochemical images of HCT-116 spheroids stained against KI67 after 96 hours of treatment with Ru(II)/Rh(III)-thiopyridone complexes (3a–3g) compared to untreated control (CTL). *Spheroids were treated with the IC_{50} + s.d. of the respective compound, tagged with a primary antibody against the cell proliferation marker KI67 and then with a fluorescently labeled secondary antibody (= red dots). Additionally, DNA was stained with DAPI to visualize the nuclei (= blue dots). Pictures of **3b**-treated spheroids were not possible to take, due to their disintegration during sample preparation. Pictures were taken with a confocal laser-scanning microscope (Zeiss LSM 800) with a 20x magnification lens.*

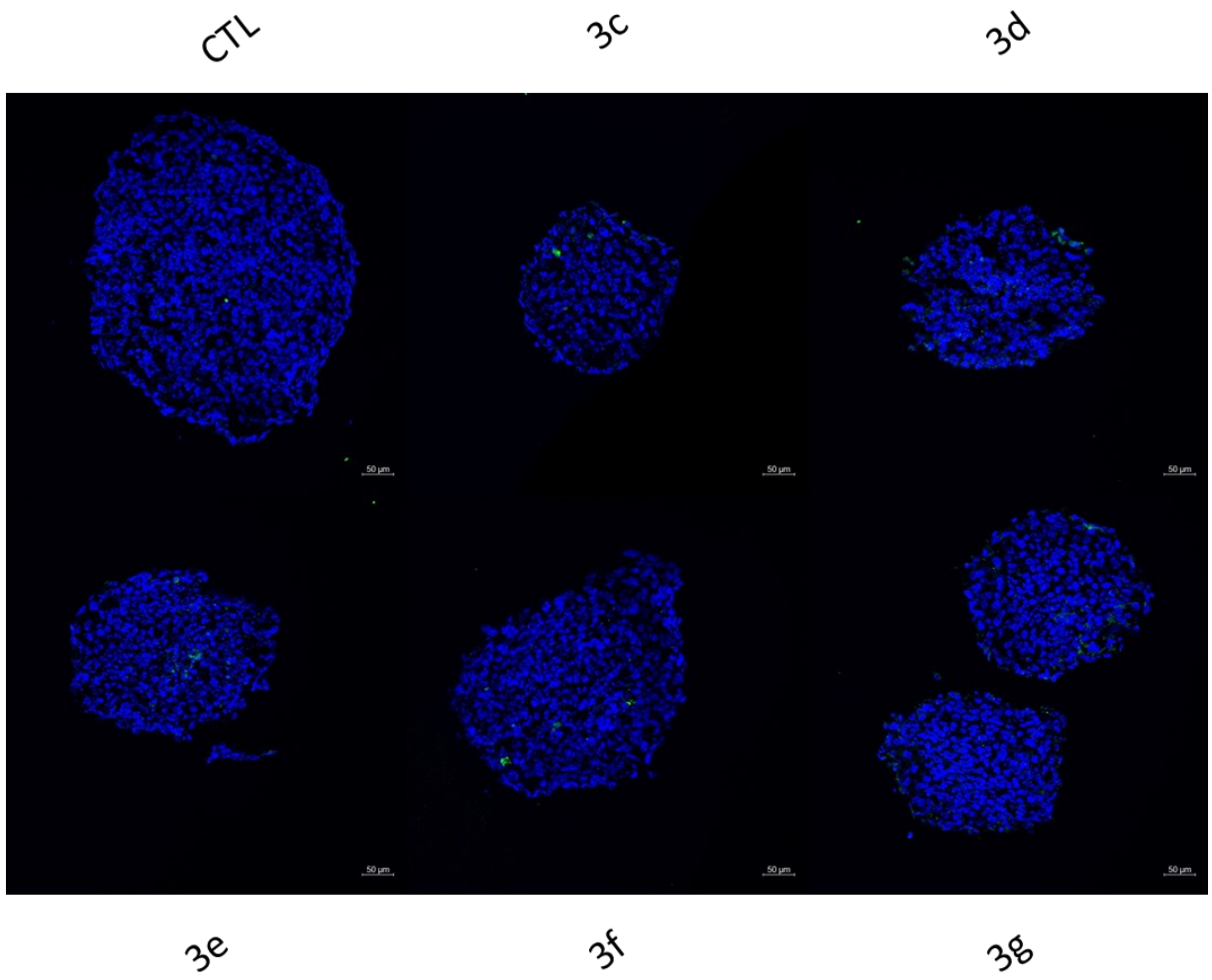

Fig. 21b: Representative immunocytochemical images of HCT-116 spheroids stained against cleaved caspase 3 after 96 hours of treatment with Ru(II)/Rh(III)-thiopyridone complexes (3c–3g) compared to untreated control (CTL). *Spheroids were treated with the IC_{50} + s.d. of the respective compound, tagged with a primary antibody against the apoptosis marker cleaved caspase 3 (active form of caspase 3) and then with a fluorescently labeled secondary antibody (= green dots). Additionally, DNA was stained with DAPI to visualize the nuclei (= blue dots). Pictures of **3a**- and **3b**-treated spheroids were not possible to take, due to their disintegration during sample preparation and. Pictures were taken with a confocal laser-scanning microscope (Zeiss LSM 800) with a 20x magnification lens.*

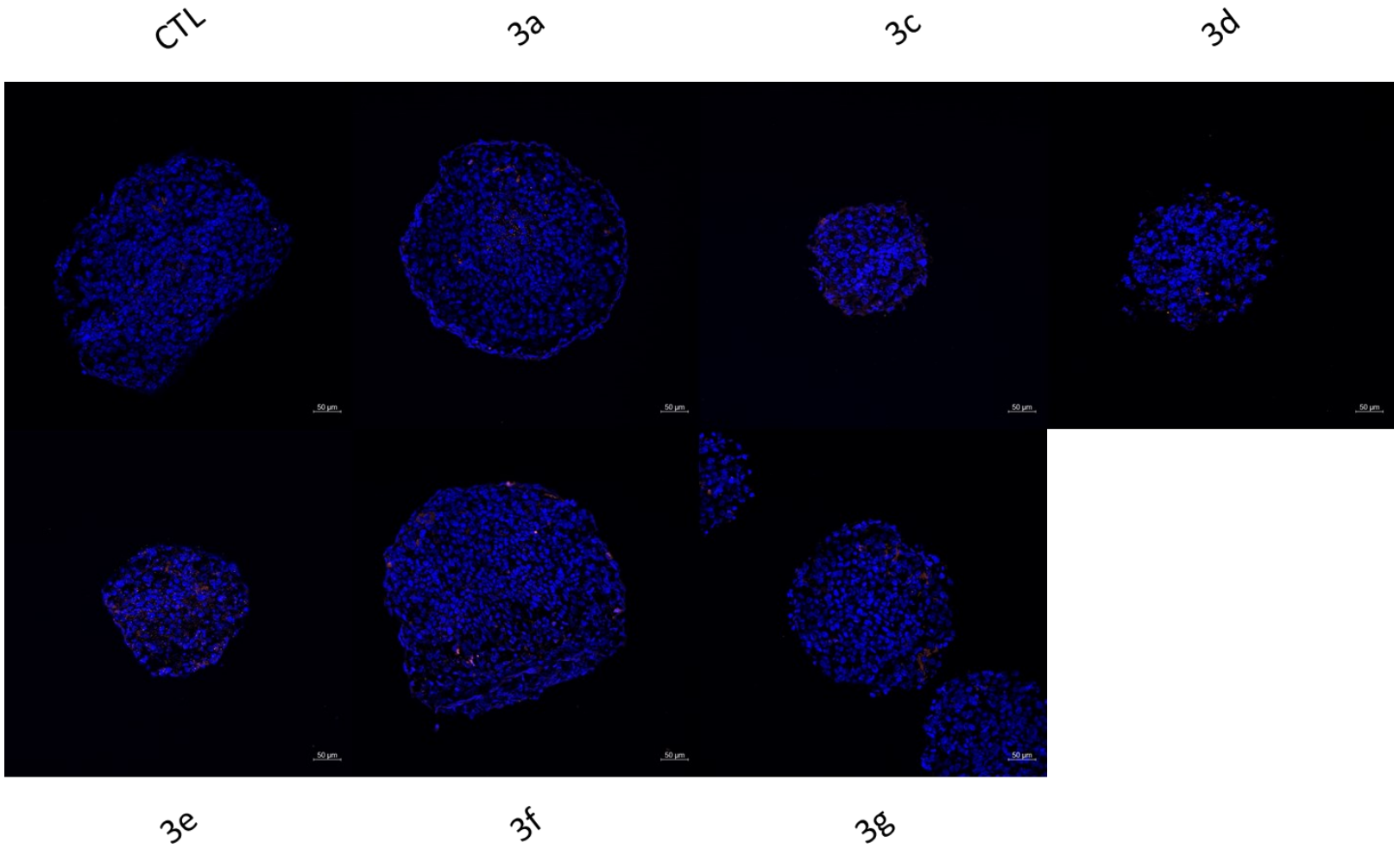

Fig. 21c: Representative immunocytochemical images of HCT-116 spheroids stained against cleaved caspase 7 after 96 hours of treatment with Ru(II)/Ru(III)-thiopyridone complexes (3a–3g). *Spheroids were treated with the IC_{50} + s.d. of the respective compound, tagged with a primary antibody against the apoptosis marker cleavedcaspase 7 (active form of caspase 7) and then with a fluorescently labeled secondary antibody (= orange dots). Additionally, DNA was stained with DAPI to visualize the nuclei (= blue dots). Pictures of **3b**-treated spheroids were not possible to take, due to their disintegration during sample preparation. Pictures were taken with a confocal laser-scanning microscope (Zeiss LSM 800) with a 20x magnification lens.*

Plasmid Assay

This approach was solely chosen for the Ru(II) and Rh(III) thiopyridone complexes, in order to gain new insights in DNA-Ru/Rh-interactions. Although this method does not employ cells, its results may still be relevant for both 2D and 3D cell culture settings.

Electrophoretic separation of different DNA conformations (of bacteria-derived plasmid DNA in this case) can prove particularly helpful, when it comes to investigating dynamic changes. For this thesis, interactions between DNA and test substances were monitored by incubating both for different periods of time (from 15 minutes to 6 hours). Then, different conformations of plasmid DNA were separated by electrophoretic flow through an agarose gel. The amounts of each DNA conformation after incubation with the respective test substance can be assessed in *Fig. 22a*. In order to quantify the bands of each lane, those electropherograms were further analyzed with ImageJ software (*Fig. 22b*).

Fig. 22b shows that interactions between DNA and the test compounds were found for five out of seven substances to a rather low, but consistent extent (only up to 15% conversion into the open-circular form). Conversion of the supercoiled (sc) plasmid to its spatially larger open-circular (oc) form can be observed when single strand breaks of plasmid DNA occur caused by the test compounds. Alternatively, cross-linking of various plasmids' strands by the test substances can yield the same apparent size, and hence the same migration speed in electrophoresis, of the oc-form. The exact mode of the conversion could not be elucidated in this work. All other complexes (**3a** and **3c**) did not induce any significant conformational change.

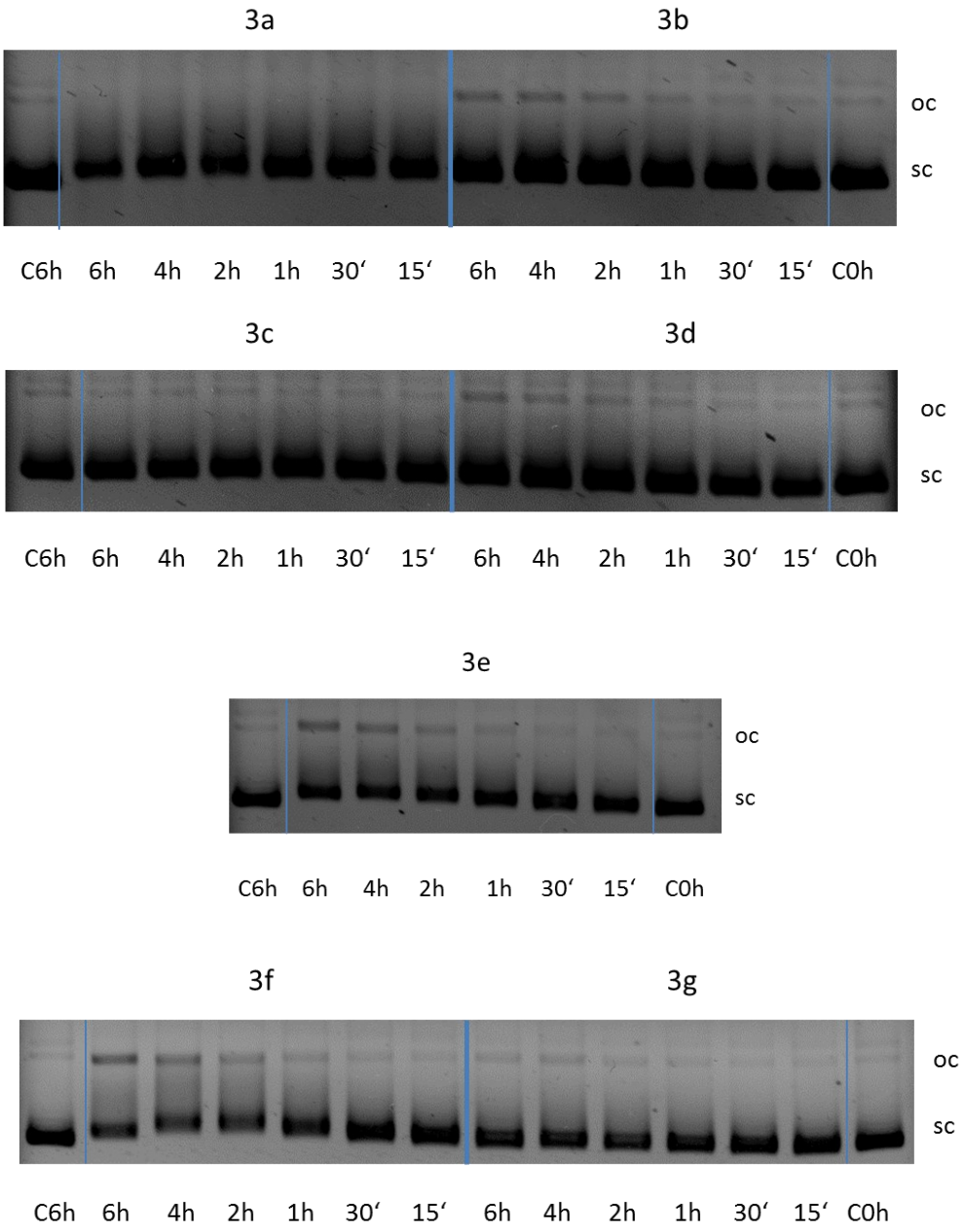

Fig. 22a: Representative electropherograms indicating pUC19 plasmid DNA conformational changes during treatment with Ru(II) and Rh(III)-thiopyridone complexes 3a–3g. *Interaction between the compounds and DNA was studied with a cell free approach after different time points (15 minutes to 6 hours) by agarose gel electrophoresis. SC (supercoiled) represents the plasmid's predominant native form, whereas the OC (open circular) form is mostly (but to low extent) induced by the interaction with test substances. C0h and C6h represent untreated DNA after 0 hours (no shaking and heating) and 6 hours (with shaking and heating as for treated samples), respectively.*

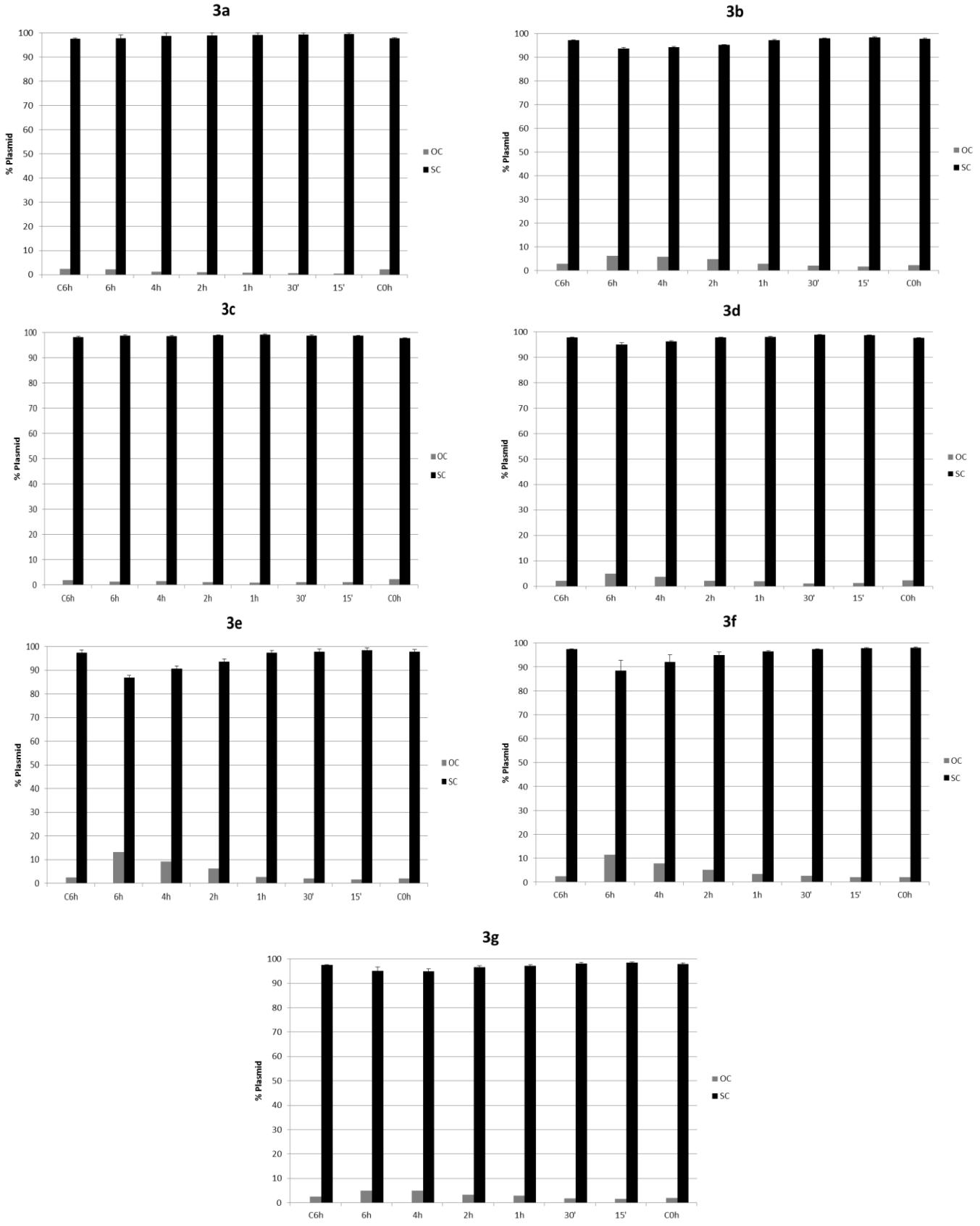

Fig. 22b: Quantitative evaluation of DNA interaction with novel Ru(II) and Rh(III)-thiopyridone complexes (3a–3g). *Electropherograms (Fig. 22a) were evaluated with FlowJo software. SC (supercoiled) represents the plasmid's predominant native form, whereas the OC (open circular) form is mostly (but to low extent) induced by the interaction with test substances. Values are means ± s.d. from at least two independent experiments.*

Synopsis of Project 3

All tested Ru(II)- and Rh(III)-comprising piano-stool complexes showed a low to moderate activity in the AlamarBlue assay, except for **3f** which was highly active in two tested cell lines (ovarian teratocarcinoma CH1/PA-1 and lung carcinoma A549).

One of seven tested compounds induced pronounced cytotoxic properties causing a shrinkage of HCT-116 spheroids, while all other ones rather seemed to have cytostatic features reducing spheroid growth only.

Cells with enhanced ROS within spheroids were observable only in three samples, whereby treatment with **3f** caused the highest numbers of those cells. On the other side, **3b**-treated spheroids showed a significant decrease in such cells.

A quantitative apoptosis assay after 48 hours of treatment showed marked induction of apoptosis by all of the compounds. In **3b**-spheroids, more apoptotic cells were observed than in any other treated sample. However, a qualitative assessment by immunocytochemical staining did not confirm those results appropriately.

A DNA-interaction study revealed quite low amounts of conformational changes in the tested plasmid, which indicated that five out of seven compounds interacted with DNA, though to a rather low extent.

Discussion

In this work, simple 3D cancer cell culture models, i.e. multicellular tumor spheroids[57-61], have been employed in order to study various aspects of the biological activity of rather diverse novel metal complexes and metal chelators. This approach creates settings that resemble actual tumor tissue much more closely than conventional 2D (monolayer) cultures which are well-established for decades, in particular with regard to extensive intercellular interactions, long diffusion paths, and physiochemical gradients, which are all relevant for the efficacy of potential antitumor drugs.

Many metal-based potential anticancer substances have been investigated since a serendipitous observation made by Rosenberg in the 1960s[36-39]. He had found that cisplatin, an already known substance then and an indispensable anticancer drug now, as well as related Pt(II) and Pt(IV) complexes inhibit cell division in *E. coli* and confirmed these effects in animal tumor models soon after. The discovery of this antiproliferative property was the starting point for investigating and widely searching for other metal-based substances with features suitable for the needs of modern cancer chemotherapy.

In the context of this work, three classes of compounds have been chosen to be studied in spheroid models:

Diverse **Pt(IV) (pro)drugs** demonstrated a broad range of cytotoxicities in the AlamarBlue assay. Obtained IC_{50} values varied between 130 nM for **1f** in CH1/PA-1 and >400 µM for **1c** and **1d** in A549 and HCT-116 spheroids. Similarly, the respective IC_{50} values in 2D cultures indicated the highest activity for **1f** in CH1/PA-1 cells (20 nM), and the lowest for **1c** as well as **1d** (>160 µM) in A549 cells.[86-89] Such remarkable differences can be caused by various structural properties, like lipophilicity of the compounds or stability of bonding between the metal center and the equatorial and axial ligands, the latter being inextricably linked with redox chemistry of the complexes. According to previous studies, di- or tetracarboxylato Pt(IV) compounds (including representatives tested in this work) might be sufficiently stable and inert to be specifically activated at the cancer site.[86-90] Hypoxic and acidic conditions within a tumor favor the reduction of inert Pt(IV) compounds to their active Pt(II) congeners.

Elongating the alkyl chains of equatorial or axial ligands influences lipophilicity, and hence in most cases cytotoxicity, tremendously: while improving lipophilic features in axial positions, in equatorial positions those chains might negatively affect compound activity.[87,88] Those aspects were confirmed in our three-dimensional studies for **1c** and **1d** in CH1/PA-1 multicellular spheroids. Another issue, which need to be considered for cytotoxic properties, is the bulkiness of the leaving groups. While ordinary alkyl chains in equatorial positions may lower the activity as in **1c**, halogenated chains have a positive impact as in **1e**. The trifluoropropanoato ligand lowers electron density around the Pt-center and enhances its reactivity.[90] The stable nitrogen ligands in Pt(IV) complexes stabilize the whole scaffold, but there is no clear evidence in 2D approaches whether mono- or bidentate nitrogen donor ligands should be employed (cf. ref. 88). While testing the seven representatives (**1a**–**1g**) in three-dimensional cytotoxicity experiments, it became obvious that small leaving equatorial moieties, as well as small monodentate equatorial nitrogen-containing groups and (large) lipophilic axial groups influence cytotoxicity tremendously, exactly analogous to the two-dimensional approaches. An apparent order of cytotoxicity was observable in all tested models: **1f** > **1b** ≥ **1g** > **1e** > **1a** > **1d** ≥ **1c**.

Compound **1b** is also known as satraplatin, which has already been evaluated in clinical phase III trials, but was rejected after no statistically significant improvement in overall survival time compared to already established therapeutics was recognizable (cf. ref. 90). In our 3D experiments, satraplatin (**1b**) showed excellently low IC_{50} values, as well as marked growth inhibition and at least a slight induction of apoptosis. Only generation of ROS was not discernible in our models. Growth inhibition of multicellular spheroids occurred after treatment with all other tested complexes, with an extraordinary effect of **1f**, which seemed to have more cytocidal impact on spheroid growth. Elevated reactive oxygen species and a possible increase of apoptotic cells are not necessarily correlated in 3D approaches though: **1d** and **1e** showed the strongest impact on ROS levels in HCT-116 multicellular spheroids, but no enhanced induction of apoptotic cells, whereas **1f** yielded elevated ROS levels as well as apoptotic cells.

While all representatives of this class demonstrated more or less distinct antiproliferative properties, compound **1f** showed in almost every employed

experiment the highest potency, hence further investigation of its cytotoxic behavior in more advanced approaches is suggested. Experiments under hypoxic conditions might also be helpful to extend our knowledge on Pt(IV) anticancer substances.

Thiosemicarbazones (applied in equimolar combination with a simple copper(II) salt) indicated in our 3D models that bi-methylation of the terminal nitrogen might be favorable for cytotoxic potency. Similar conclusions have been made by *Heffeter et al*.[51] Terminal bi-methylation of thiosemicarbazones was shown to enhance cytotoxic activity enormously. *Enyedi et al.*[91] showed that differences in thiosemicarbazone stability occurred, when Ga(III), instead of Cu(II), was chelated. Results demonstrated a fairly more stable chelation with Cu(II), whereas ordinary semicarbazones seem to bind Ga(III) more tightly. This might be explainable according to the HSAB concept: Cu(II) as a relatively soft Lewis acid binds preferably and tightly to the sulfur atom in thiosemicarbazones, while Ga(III) needs the "hard" properties of the oxygen atom in semicarbazones. Additionally, this study employed semicarbazones (combined with a Cu(II) salt solution) in 2D cell experiments. Estrone, as well as tetrahydronaphthalene, demonstrated low (CH1/PA-1) to moderate (A549) IC_{50} values, comparable to those obtained in this work for the 3D approach. All methylated thiosemicarbazones (**2a**–**2d**) seem to be more active (two- to four-fold higher activity) in A549 multicellular spheroids than unmethylated semicarbazones in 2D, and only slightly more inert in CH1/PA-1 spheroids than in monolayers. All tested compounds showed growth inhibition and apoptosis induction after 48 hours of treatment. Terminal di-methylation seemed to be favorable for inducing apoptosis; however, for the other experiments there was no clear consistence observable between compound structure and their respective activities.

Ru(II) and Rh(III) complexes with thiopyridone-derived and arene ligands in piano-stool conformation showed promising cytotoxic behavior.[54, 55] Exceptionally low IC_{50} values were observable for compound **3f** with 440 nM in A549 and 1.4 µM in CH1/PA-1 multicellular spheroids. On the other hand, colon carcinomas HCT-116 and HT29 seemed not to be affected by this complex. Compared to their respective values (600 nM and 0.96 µM in A549 and CH1/PA-1, respectively) reported from 2D experiments, **3f** is comparable active in spheroids as in monolayers of both A549 and CH1/PA-1 cells. This RAPTA-containing complex also contains a relatively small

methylated thiopyridone. Compared to its benzylated congener **3e** its activity is almost 400-fold and 30-fold higher in the non-small cell lung cancer (A549) and ovarian teratocarcinoma (CH1/PA-1) spheroids. According to our 3D cytotoxicity results, it might be possible for Ru(II) thiopyridone piano-stool complexes that smaller bidentate ligands and a bulky leaving group are more favorable for cytotoxic potency in selected cancer cell lines, as it is true for **3f,** compared to all the other Ru(II)-containing compounds. This hypothesis should be confirmed by further testing. For Rh(III) thiopyridone complexes (**3c** and **3d**), results did not hint on preferable structures. All tested compounds inhibited spheroid growth, with exceptional cytotoxic properties of **3g** compared to the other complexes.

Regarding ROS and apoptosis experiments, they demonstrated intriguing effects of a few compounds, especially **3b** and **3f**. On one side, **3b** revealed high induction of apoptosis, but diminished ROS levels in HCT-116 multicellular spheroids. **3f**, on the other hand, induced highest levels of ROS and only moderate amounts of apoptotic cells. Due to the apoptosis induction of all representatives of this class, the mode of action would be intriguing. Therefore, a cell-free interaction assay with plasmid DNA was performed, which revealed interaction of a low extent of a few tested compounds with DNA. These findings do not suggest DNA interactions as the preferred mode of action for this class of substances. After considering all experiments employed, further research on **3f** (or other RAPTA complexes with similar scaffolds) is recommended.

In summary, all of the compounds included in the above-mentioned projects showed advantages and drawbacks in the approach of using multicellular tumor spheroids as 3D cancer models, which had not been applied to these compounds before. Overall, *in-vitro* anti-neoplastic properties could be demonstrated for the majority of tested complexes of Pt(IV) and Ru(II)/Rh(III) as well as copper-chelating thiosemicarbazones.

Their biological activity could be shown excellently with this work. However, to gain more detailed insights into tumor-specific issues, more advanced experiments are suggested. Commonly, signals and activity of tested compounds are lower in spheroids than in conventional 2D cell culture experiments, but results in the former

are expected to be more predictive, due to the higher similarity of 3D cancer models to tumors *in vivo*.[59] Along the already established 2D approaches, 3D models (simple or more advanced) are recommended to be applied more frequently for assessing the activity of novel compounds before *in vivo* experiments are considered. Despite their time and cost intensity, three-dimensional test approaches and their contribution to future cancer-therapeutic strategies should not be underestimated.

List of publications

Harringer, S., Wernitznig, D., Gajic, N., Diridl, A., **Wenisch, D.**, Hejl, M., Jakupec, M. A., Theiner, S., Koellensperger, G., Kandioller, W. & Keppler, B. K., Introducing N-, P-, and S-donor leaving groups: an investigation of the chemical and biological properties of ruthenium, rhodium and iridium thiopyridone piano stool complexes, *Dalton Transactions*, 2020, **49**(44), 15693-15711. doi: 10.1039/d0dt03165h

Wernitznig, D., Meier-Menches, S. M., Cseh, K., Theiner, S., **Wenisch, D.**, Schweikert, A., Jakupec, M. A., Koellensperger, G., Wernitznig, A., Sommergruber, W. and Keppler, B. K., Plecstatin-1 induces an immunogenic cell death signature in colorectal tumour spheroids, *Metallomics*, 2020, **12**, pp. 2121. doi: 10.1039/d0mt00227e

Songoen, W., Phanchai, W., Brecker, L., **Wenisch, D.**, Jakupec, M. A., Pluempanupat, W., and Schinnerl, J., Highly Aromatic Flavan-3-ol Derivatives from Palaeotropical Artocarpus lacucha Buch.-Ham Possess Radical Scavenging and Antiproliferative Properties, *Molecules,* 2021, **26**(4), pp. 1078. doi:10.3390/molecules26041078

Enyedi, É. A., Petrasheuskaya, T. V., Kiss, M. A., Wernitznig, D., **Wenisch, D.**, Keppler, B. K., Spengler, G., May, N. V., Frank, È. and Dömötör, O., Complex formation of an estrone-salicylaldehyde semicarbazone hybrid with copper(II) and gallium(III): Solution equilibria and biological activity, *J. Inorg. Biochem.*, 2021, **220**, pp. 111468. doi: 10.1016/j.jinorgbio.2021.111468

References

1) WHO - World Health Organization (2020), Cancer, accessed on 22. June 2021 from https://www.who.int/health-topics/cancer
2) Ritchie, H. (2018), Causes of Death, accessed on 12. April 2020 from https://ourworldindata.org/causes-of-death
3) WHO – World Health Organization, Globocan 2020 statistics, accessed on 22. June 2021 from https://gco.iarc.fr
4) United Nations (2019), Worldometer, accessed on 15. April 2020 from https://www.worldometers.info/world-population
5) Statistik Austria, Bundesanstalt Statistik, Todesursachen, accessed 24. July 2020 from Todesursachen (statistik.at)
6) ECIS- European Cancer Information System (2020), Austrian cancer estimates, accessed on 22. June 2020 from https://ecis.jrc.ec.europa.eu/
7) IARC – International Agency for Research on Cancer (2010), accessed on 12. April 2020 from http://www-dep.iarc.fr/WHOdb/glossary.htm
8) NCI – National Cancer Institute (2020), What is cancer?, accessed on 25. April 2020 from https://www.cancer.gov
9) Goustin, A. S., Growth Factors and Cancer, *Cancer Research*, 1986, **46**(3), 1015-1029.
10) Dhillon, A. H., MAP kinase signaling pathways in cancer, *Oncogene*, 2007, **26**, 3279-3290. doi: https://doi.org/10.1038/sj.onc.1210421
11) Sherr, C. J., McCormick, F., The RB and p53 pathways in cancer, *Cancer Cell*, 2002, **2**(2), 103-112. doi: https://doi.org/10.1016/S1535-6108(02)00102-2
12) Yang, J., Weinberg, R. A., Epithelial-Mesenchymal Transition: At the Crossroads of Development and Tumor Metastasis, *Developmental Cell*, 2008, **14**(6), 818-829. doi: https://doi.org/10.1016/j.devcel.2008.05.009
13) NCI – National Cancer Institute (2020), benign tumor, accessed on 27. April 2020 from https://www.cancer.gov
14) NCI – National Cancer Institute (2020), malignancy, accessed on 27. April 2020 from https://www.cancer.gov
15) Kim, J., Dang, C. V., Cancer's Molecular Sweet Tooth and the Warburg Effect, *Cancer Research*, 2006, **66**(18), 8927-30.
16) Berufsverband Deutscher Internisten e.V., Klassifikation von Tumoren, accessed on 27. April 2020 from https://www.internisten-im-netz.de
17) NCI – National Cancer Institute (2020), Types of Cancer Treatment, accessed 25. April 2020 from https://www.cancer.gov
18) NCI – National Cancer Institute (2020), Surgery to Treat Cancer, accessed 25. April 2020 from https://www.cancer.gov
19) Noldus, J., Wann ist bei eingetretener Metastasierung des Prostatakarzinoms die operative Entfernung des Primärtumors angezeigt und gibt es eine wissenschaftliche Grundlage dafür? *Urologe,* 2017, **56,** 591–594. doi: https://doi-org.uaccess.univie.ac.at/10.1007/s00120-017-0359-7
20) Baskar, R., et al., Cancer and Radiation Therapy: Current Advances and Future Directions, *Int. J. Med. Sci*, 2012, **9**(3), 193-199. doi: 10.7150/ijms.3635
21) NCI – National Cancer Institute (2020), Radiation Therapy to Treat Cancer, accessed 04. May 2020 from https://www.cancer.gov

22) NCI – National Cancer Institute (2020), Chemotherapy to Treat Cancer, accessed 04. May 2020 from https://www.cancer.gov
23) Kratz, F., et al., Prodrug Strategies in Anticancer Chemotherapy, *Chem. Med. Chem*, 2008, **3**(1), 20-53. doi: https://doi.org/10.1002/cmdc.200700159
24) NCI – National Cancer Institute (2020), Immunotherapy to Treat Cancer, accessed 04. May 2020 from https://www.cancer.gov
25) Smyth, M. J., et al., Cytokines in cancer immunity and immunotherapy, *Immun. Reviews*, 2004, **202**(1), 275-293. doi: https://doi.org/10.1111/j.0105-2896.2004.00199.x
26) NCI – National Cancer Institute (2020), Targeted Therapy to Treat Cancer, accessed 09. May 2020 from https://www.cancer.gov
27) Brown, C., Targeted Therapy: An elusive cancer target, Nature, 2016, 537, 106-108. doi: https://doi.org/10.1038/537S106a
28) NCI – National Cancer Institute (2020), Hormone Therapy to Treat Cancer, accessed 09. May 2020 from https://www.cancer.gov
29) Davies, C., et al., Long-term effects of continuing adjuvant tamoxifen to 10 years versus stopping at 5 years after diagnosis of oestrogen receptor-positive breast cancer: ATLAS, a randomised trial, *Lancet*, 2013, **381**, 805-816. doi: 10.1016/S0140-6736(12)61963-1
30) Day, J. M., et al., The Development of Steroid Sulfatase Inhibitors for Hormone-Dependent Cancer Therapy, *Steroid Enzymes and Cancer: Ann. N.Y. Acad. Sci.*, 2009, 1155, 80-87. doi: 10.1111/j.1749-6632.2008.03677.x
31) NCI – National Cancer Institute (2020), Precision Medicine in Cancer Treatment, accessed 11. May 2020 from https://www.cancer.gov
32) Your Dictionary, Metallodrug Definiton, accessed 01. April 2020 from https://www.yourdictionary.com
33) Mukherjee, A., Sadler, P. J., Metals in Medicine: Therapeutic Agents. Abstract in: Bagley, T. P., *Wiley Encyclopedia of Chemical Biology* (2007), accessed 15. June 2020. doi: https://doi.org/10.1002/9780470048672.wecb333
34) Mjos, K. D., Orvig, C., Metallodrugs in Medicinal Inorganic Chemistry, *Chem. Rev.*, 2014, **114**, 4540-4563.
35) Guha, R., On Exploring Structure–Activity Relationships. Abstract in: Kortagere, S*., In Silico Models for Drug Discovery. Methods in Molecular Biology (Methods and Protocols)*, 2013, **993,** accessed 15. June 2020**.** doi: https://doi.org/10.1007/978-1-62703-342-8_6
36) Kauffman, G. B., et al., Michele Peyrone (1813-1883), Discoverer of Cisplatin. In: *Platinum Metals Rev.*, 2010, **54**(4), 250-256, accessed 04. Juned 2020. doi: 10.1595/147106710X534326
37) Rosenberg, B., et al., Inhibition of Cell Division in Escherichia coli by Electrolysis Products from a Platinum Electrode. Abstract in: *Nature*, 1965, **205**, 698-699. doi: https://doi-org.uaccess.univie.ac.at/10.1038/205698a0
38) Rosenberg, B., Chapter 2 – Cisplatin: Its history and possible mechanisms of action. Publisher Summary in: *Cisplatin. Current Status and New Developments*, 1980. doi: https://doi.org/10.1016/B978-0-12-565050-2.50006-1
39) Dasari, S., Tchounwou, P. B., Cisplatin in cancer therapy: Molecular mechanisms of action, *European Journal of Pharmacology*, 2014, **740**, 364-378. doi: https://doi.org/10.1016/j.ejphar.2014.07.025
40) Kelland, L., The resurgence of platinum-based cancer chemotherapy, *Nature Reviews Cancer*, 2007, **7**, 573-584.

41) Zhou, J., et al., Immunogenic cell death in cancer therapy: Present and emerging inducers, *J. Cell. Mol. Med.*, 2019, **23**, 4854-4865. doi: 10.1111/jcmm.14356
42) Wernitznig, D., et al., First-in-class ruthenium anticancer drug (KP1339/IT-139) induces an immunogenic cell death signature in colorectal spheroids in vitro, *Metallomics*, 2019, **11**, 1044-1048. doi: 10.1039/c9mt00051h
43) Shu-An Liu, Y. S., et al., Pt(IV) complexes as prodrugs for cisplatin, *Journal of Inorganic Biochemistry,* 2012, **107**(1), 6-14. doi: https://doi.org/10.1016/j.jinorgbio.2011.10.012
44) Johnstone, T. C., et al., Understanding and Improving Platinum Anticancer Drugs-Phenanthriplatin, Anticancer Res., 2014, 34(1), 471-476.
45) Ding, D., et al., Review: Ototoxic Characteristics of Platinum Antitumor Drugs, *The Anatomical Record*, 2012, **295**, 1851-1867. doi: https://doi.org/10.1002/ar.22577
46) Slator, C., et al., Di-copper metallodrugs promote NCI-60 chemotherapy via singlet oxygen and superoxide production with tandem TA/TA and AT/AT oligonucleotide discrimination, *Nucleic Acids Research*, 2018, **46**(6), 2733-2750. doi: https://doi.org/10.1093/nar/gky105
47) Heffeter, P., et al., Anticancer Thiosemicarbazones: Chemical Properties, Interaction with Iron Metabolism, and Resistance Development, *Antioxidants & Redox Signaling*, 2019, **30**(8), 1062-1082. doi: https://doi-org.uaccess.univie.ac.at/10.1089/ars.2017.7487
48) Tisato, F., et al., Copper in Diseases and Treatments, and Copper-Based Anticancer Strategies, *Medicinal Research Reviews*, 2010, **30**(4), 708-749. doi: https://doi-org.uaccess.univie.ac.at/10.1002/med.20174
49) Zhang, Z., et al., Novel copper complexes as potential proteasome inhibitors for cancer treatment (Review), *Molecular Medicine Reports*, 2017, **15**(1), 3-11. doi: https://doi.org/10.3892/mmr.2016.6022
50) Jungwirth, U., et al., Anticancer Activity of Metal Complexes: Involvement of Redox Processes, *Antioxidants & Redox Signaling*, 2011, **15**(4), 1085-1127. doi: http://doi-org.uaccess.univie.ac.at/10.1089/ars.2010.3663
51) Heffeter, P., et al., Impact of terminal dimethylation on the resistance profile of α-N-heterocyclic thiosemicarbazones, *Biochem Pharmacol*, 2012, **83**(12), 1623-1633. doi: 10.1016/j.bcp.2012.03.004
52) Almodares, Z., et al., Rhodium, Iridium, and Ruthenium Half-Sandwich Picolinamide Complexes as Anticancer Agents, *Inorg. Chem.*, 2014, **53**(2), 727-736. doi: https://doi-org.uaccess.univie.ac.at/10.1021/ic401529u
53) Lin, K., et al., Applications of Ruthenium Complex in Tumor Diagnosis and Therapy, Mini Review Article in: *Front. Pharmacol.*, 2018, **9**, pp 1323. doi: https://doi.org/10.3389/fphar.2018.01323
54) Harringer, S., et al., Synthesis, Modification, and Biological Evaluation of a Library of Novel Water-Soluble Thiopyridone-Based Organometallic Complexes and Their Unexpected (Biological) Behavior, *Chemistry – A European Journal*, 2020, **26**(24), 5419-5433. doi: https://doi.org/10.1002/chem.201905546
55) Geisler, H., et al., Novel phthiocol-based organometallics with tridentate coordination motiv and their unexpected cytotoxic behaviour, *Dalton Trans.*, 2020, **49**, 1393.1397. doi: https://doi.org/10.1039/C9DT04462K
56) Suntharalingam, K., et al., A Breast Cancer Stem Cell-Selective, Mammospheres-Potent Osmium(VI) Nitrido Complex, *J. Am. Chem. Soc.*, 2014, **136**, 14413-14416. doi: dx.doi.org/10.1021/ja508808v
57) Ravi, M., et al., 3D Cell Culture Systems: Advantages and Applications, *J. Cell. Physiol.*, 2015, **230**, 16-26. doi: 10.1002/jcp.24683

58) Duval, K., et al., Modeling Physiological Events in 2D vs. 3D Cell Culture, *Physiology*, 2017, **32**(4), 266-277. doi: 10.1152/physiol.00036.2016
59) Carvalho, M. P., et al., *Tumour Spheroid Assembly on Hyaluronic Acid-Based Structures: A Review*, *Carbohydr. Polym.*, 2016, **150**, 139-148. doi: https://doi.org/10.1016/j.carbpol.2016.05.005
60) Edmondson, R., et al., Three-Dimensional Cell Culture Systems and Their Application in Drug Discovery and Cell-Based Biosensors, *ASSAY and Drug Development Technologies*, 2014, **12**(4), 207-218. doi: http://doi.org/10.1089/adt.2014.573
61) Kenny, P. A., et al., The morphologies of breast cancer cell lines in three-dimensional assays correlate with their profiles of gene expression, *Mol. Oncol.*, 2007, **1**(1), 84-96. doi: 10.1016/j.molonc.2007.02.004
62) ATCC – American Type Culture Collection (2016), HCT 116, accessed on 14. September 2020 from https://www.lgcstandards-atcc.org
63) ATCC – American Type Culture Collection (2016), HT 29, accessed on 14. September 2020 from https://www.lgcstandards-atcc.org
64) ATCC – American Type Culture Collection (2016), A549, accessed on 14. September 2020 from https://www.lgcstandards-atcc.org
65) Expasy (Cellosaurus, 2012), CH1, accessed on 14. September 2020 from https://web.expasy.org/
66) Al-Nasiry, S., et al., The use of Alamar Blue assay for quantitative analysis of viability migration and invasion of choriocarcinoma cells, *Human Reproduction*, 2007, **22**(5), 1304-1309. doi: https://doi.org/10.1093/humrep/dem011
67) Lama, R., et al., Development, validation and pilot screening of an in vitro multi-cellular three-dimensional cancer spheroid assay for anti-cancer drug testing, *Bioorganic & Medicinal Chemistry*, 2013, **21**(4), 922-931. Doi: https://doi.org/10.1016/j.bmc.2012.12.007
68) Yokoyama, C., et al., Induction of oxidative stress by anticancer drugs in the presence and absence of cells, *Oncology Letters*, 2017, **14**(5), 6066-6070. doi: https://doi.org/10.3892/ol.2017.6931
69) Kalyanaraman, B., et al., Measuring reactive oxygen and nitrogen species with fluorescent probes: challenges and limitations, *Free Radic. Biol. Med.*, 2012, **52**(1), 1-6. doi: 10.1016/j.freeradbiomed.2011.09.030
70) McKinnon, K. M., Flow Cytometry: An Overview, *Curr. Protoc. Immunol.*, 2018, **120**, 5.1.1-5.1.11. doi: 10.1002/cpim.40
71) Van Engeland, M., et al., Annexin V-Affinity Assay: A Review on an Apoptosis Detection System Based on Phosphatidylserine Exposure, Cytometry, 1998, 31, 1-9.
72) Rieger, A. M., et al., Modified Annexin V/Propidium Iodide Apoptosis Assay For Accurate Assessment of Cell Death, Video Article in: *Journal of Visualized Experiments*, 2011, **50**, 1-4. doi: 10.3791/2597
73) Howat, W. J., Wilson, B. A., Tissue fixation and the effect of molecular fixatives on downstream staining procedures, *Methods,* 2014, **70**(1), 12-19. Doi: 10.1016/j.ymeth.2014.01.022
74) Lazzari, G., et al., Light sheet fluorescence microscopy versus confocal microscopy: in quest of a suitable tool to assess drug and nanomedicine penetration into multicellular tumor spheroids, *European Journal of Pharmaceutics and Biopharmaceutics*, 2019, **142**, 195-203. doi: https://doi.org/10.1016/j.ejpb.2019.06.019

75) Li, L. T., et al., Ki67 is a promising molecular target in the diagnosis of cancer (Review), *Molecular Medicine Reports*, 2015, **11**(3), 1566-1572. doi: https://doi.org/10.3892/mmr.2014.2914
76) Bressenot, C., et al., Assessment of Apoptosis by Immunohistochemistry to Active Caspase-3, Active Caspase-7, or Cleaved PARP in Monolayer Cells and Spheroid and Subcutaneous Xenografts of Human Carcinoma, *Journal of Histochemistry & Cytochemistry*, 2009, **57**(4), 289-300. doi: https://doi.org/10.1369/jhc.2008.952044
77) Walsh, J. G., et al., Executioner caspase-3 and caspase-7 are functionally distinct proteases, *PNAS*, 2008, **105**(35), 12815-12819. doi: 10.1073pnas.0707715105
78) Odell, I. D., Cook, D., Immunofluorescence Techniques, *Society for Investigative Dermatology*, 2013, **133**, 1-4. doi: 10.1038/jid.2012.455
79) NEB - New England Biolabs (2020), pUC-19-Vector, accessed on 16. October 2020, from https://www.neb.uk.com
80) Víglasky, V., et al., Anthracycline-dependent heat-induced transition from positive to negative supercoiled DNA, *Electrophoresis*, 2003, **24**, 1703-1711. doi: https://doi.org/10.1002/elps.200305388
81) Li, Q.-L., et al., Monometallic complexes of 1,4,7,10-tetraazacyclododecane containing an imidazolium side: Synthesis, characterization, and their interaction with plasmid DNA, *Bioorganic & Medicinal Chemistry*, 2006, **14**(12), 4151-4157. doi: https://doi.org/10.1016/j.bmc.2006.01.069
82) Kasprzak, K. S., Oxidative DNA and protein damage in metal-induced toxicity and carcinogenesis, Serial Review: Oxidative DNA damage and repair in: *Free Radical Biology and Medicine*, 2002, **32**(10), 958-967. doi: https://doi.org/10.1016/S0891-5849(02)00809-2
83) Balagurumoorthy, P., et al., Method to eliminate linear DNA from mixture containing nicked circular, supercoiled, and linear plasmid DNA, *Analytical Biochemistry*, 2008, **381**, 172-174. doi: https://doi.org/10.1016/j.ab.2008.06.037
84) Harringer, S., et al., Introducing N-, P-, and S-donor leaving groups: an investigation of the chemical and biological properties of ruthenium, rhodium and iridium thiopyridone piano stool complexes, *Dalton Trans.*, **49**, 2020, pp 15693. doi: 10.1039/D0DT03165H
85) Schreiber-Brynzak, E., et al., Behavior of platinum(IV) complexes in models of tumor hypoxia: cytotoxicity, compound distribution and accumulation, *Metallomics*, 2016, **8**, 422-433. doi: 10.1039/c5mt00312a
86) Göschl, S., et al., Comparative studies of oxaliplatin-based platinum(IV) complexes in different in vitro and in vivo tumor models, *Metallomics*, 2017, **9**(3), 309-322. doi: 10.1039/c6mt00226a
87) Höfer, D., et al., Tetracarboxylatoplatinum(IV) complexes featuring monodentate leaving groups - A rational approach toward exploiting the platinum(IV) prodrug strategy, *J. Inorg. Biochem.*, 2015, **153**, 259-271. doi: 10.1016/j.jinorgbio.2015.08.018.
88) Höfer, D., et al., Impact of the equatorial coordination sphere on the rate of reduction, lipophilicity and cytotoxic activity of platinum(IV) complexes, *J. Inorg. Biochem.*, 2017, **174**, 119-129. doi: 10.1016/j.jinorgbio.2017.06.005
89) Göschl, S., et al., The role of the equatorial ligands for the redox behavior, mode of cellular accumulation and cytotoxicity of platinum(IV) prodrugs, *J. Inorg. Biochem.*, 2016, **160**, 264-274. doi: 10.1016/j.jinorgbio.2016.03.005
90) Höfer, D., et al., Synthesis, characterization, cytotoxic activity, and 19F NMR spectroscopic investigations of (OC-6-33)-diacetato(ethane-1,2-diamine)bis(3,3,3-

trifluoropropanoato)platinum(IV) and its platinum(II) counterpart, *Inorg. Chim. Acta*, 2019, **490**, 190-199. doi: 10.1016/j.ica.2019.02.017

91) Enyedi, É. A., et al., Complex formation of an estrone-salicylaldehyde semicarbazone hybrid with copper(II) and gallium(III): Solution equilibria and biological activity, *J. Inorg. Biochem.*, 2021, **220**, pp 111468. doi: 10.1016/j.jinorgbio.2021.111468